THESIS FOR THE DEGREE OF LICENTIATE OF ENGINEERING

Energy Evaluation for DC/DC Converters in DC-Based Wind Farms

LENA MAX

Division of Electric Power Engineering
Department of Energy and Environment
CHALMERS UNIVERSITY OF TECHNOLOGY
Göteborg, Sweden 2007

Energy Evaluation for DC/DC Converters in DC-Based Wind Farms
LENA MAX

Licentiate Thesis at the Graduate School in Energy and Environment

Division of Electric Power Engineering
Department of Energy and Environment
Chalmers University of Technology
SE–412 96 Göteborg
Sweden
Telephone +46 (0)31–772 1000

Chalmers Bibliotek, Reproservice
Göteborg, Sweden 2007

Energy Evaluation for DC/DC Converters in DC-Based Wind Farms
LENA MAX
Division of Electric Power Engineering
Department of Energy and Environment
Chalmers University of Technology

Abstract

In this thesis the suitability of three topologies for DC/DC converters in a DC wind farm grid is investigated from an energy efficiency and energy production cost point of view. The three selected topologies are the fullbridge converter, the single active bridge converter and the series parallel resonant converter. The losses are calculated for all three topologies as a function of the wind speed considering the losses in the semiconductor components and in the transformer. To obtain the average losses, the losses for each converter are integrated over the wind distribution for different average wind speeds.

It is found that the resonant converter and the fullbridge converter have the lowest losses of the three types for the DC wind farm application with about 1.79 - 2.47 % power losses for the resonant converter and about 1.47 - 2.92 % for the fullbridge converter depending on the position in the wind turbine grid. The single active bridge converter has considerably higher losses than the other two topologies with 3.18 - 4.44 % losses. It is shown that the variable operating conditions create problems for all three converters, and as mentioned the single active bridge converter is most affected by the wide range of operation conditions. When comparing the resonant converter and the fullbridge converter, the fullbridge converter has a smaller transformer as well as lower peak current and peak voltage, but also a higher number of diode modules in the output bridge. Comparing the contribution to the energy production cost for the converters, the topology with the lowest contribution varies between the positions in the wind turbine grid. For all positions except position 2b, the resonant converter of the fullbridge converter has the lowest losses. Considering the resonant capacitor, the higher peak voltage and the variable frequency control for the resonant converter, the fullbridge converter is here found to be the most suitable choice for the wind farm application. A measurement verification is conducted for the fullbridge converter, and the result found is that the simulated waveforms and the calculated losses agree with the measured values.

Index Terms: DC/DC converter, loss evaluation, wind energy, hard switching converters, resonant converters, snubber design and measurements.

Acknowledgements

The financial support for this research project given by Statens Energimyndighet (Swedish Energy Agency) is gratefully acknowledged.

First, I would like to thank my supervisors Dr. Ola Carlson and Dr. Torbjörn Thiringer for all help and support during the project. I would also like to thank my examiner Prof. Tore Undeland for his support and valuable comments. The reference group consisting of Dr. Philip Kjær, Dr. Georgios Demetriades, Dr. Per Karlsson and Sven Sjöberg is also gratefully acknowledged.

I also would like to thank the master thesis workers Thomas Nyikos and Tobias Tomaschett from ETH for the experimental setup and Robert Karlsson for the help during the experimental work. Further I would like to thank my friends and colleagues in the Division of Electric Power Engineering and in the Division of High Voltage Engineering for making the working environment enjoyable, especially Johan Andersson, Jimmy Ehnberg, Ramona Huuva, Elisabeth Lindell and Dr. Stefan Lundberg.

Finally, I would like to thank my family and Mattias for their love and support.

Lena Max
Göteborg, Sweden
February, 2007

Contents

Chapter 1

Introduction

1.1 Problem Background

For utilization of wind energy, an attractive option is to build large offshore wind farms. The planned offshore wind farms have large power ratings compared to the offshore wind farms existing today, and there will also be an increasing distance to the shore and to the point of common coupling, PCC. For all offshore wind farms, cable transmission will be the only solution [1]. If the transmission distance is long or if the grid to which the farm is connected to is weak, a high voltage direct current (HVDC) cable transmission could be an attractive transmission system, instead of using a high voltage AC cable transmission [1, 2, 3]. In [4] different configurations of electrical systems for large wind farms have been investigated. From this investigation it is shown that wind farms with DC-grids is an interesting option for future wind farms from an energy cost point of view, providing that the losses and cost of the DC/DC converters will not be too high.

Assuming that the wind turbines produce a DC voltage as output (after a rectification of the generator output), they can be connected in different ways to achieve the desired voltage level for the HVDC transmission. One possibility is to connect the turbines in parallel, which can be done in different ways and an example is shown in Fig. 1.1. A suitable number of turbines are connected in parallel to a DC/DC converter to raise the voltage level. These groups are then connected in parallel to a DC/DC converter which makes up the transmission voltage. In these DC-based wind farms, there is a need of DC/DC converters, both converters for the single turbines and for converters with higher power designed to handle a group of turbines or a whole wind farm. A key component for the realization of a DC-based wind farm is the high-power DC/DC converter. This DC/DC converter will have the same function in a DC wind farm as the AC transformer in a traditional AC wind farm.

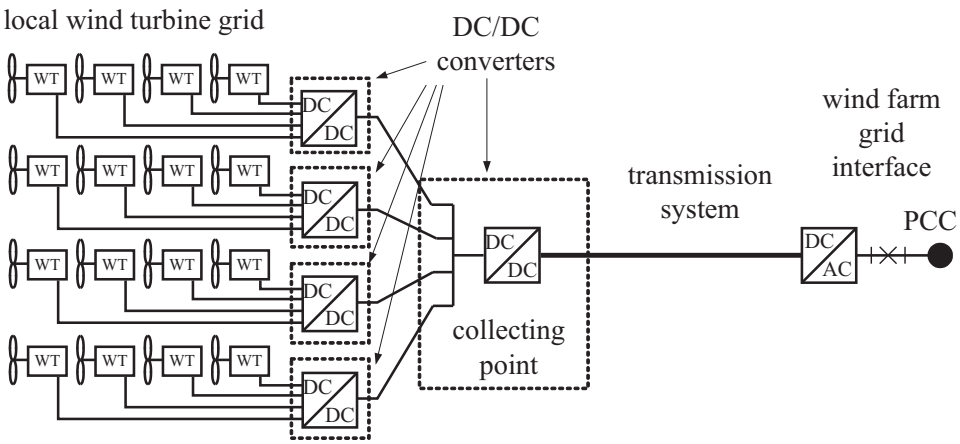

Fig. 1.1 Possible layout of a DC wind farm with DC/DC converters

1.2 Overview of Previous Work

Different topologies for low power DC/DC converters have been extensively studied in earlier literature. Recently, also interesting work concerning high power DC/DC converters has started to emerge. Since there is a general demand for smaller and less heavy converters, the switching frequency tends to be higher since that reduce the size of transformers, capacitors and inductors [5]. The resulting increase of the switching losses leads to a demand for a reduction of these losses by achieving soft switching conditions for the power devices.

1.2.1 Topologies for DC/DC Converters

The fullbridge (FB) converter, seen in Fig. 1.2, with different control schemes have been extensively studied in literature. Common for most of the studies is that there has to be some kind of soft-switching to reduce the switching losses. A common way of achieving reduced switching losses is to use the phase-shifted pulse-width modulation technique [6, 7, 8], which requires snubber capacitors connected across the switches as seen in Fig. 1.2. This will be further investigated in Chapter 3.

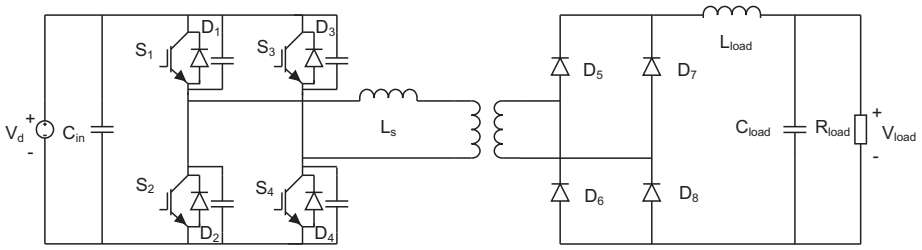

Fig. 1.2 Topology for the FB converter using phase shift control.

The single active bridge (SAB) converter was first presented in [9] and then further investigated in [10]. The topology is the same as for the fullbridge converter shown in Fig. 1.2 except for the voltage stiff output instead of the current stiff output for the FB converter. As a consequence it behaves differently and accordingly it is controlled in a different way [10]. Soft switching at turn-off is achieved by adding turn-off snubbers across the switches and turn on occurs at zero current.

Resonant converters are introduced that use a resonant tank to achieve soft-switching [9, 11, 12], which has the advantage of reduced switching losses but has to contain a resonant inductance and resonant capacitance resulting in large circulating currents and high conduction losses. The resonant tank consists of inductive and capacitive components and is located in between the input bridge and the rectifying output bridge. In addition, the components in the resonant tank must be rated for high currents and high voltages. There is no need for snubber capacitors since switching occurs under zero current and/or zero voltage conditions due to the resonant tank.

1.2.2 Loss Comparison

There are different methods for loss calculations for the different components. The calculation of losses in an inductance is described in [13, 14, 15], the switching losses are described in [5, 16, 17] and the losses in the transformer are treated in [18, 19].

There is a number of papers presenting different loss evaluations of soft switched and hard switched converters. In [20], it is proposed to add capacitor snubbers across the switches in a traditional H-bridge to reduce the turn-off losses. However, the losses are not completely removed, but a part of the losses can be moved to external capacitors and there can also be turn-on losses in the switches due to the discharge of the snubber capacitors. Many different solutions have been proposed to reduce the losses, and in [20] it has been shown that the efficiency can be increased from 92 % to 99 % for a 50 kVA DC/DC converter. In [5], the losses were compared for a 100 kW DC/DC converter for the hard switched fullbridge converter, the phase shifted fullbridge converter, the series parallel resonant converter, the dual active bridge and the auxiliary resonant commutated bridge. It was found that the resonant converter has the lowest efficiency with 94.3 % while the other topologies had an efficiency around 96 %. The only exception was the hard-switched fullbridge converter that also had an efficiency of 96 %, however it had a lower switching frequency, 5 kHz compared to 20 kHz for the other topologies. In [9] the operation and component stresses are studied for a 7 MW converter comparing the fullbridge, single active bridge and resonant topologies. However, there is no loss comparison for these converters.

1.3 Purpose of the Report

For the application in a wind farm, there is a lack of information in how the variable low output DC voltage from the wind turbines can be transformed into a high constant DC voltage suitable for transmission in an energy efficient way. For this, knowledge is needed of how high-power DC/DC converters behave in the wide range of operating conditions that occurs in a DC-based wind farm. Accordingly, the purpose of this report is to investigate these issues and present key results. One specific goal is, since the operating conditions vary strongly, to study the difficulties in operating the DC/DC converters at high efficiency at all wind speeds, and also to investigate if there are any difficulties due to the high power ratings for the converters. Moreover, an aim here is to find how the variable voltage from the turbines is transformed to the wind farm output voltage in the most energy-efficient way and with the lowest possible contribution to the energy production cost. Finally, a goal is to verify some of the results from the simulations using an experimental setup.

1.4 Layout of the Report

First, there is a general introduction to wind power and offshore wind farms in Chapter 2. The conversion of wind energy into mechanical and electrical energy is described as well as some introduction to offshore wind farms, the transmission to shore and grid integration. In Chapter 3, three possible topologies for high power DC/DC converters are presented along with the components needed to realize these converters. In Chapter 4, the loss calculations are described for the different components in the converter. These loss calculations are needed to optimize the converters and compare the efficiencies. In Chapter 5 the operating conditions for the DC/DC converters in a DC based wind farm are lined out using a local wind turbine grid with different control strategies to adjust the voltage levels from the varying output voltage from the generator to a constant transmission voltage. For these obtained operating conditions, converters are designed using the three described topologies for all positions in the local wind turbine grid. The losses and performance of the three topologies using the different control strategies are compared. From the losses and the designs of the converters, the contribution to the energy production cost from each converter is calculated. Finally, in Chapter 6, the results from the experimental setup verifies the loss calculations for the converters.

1.5 Publications

The publications originating from this project are:

I **L. Max** and S. Lundberg, "System efficiency of a DC/DC converter based wind turbine grid system," in *Nordic Wind Power Conference (NWPC) 2006*, May., 2006. The paper has been recommended for consideration for a special issue of the Wind Energy journal.

II **L. Max**, "Energy efficiency for DC/DC converters in a DC grid system for wind farms," in *Nordic Workshop on Power and Industrial Electronics (NORPIE) 2006*, June 2006.

III **L. Max** and T. Thiringer, " Snubber and control method selection for a 5 MW wind turbine single active bridge DC/DC converter", submitted to *12th European Conference on Power Electronics and Applications (EPE) 2007*.

Chapter 2

Wind Turbines and Grid Connection

Wind power is an area under rapid development. The installed wind power capacity has increased significantly during the last ten years [21], and the trend is to install larger wind turbines and group them together to large wind farms. For these large wind farms that require a vast area, offshore locations is an interesting option. In this chapter, the basics of wind energy will be described and also some of the challenges with offshore wind farms.

2.1 Conversion of Wind Energy

The basic principle for a wind turbine is to convert the energy in the wind into mechanical power and then into electrical power. The mechanical energy obtained from the wind is a function of the wind speed as well as the design and control of the wind turbine.

2.1.1 Wind Distribution

The most common probability density function to describe the wind speed is the Weibull function [22], which has the probability function

$$f(\omega_w) = \frac{k}{c}\left(\frac{\omega_w}{c}\right)^{k-1} \exp\left[-\left(\frac{\omega_w}{c}\right)^k\right]. \tag{2.1}$$

In (2.1), k is a shape parameter, c is a scale parameter and ω_w is the wind speed. If $k = 2$, the Weibull distribution is known as the Rayleigh distribution where c is given by the average wind speed $\bar{\omega}_w$ [23] as

$$c = \frac{2}{\sqrt{\pi}}\bar{\omega}_w. \tag{2.2}$$

The probability distribution is then given by the average wind speed [22] as

$$f(\omega_w) = \frac{\pi\omega_w}{2\bar{\omega}_w^2} \exp\left[-\frac{\pi\omega_w^2}{4\bar{\omega}_w^2}\right]. \tag{2.3}$$

The average wind speed varies between different locations, average values of 7.2 m/s and 5.4 m/s have been measured at two different sites in Sweden [24]. At the wind farm Horns Rev at the Danish west coast, the average wind speed is 10 m/s [25]. The probability distributions for these different average wind speeds using the Rayleigh distribution are shown in Fig. 2.1.

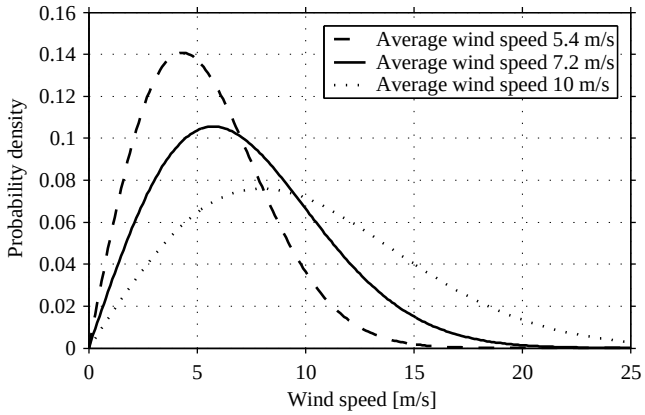

Fig. 2.1 Probability distribution for the wind speed.

2.1.2 Aerodynamic Conversion

A part of the available power in the wind is then converted to mechanical power by the rotor blades. The amount of energy converted from energy in the wind to mechanical energy on the shaft of the generator is given by [22]

$$P_{mech} = \frac{1}{2}\rho_{air} A_r C_P(\lambda_{tip}, \beta)\omega_w^3. \tag{2.4}$$

In the so called $C_P(\lambda_{tip}, \beta)$-curve, C_P is the power coefficient and β is the pitch angle. Further, λ_{tip} is the tip speed ratio, ω_w is the wind speed, ρ_{air} is the air density and A_r is the area swept by the rotor. The tip speed ratio λ_{tip} is calculated from the rotor speed Ω_r, the radius of the rotor r_r and the wind speed ω as

$$\lambda_{tip} = \frac{\Omega_r r_r}{\omega_w}. \tag{2.5}$$

Since the mechanical power is a function of the tip speed ratio λ_{tip}, the speed of the rotor should be adjusted so the maximum mechanical power is achieved at every wind speed. However, at high wind speeds it is necessary to limit the power. It can basically be done in two ways, either by stall control or by pitch control. With stall control, the blades are designed to stall at high wind speeds and no pitch control is needed. The second and most common method used in almost all variable speed wind turbines is pitch control [23].

Below rated wind speed the pitch angle maximizes the energy capture, and at higher wind speeds the mechanical power is reduced by changing the pitch angle. In Fig. 2.2 output power, voltage and current are shown for an ideal variable speed wind turbine with a synchronous generator.

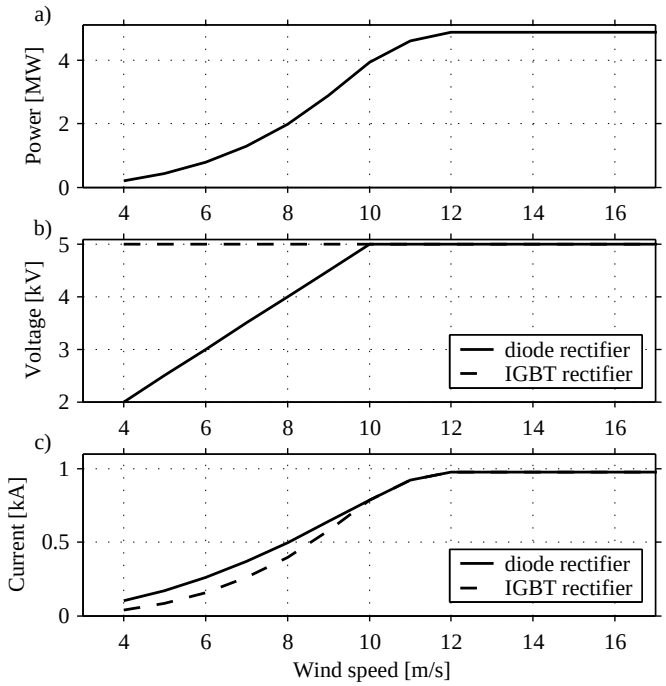

Fig. 2.2 Output from the wind turbine rectifier. a) power, b) voltage and c) current.

The output voltage from the turbine can be rectified either using a diode rectifier or an IGBT rectifier. In Fig. 2.2 the difference in the output voltage for these different rectifiers is shown. It is seen that when the diode rectifier is used, the output voltage is proportional to the speed and when the IGBT rectifier is used, the voltage level can be adjusted to the same voltage for all wind speeds. As long as the wind speed is below the rated wind speed, the speed of the rotor is adjusted to give the maximum output power. At higher wind speeds the power should be limited and the speed of the turbine will therefore stay constant. In reality, the voltage in Fig. 2.2 b) will not always stay constant for wind speeds higher than 10 m/s, instead the voltage can decrease with increasing wind speed if the generator has a significant synchronous reactance.

2.2 Wind Turbine Systems

There are different ways to convert the mechanical power from the rotor blades to electrical energy. It could either be done with a fixed speed generator or with a variable speed

generator. Different types of generator systems are described in [3, 23] and will here only be described briefly. For all systems, the rotational speed of the wind turbine is fairly slow and a gearbox is therefore needed to adjust it to the electrical frequency. In case of a synchronous machine it is possible to use a multipole generator and in this way avoid a gearbox.

2.2.1 Fixed Speed Turbine

The fixed-speed generator in Fig. 2.3 consists of an induction generator (IG) directly connected to the grid. The speed of the turbine is fixed and determined by the grid frequency, the gearbox and the pole-pair number of the generator. The ”locked” speed operation makes that it is not possible to store the energy in the turbulence as rotational energy. The turbulence will then result in power variations leading to mechanical wear and also affect the power quality of the grid. The fixed speed turbine system often have two fixed speeds, which can be achieved either with two generators with different ratings and pole pairs or by a generator with two windings with different ratings and pole pairs.

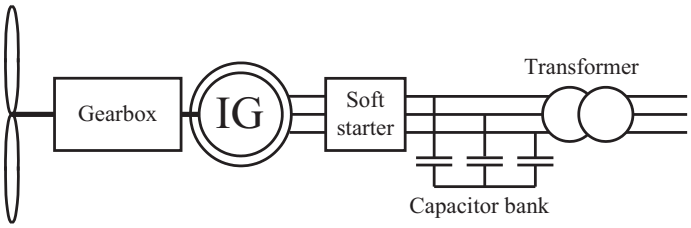

Fig. 2.3 Fixed speed turbine with an induction generator.

2.2.2 Full Variable Speed Turbine

For the variable speed wind turbine in Fig. 2.4, the rotational speed of the turbine is controlled by power electronics. The generator could be either a synchronous generator or an induction generator. If the generator is designed with multiple poles there is no need for a gearbox. In the variable speed wind turbine, power fluctuations caused by varying wind speed can be absorbed by slightly changing the rotor speed.

2.2.3 Variable Speed Turbine with Doubly Fed Induction Generator

The system in Fig. 2.5 consists of a wind turbine with a doubly fed induction generator (DFIG). In the DFIG, the stator is directly connected to the grid while the rotor is connected to a converter via slip rings. The converter only has to handle 20-30 % of the total power and the losses in the converter can be reduced compared to the converter that has

to handle the whole power. This system has a sufficient speed range to also smoothen out incoming wind power variations.

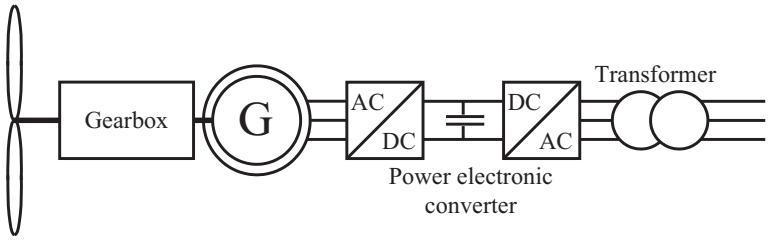

Fig. 2.4 Variable speed turbine with an induction or synchronous generator.

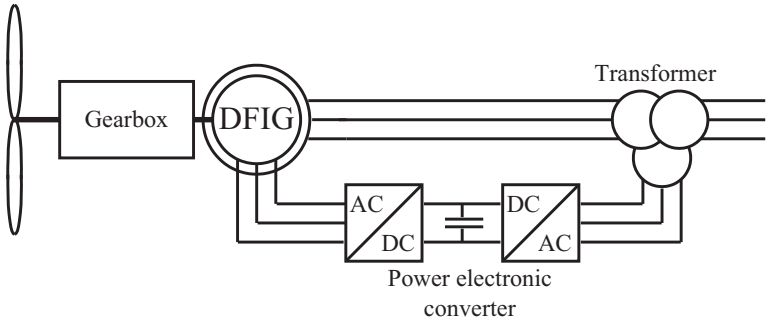

Fig. 2.5 Variable speed turbine with a doubly-fed induction generator (DFIG).

2.3 Offshore Wind Farms

Today, there is a large interest for placing wind turbines offshore in large wind farms. A large offshore wind farm is more complicated to design than a small onshore wind farm. Offshore wind turbines require maintenance as well as onshore wind turbines, but to reach the offshore turbines can be costly and difficult [26, 27]. Moreover, important to point out is that since the planned wind farms include a large number of turbines, they require a large space and the internal grid in the wind farm needs special attention during the design process. For offshore locations, the foundation for each turbine is the only item that can not be standardized [28]. A common foundation for offshore wind turbines is the steel monopile foundation [28, 29, 30], but also concrete gravity foundations have been used with success [29]. The monopile structure is used extensively in the offshore and nearshore environment for supporting oil and gas platforms and other structures [30]. Other possible solutions for offshore foundations are the tripod and the jacket structures, which are described in [30].

There are some different suggestions for layout of offshore wind farms presented in [4]. This include an AC based wind farm as well as two different DC based wind farms. One of these options is the wind farm that was shown in Fig. 1.1 which has replaced the AC cables and AC transformers in a traditional AC wind farm with DC cables and DC transformers. Another option presented in [4] is to connect the wind turbines in series until the transmission voltage has been reached. This will eliminate the need for DC/DC converters, but on the other hand the control will be more difficult and every wind turbine has to be isolated for a high transmission voltage. In [31] a medium frequency (500 Hz) wind turbine grid is proposed using cycloconverters for the turbines. This solution will reduce the number of series connected IGBTs in the voltage source converter and is also resulting in lighter transformers (compared to transformers for 50 Hz) since they are operating at medium frequency.

2.4 Transmission Systems for Offshore Wind Farms

The first offshore wind farm has been in operation since the beginning of the 1990's. At that time, the installed capacity was less than 10 MW and the size of the offshore wind farms have increased since then [1]. However, the offshore wind farms existing today still have relatively small installed capacity and are placed within a short distance from the shore [2, 32]. At mid 2005, all existing offshore wind farms are connected by HVAC cables and only three of them have offshore substations [2, 33]. The wind farm Horns Rev in Denmark is the first large offshore wind farm constructed in 2002. It has a capacity of 160 MW and is connected to the shore with an approximately 15 km long AC cable [25]. In several countries in Northern Europe offshore wind farms are planned with power rating from 100 MW to above 1000 MW [1]. Besides the larger size of the offshore wind farms there will be an increasing distance to the shore and cable transmission will be the only solution. The transmission distance from the wind farm to the shore together with the distance on land to reach a suitable interconnection point often end up with a distance of 50 - 100 km [1]. As a result, for offshore wind farms that have long transmission distances to the grid and often a large installed capacity, the transmission of power and integration to the grid needs to be considered carefully.

If the offshore wind farm is large and situated at a long distance from the shore, there is a need for one or several substations for stepping up the voltage to the voltage level for HVAC transmission or converting the power for HVDC transmission. For the transmission system for offshore wind farms there are basically two options, either an HVAC cable or an HVDC cable [1, 2, 3].

2.4.1 High Voltage AC (HVAC) Transmission

The experience of very long (about 100 km) offshore cable connections using AC cable are limited [34]. For long transmission distances, the production of large amounts of reactive power can be considered as the limiting factor for the HVAC cable [2, 33]. The high capacitance in the AC cables generate a considerable reactive current which reduces the active current carrying capacity of the cable and requires compensation devices for large distances [3]. The capacitance in the cable is much higher than the one for an overhead line and the reactive power is increasing with voltage and transmission capacity, and therefore there is a limited transmission distance for AC cables [1]. A possible solution is compensation, for example by several FACTS (Flexible AC Transmission System) devices such as thyristor controlled reactors (TCR) distributed along the cable. However, in practice the submarine cable for transmission to shore can only be compensated at the platform for the wind farm and on shore, effectively limiting the possible power transfer for a given cable length. The critical distance for HVAC cables has been found to be 202 km for 400 kV and 370 km for 132 kV [2, 33] for a transferred power of between 500 MW and 1000 MW. The critical length is defined as when half of the reactive current produced by the cable reaches nominal current at the end of one cable. Further, when the HVAC cable is used, the AC local wind turbine grid and the main grid are synchronously coupled and all faults in either grid can affect the other grid [3].

For the realization of an HVAC transmission system, the needed components are HVAC submarine transmission cables, offshore transformers, compensation units both onshore and offshore and onshore transformers depending on the transmission voltage. When calculating the losses of an HVAC transmission system, it has been found that the major part (above 80 %) of the losses are losses in the cables [2, 33]. The cost of the substations is low compared to the HVDC transmission, but the cost for the cables is higher [3].

2.4.2 High Voltage DC (HVDC) Transmission

For HVDC transmission, there are two alternatives, the Line Commutated Converter based and the Voltage Source Converter (VSC) based HVDC transmission system. Both the losses and the voltage drop in the HVDC cable is lower than the losses in the HVAC cable and there is no critical cable length except the practical limitations [1, 3]. Further, HVDC only requires two cables instead of three and the HVDC cables are also smaller in size and lighter [1].

Line Commutated Converter HVDC System

The line commutated converter HVDC transmission system (also called HVDC classic) is the traditional HVDC system using thyristor based converters that has been developed

over 50 years [1]. It is available for power up to 3000 MW [35] and the remaining development is to build systems for power above 3000 MW and distances longer than 1500 km in China [1]. Since the thyristor can not be turned off except when the current through it reverses direction, it is called a line commutated converter. To realize this transmission system, a number of components are needed including the converter based on thyristor valves. For the line commutated converter HVDC system, the major part of the losses originate from the converters at both ends of the HVDC cable. The cable itself contribute with approximately 20 % of the losses for an example with rated power of 500 and 1000 MW and transmission distances of 100 and 200 km [2, 33]. The line commutated converter HVDC system often uses the abbreviation LCC. This is not done in this thesis in order to avoid confusion sine the abbreviation for the series parallel resonant converter used in this thesis also is LCC.

Voltage Source Converter (VSC) HVDC System

The VSC HVDC transmission system is a newer technology based on converters using IGBT modules. This new technology is manufactured by both ABB where it is called HVDC Light^{TM} and by Siemens where it is called HVDC PLUS. The first HVDC Light^{TM} installation made by ABB was the 50 MW and 70 km link on Gotland in 1999 [1]. An advantage with the VSC HVDC is its capability to supply and absorb reactive power and thereby support power system stability [2, 3, 33] and take part in voltage regulation. Also for the VSC HVDC transmission, the major part of the losses is caused by the two converters. For the VSC HVDC the high losses in the converters caused by the high switching losses due to the high switching frequency and the higher conduction losses in the switches is a clear drawback. The losses in the cables is between 20 and 30 % of the total losses for example with rated power of 500 and 1000 MW and transmission distances of 100 and 200 km [2, 33]. Presently, the so called HVDC Light^{TM} from ABB is developed to approximately 550 MW [35], and the HVDC PLUS from Siemens is available with power rating from 50 MVA to 250 MVA [36].

2.4.3 Comparison Between HVDC and HVAC Transmission

In the comparison between HVAC, HVDC classic and VSC HVDC, it has been found in [2, 33] that for very large wind farms (above 200 MW), HVAC has the lowest losses for distances up to 55-70 km from shore depending on the transmitted power. For longer transmission distances it has been found that the HVDC classic solution has the lowest losses. In [3], the losses in HVAC and VSC HVDC transmission systems have been compared for wind farms between 100 and 500 MW and a transmission distance of 60 km. It was found that the VSC HVDC transmission has the highest losses, mainly due to the high losses in the converters. Also considering the total costs, the VSC HVDC solution is more expensive than the HVAC solution [3]. In [1] it was found that for an offshore

application for VSC HVDC with 350 MW transmitted power and 70 km sub sea cable and 30 km land cable, the direct investment cost would be the same for VSC HVDC and HVAC, which is about 110 - 140 MEuro. Further, it should be noted that the grid reinforcement costs may be significant when using HVAC but non-existing when using VSC HVDC [1]. The competitiveness of the HVDC transmission increases with the size of the wind farm and the transmission distance. HVDC can be an interesting alternative if the transmitted power is 200 - 1000 MW, if there is a need for a fast and accurate control and if the distance is more than 50 km. It can also be an interesting alternative if it is difficult to obtain permits for OH-lines, if there is a weak AC network and it can also increase both the long-term and short-term voltage stability [1]. It should be kept in mind that there is also other properties that affect the choice of transmission system, for example the number of cables required, reliability and integration into the onshore power system. For example, in the HVDC classis transmission the converter station are much larger than in VSC HVDC [1, 35] and therefore not suitable for offshore applications where the converter is situated on a platform. Further, the VSC HVDC has the ability to control the supplied reactive power and can thereby help to control the voltage stability of the network. Another possibility with HVDC connection is to connect a wind farm directly to an HVDC link used as interconnector between two electrical power systems [32]. This interconnector is preferably done with an HVDC link which then can be used for two purposes, both connecting an offshore wind farm and creating a link between two power systems. A condition for this is that the interconnector crosses a site that is suitable for an offshore wind farm.

2.5 Connection to the Grid

When the penetration of wind power increases, it can have a substantial impact on the electric transmission system. This is caused by the remote siting and possible problems for system security. As a result of the varying output power from wind generation and the fact that energy cannot be stored in a substantial way, there could be a need for both long term and short term power balancing, in addition to the reactive power aspects [3]. The operational strategy of the power system must consider the level of wind power penetration. Even the voltage control capability of a network is affected by wind generation since wind turbines can require a large amount of reactive power and wind power can replace conventional power plants with excellent voltage control capabilities [3]. The voltage control can be improved by using a VSC HVDC connection to the wind farm, the reactive power supplied can then be controlled which supports the voltage at the point of common coupling [3].

Chapter 3

DC/DC Converter Topologies for Wind Farm Applications

There are different ways to realize high power DC/DC converters for the application in a DC-based wind farm. From literature, three topologies that have been shown to have good characteristics have been selected. They are the fullbridge converter using phase shift control [5, 7, 37], the single active bridge converter [9, 10] and the series parallel resonant converter [38].

In this section, first the transformer and semiconductor components used in the DC/DC converters will be studied and then the three converter topologies will be described. It should be stressed that the transformer design is not a full-covering description of this subject, but instead the background theory for the transformers used in this thesis.

3.1 Components

For the design and loss calculations for the converters, the design of the transformer and the semiconductor switches and diodes must be known. First, the transformer is described, including the choice of core material, the design process and the cause of the losses in the transformer. Then the basics of the semiconductor components are described including the diode and the MOSFET and the IGBT transistors. Finally, the snubber circuits are introduced that limit the turn-off losses.

3.1.1 Transformer

The transformer is a magnetic component needed in a converter which is often designed for a specific application and is not commercially available in a wide range of properties. In [12, 37], the magnetic properties as well as the design process and considerations for a

transformer are explained in detail. In this thesis, a basic transformer design is made for each converter providing data for calculation of the losses in this component.

Magnetic Materials

The properties of the magnetic core material are important for the performance of the transformer. For different core materials, the losses are different and may vary differently with frequency and flux levels. These factors must be carefully considered in the design of the transformer.

There are mainly two classes of materials used for magnetic cores in transformers [12]. The first class includes alloys of iron and small amounts of other elements like chrome and silicon. These materials have a large electric conductivity compared to ferrites and the saturation flux density can be as high as 1.8 T. In the iron alloy materials, there exist both hysteresis losses and eddy current losses. The presence of eddy current losses makes the materials suitable for lower frequencies, approximately 2 kHz and below, and the material must be laminated to reduce eddy current losses for frequencies as low as 60 Hz [12]. Cores made from powdered iron or powdered iron alloys have a larger resistivity and a lower eddy current loss than laminated cores and can thereby be used at higher frequencies. However, the reluctance in these materials is lower than for classical iron shells. There is also a possibility to use various amorphous alloys of iron and other metals together with approximately 20 atomic percent of boron, silicon and other glass-forming elements. These alloys have the trade name METGLAS and have larger electric resistivity as well as larger saturation inductance at high temperatures than ferrites. The second class of materials is ferrites, which is an oxide mixture of iron and other materials [12]. For the ferrites, the electric resistivity is high but the saturation flux density is low and the ferrites have only hysteresis loss since the high resistivity reduce the eddy current loss.

The hysteresis loss is caused by the hysteresis in the B-H characteristics of a magnetic material [12, 37]. The area inside the B-H curve represents work done to the material by the applied field which causes heat and a temperature rise in the material. In [12, 39, 40] the general expression for the core losses in the case of a sinusoidal voltage exciting the core is

$$P_{core} = K_1 f_{tr}^{K_2} (B_{max})^{K_3} V_{core}. \tag{3.1}$$

Here the core loss P_{core} is a function of the peak value of the ac flux density B_{max} and the switching frequency f_{tr}. Further, K_1, K_2 and K_3 are constants that vary between the materials and V_{core} is the volume of the core. However, loss coefficients are often provided from the manufacturer of the core only for sinusoidal excitation. For non sinusoidal

excitation, the core losses can be given by

$$P_{core} = \frac{1}{\tau} K_1 f_{eq}^{K_2 - 1} (B_{max})^{K_3} V_{core} \tag{3.2}$$

assuming no temperature dependence of the core losses [41, 42]. Here, τ is the switching period and f_{eq} is the equivalent frequency. In the case of a PWM-type DC/DC converter the equivalent frequency can be calculated with

$$f_{eq} = \frac{2}{\pi^2} f_{tr} \frac{1}{D(1-D)} \tag{3.3}$$

where D is the duty cycle [41, 42].

Further, it has been shown in [39] that the core losses are lower for a core with square wave excitation than for a core with sinusoidal excitation, when the peak flux B_{max} has the same value.

Copper Windings

Copper is used for transformer windings because of its high conductivity and that it is easy to bend to tight windings [12]. The winding losses P_w are given by

$$P_w = I_{pri}^2 R_{pri} + I_{sec}^2 R_{sec} \tag{3.4}$$

for the primary and secondary windings [41]. The dc-resistance R_{pri} of the primary winding and R_{sec} of the secondary winding are given by

$$R_{pri} = \sigma \frac{l_{w,pri} N_{pri}}{A_{Cu,pri}} \tag{3.5}$$

and

$$R_{sec} = \sigma \frac{l_{w,sec} N_{sec}}{A_{Cu,sec}}. \tag{3.6}$$

Here σ is the resistivity of copper, $l_{w,pri}$ and $l_{w,sec}$ the average lengths of winding turn, $A_{Cu,pri}$ and $A_{Cu,sec}$ the areas of the windings and N_{pri} and N_{sec} the number of turns. Neglecting any leakage and magnetizing currents, the ratio between the primary and the secondary currents are given by

$$I_{sec} = I_{pri} \frac{N_{pri}}{N_{sec}}. \tag{3.7}$$

Due to the skin effect, the current in a conductor concentrates towards the surface at high frequencies and the result will be an increase in the current density and thereby also the effective resistance [12, 18, 37]. If the diameter of the conductor is larger than the skin

depth, the loss will increase significantly in the conductor at higher frequencies. This increase can be reduced by making the diameter of the conductor less than the skin depth. Another advantage with a conductor with small diameter is that the eddy current losses are reduced. However, to only reduce the conductor diameter is not a solution since a smaller diameter will give higher resistive losses. Connecting several small twisted cables with diameters significantly smaller than the skin depth in parallel (called Litz wire) will reduce the resistive losses but not increase the eddy current losses. The small diameter of the conductors in the Litz wire, also called strands, will result in that the resistance is not significantly increased at higher frequencies. Also, in a Litz wire, all strands occupy each position in the cable equally [39].

For the Litz wire, the number of strands multiplied by the conductor area $A_{Cu,st}$ for each strand gives the total copper area A_{Cu} for the Litz wire. The total copper area multiplied by the number of turns will be less than the cross sectional area of the winding A_w, and the resulting ratio is called the copper fill factor which is given by

$$k_{Cu} = \frac{NA_{Cu}}{A_w}. \tag{3.8}$$

Reasonable values for the copper fill factor is from 0.3 for Litz wire to 0.5-0.6 for round conductors.

In [40], the power loss P_w in a conductor carrying ac current I_{rms} is calculated as

$$P_w = K_{ac}\frac{\sigma \cdot l_{w,tot}}{A_{Cu}} I_{rms}^2. \tag{3.9}$$

In (3.9) $K_{ac} = \frac{R_{ac}}{R_{dc}}$ is the ac-resistance coefficient which is given by [40, 41]

$$K_{ac} = \frac{R_{ac}}{R_{dc}} = 0.5y\left[M(y) + (2m-1)^2 D(y)\right] \tag{3.10}$$

where

$$y = hc/\delta \tag{3.11}$$

is the normalized conductor thickness. For a round conductor $hc = \frac{\sqrt{\pi}}{2}d$ where d is the wire diameter and $\delta = \frac{0.071}{\sqrt{f_{tr}}}$ where f_{tr} is the frequency. For a foil conductor, hc is the conductor thickness and δ is the skin depth at 100°C. In (3.10) m is the number of layers,

$$M(y) = \frac{\sinh(y) + \sin(y)}{\cosh(y) - \cos(y)} \tag{3.12}$$

and

$$D(y) = \frac{\sinh(y) - \sin(y)}{\cosh(y) + \cos(y)}. \tag{3.13}$$

The power loss in the windings can then be obtained by adding the losses of each harmonic component [41], which is done by

$$P_w = \sum_{h=0}^{\infty} (I_{pri,h}^2 R_{pri} + I_{sec,h}^2 + R_{sec}) \left(\frac{R_{ac}}{R_{dc}} \right)_h . \tag{3.14}$$

Design of a Transformer

The transformer is complicated because it requires two or more conductor windings on the magnetic core. The medium frequency transformer have different properties compared to the line frequency transformer [39], both the power density and the loss density are high compared to the line frequency transformer. Since the voltage level used is high and the core is small, the space needed for insulation can cause a problem. In the design of a transformer for soft switching DC/DC converters, the leakage inductance needs to be carefully controlled [18].

In this design, two c-cores are used as shown in Fig. 3.1 with the winding arrangement shown in Fig. 3.2. Here, only two c-cores are used but if the maximum winding radius is large, a larger number of c-cores can be distributed along the windings.

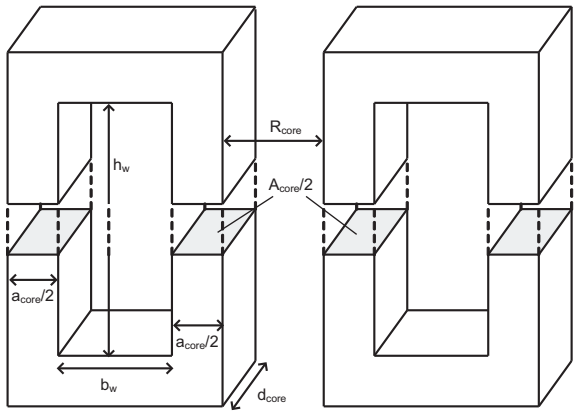

Fig. 3.1 Two c-cores used for transformer design

As a first step, the winding design for the converter is determined. The number of primary turns N_{pri} in the winding is determined and can be varied in order to find a suitable design. Knowing the number of primary turns, the number of secondary turns are given by

$$N_{sec} = N_{pri} \frac{V_{sec}}{V_{pri}}. \tag{3.15}$$

For the primary winding, which is the low-voltage winding, a foil conductor is used and for the secondary winding, which is the high voltage winding, a Litz wire is used. The in-

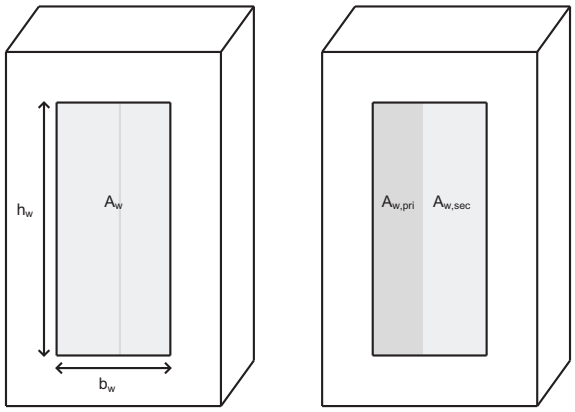

Fig. 3.2 Winding arrangement for the transformer

sulation is supposed to withstand a maximum electric field of E_{max} = 10 kV/mm, which is lower than the maximum field for transformers used for 50 Hz sinusoidal voltage. The insulation distance $d_{i,pri}$ and $d_{i,sec}$ for the windings are then obtained from the peak voltages as

$$d_{i,pri} = \frac{V_{pri,max}}{E_{max}}, \;\; d_{i,sec} = \frac{V_{sec,max}}{E_{max}}. \tag{3.16}$$

The width of the foil $e_{w,pri}$ for the primary winding is assumed to be equal to the skin depth δ and calculated with

$$e_{w,pri} \leq \delta = \sqrt{\frac{2\sigma}{\omega\mu_{cu}}}. \tag{3.17}$$

For the foil conductor in the primary winding, the copper area for one turn is calculated by

$$A_{cu,pri} = \frac{I_{pri}}{J_{pri}}. \tag{3.18}$$

The height of the winding is then dependent on the number of parallel layers np_{pri} for the primary winding as seen in Fig. 3.3.

The height of the winding is then calculated by

$$h_{w,pri} = \frac{A_{cu,pri}}{e_{w,pri} np_{pri}}. \tag{3.19}$$

With the insulation distance of $d_{i,pri}$ between the windings and N_{pri} number of turns, the winding height $h_{w,pritot}$ and width $b_{w,pritot}$ for the primary winding can be calculated as

$$h_{w,pritot} = h_{w,pri} + 2d_{i,pri} \tag{3.20}$$

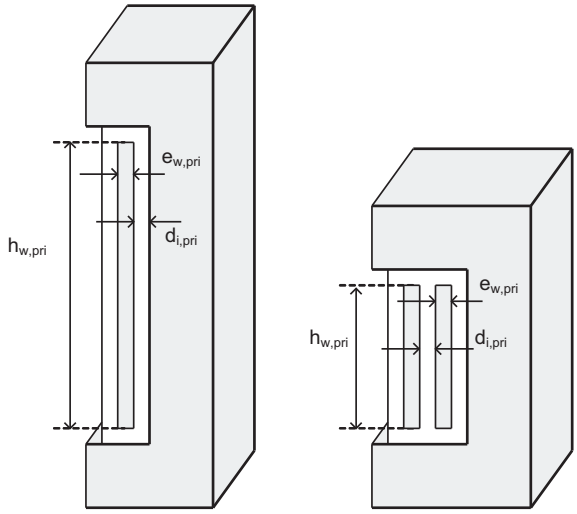

Fig. 3.3 Foil winding for the primary side with 1 or 2 parallel layers.

and

$$b_{w,pritot} = N_{pri} np_{pri}(e_{w,pri} + d_{i,pri}) + d_{i,pri}. \tag{3.21}$$

For the secondary winding, a Litz wire is used with a copper fill factor of about 0.75 (excluding insulation between the wires). The copper area $A_{cu,sec}$ of the Litz wire is then calculated as

$$A_{cu,sec} = \frac{I_{sec}}{J_{sec} 0.75}. \tag{3.22}$$

The diameter for the copper wire is obtained by

$$e_{w,sec} = 2\sqrt{\frac{A_{cu,sec}}{\pi}}. \tag{3.23}$$

For the secondary winding, the number of turns N_{sec} is assumed to be divided into np_{sec} layers. In Fig. 3.4, the secondary winding can be seen when it is divided into 1 or 2 layers. It should be noted that this is the high voltage side and each cable is one turn unlike the primary winding where each turn can be divided into several parallel foil turns.

Just as for the primary winding, the winding height $h_{w,sectot}$ and width $b_{w,sectot}$ for the secondary winding can be calculated using the insulation distance $d_{i,sec}$ as

$$h_{w,sectot} = \frac{N_{sec}}{np_{sec}}(e_{w,sec} + d_{i,sec}) + d_{i,sec} \tag{3.24}$$

and

$$b_{w,sectot} = np_{sec}(e_{w,sec} + d_{i,sec}) + d_{i,sec}. \tag{3.25}$$

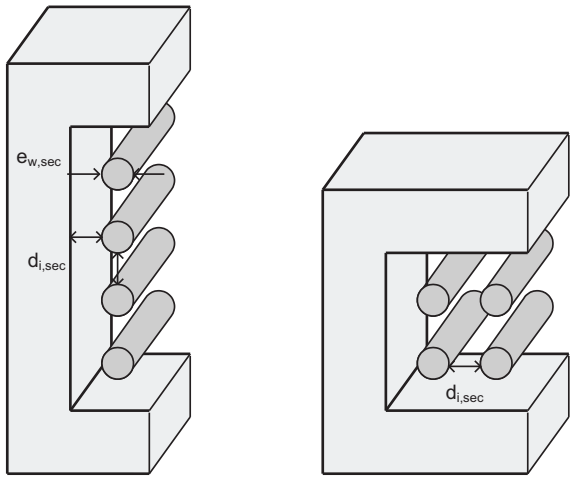

Fig. 3.4 Litz winding for the secondary side with 1 or 2 layers.

The resulting height h_w of the winding window is then the maximum height of the secondary and the primary winding, and the width b_w is the sum of the widths of the windings as shown in

$$h_w = \max(h_{w,pritot}, h_{w,sectot}), \quad b_w = b_{w,pritot} + b_{w,sectot}. \tag{3.26}$$

For the complete dimensions of the transformer, also the area of the core needs to be determined. For this, the peak flux density B_{max} in the core is determined and should be lower than the saturation flux density B_{sat}. The core area can be calculated using

$$A_{core} = \frac{\lambda_{pri}}{2N_{pri}B_{max}} \tag{3.27}$$

where

$$\lambda_{pri} = \int_{t_{pos}} v_{pri}(t)dt \tag{3.28}$$

is the integral of the voltage across the primary winding during the positive period t_{pos} [37]. Knowing A_{core} and assuming that $a_{core} = d_{core}$ these dimensions are given for the core.

Knowing all the dimensions, the volume V_{core} and weight of the core can be calculated and the core loss is obtained by

$$P_{core} = K_1 f_{tr}^{K_2} (B_{max})^{K_3} V_{core}. \tag{3.29}$$

The mean turns length $l_{w,pri}$ and $l_{w,sec}$ of the windings can be calculated from the known dimensions and the DC resistance in the windings are obtained as

$$R_{pri} = \frac{\sigma l_{w,pri} N_{pri}}{A_{Cu,pri}}, \quad R_{sec} = \frac{\sigma l_{w,sec} N_{sec}}{A_{Cu,sec}}. \tag{3.30}$$

The copper losses in the windings are then calculated by

$$P_w = K_{ac,pri} R_{pri} I_{pri} + K_{ac,sec} R_{sec} I_{sec}. \tag{3.31}$$

The total losses P_{tr} of the transformer are then given by the sum of the core losses and the winding losses as

$$P_{tr} = P_{core} + P_w. \tag{3.32}$$

For a transformer, the leakage inductance L_{leak} is an important design parameter that is calculated by [12]

$$L_{leak} = \frac{\mu_0 N_{pri}^2 l_w b_w}{3 h_w}. \tag{3.33}$$

In the design process of the transformer an iterative process is used. In this design process, the starting point is the demanded ratings of the transformer. From these values, designs are obtained for different values of for example the number of turns, the maximum flux density and the current density. The chosen design is then the design that gives the lowest losses or the lowest weight depending on what gives the lowest cost for the application.

3.1.2 Diodes

The power diode has the same principle of operation as the small signal diode, but a more complicated structure due to the higher power rating. This is described in detail in [12] and will here be explained briefly. The Shottky diode is not considered here since the reverse blocking voltage is too low for the high-voltage application in a wind farm, instead the focus is on the pn-diodes.

Fundamental Power Diode Physics

For explaining the fundamental physics of the power diode, the vertical cross section shown in Fig. 3.5 is used.

For the power diode, the n^--layer is the main difference from the low power diodes. In this region, the depletion region of the reverse-biased p^+n^-junction is absorbed. The reverse breakdown voltage is dependent of the width of the drift region. There are two main types of diodes, the non-punch-through diode and the punch-through diode. For a non-punch-through diode, the drift region is longer than the depletion layer at breakdown. The other option is the punch-through diode where the depletion region has extended all the

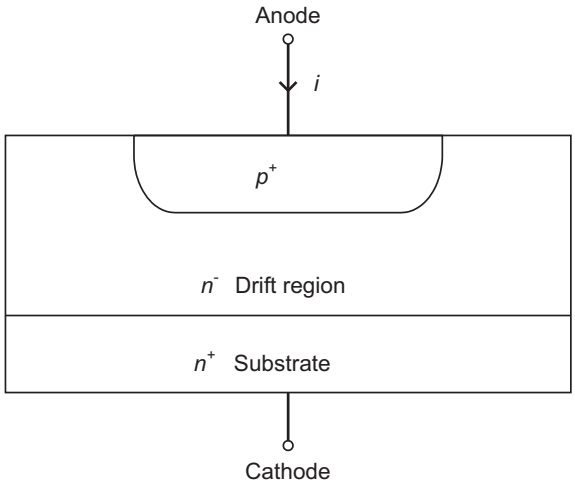

Fig. 3.5 Vertical cross section of a power diode.

way through the drift region.

In the on-state, the ohmic resistance is much less than the resistance calculated from the geometric size and and the thermal equilibrium power densities. This is a result of the large amount of excess-carrier injection into the drift region, called conductivity modulation.

An emerging technology today is the SiC power diode [43], and SiC p-n diodes rated at 19 kV have been reported. The SiC devices can operate at high junction temperature because of the wide band gap of SiC and they also have low thermal resistivity.

3.1.3 MOSFET

The Metal Oxide Field Effect Transistor (MOSFET) is widely used in low-power applications due to its fast switching and thereby low switching losses. However, the on-state losses are larger than for the IGBT which makes the IGBT more suitable for high-power applications. Even though the MOSFET is not used in this thesis it will be described here briefly since the section about the operation of the IGBT will refer to the operation of the MOSFET. A more detailed explanation of the MOSFET can be found in [12].

Fundamental MOSFET Physics

For understanding the physics of the MOSFET, the vertical cross section of a MOSFET is shown in Fig. 3.6. The transistor shown in the figure is called a n-channel MOSFET, since a n-channel is created when the device is conducting. In the off-state when no voltage is applied at the gate, the device is blocking since one of the pn-junctions is blocking

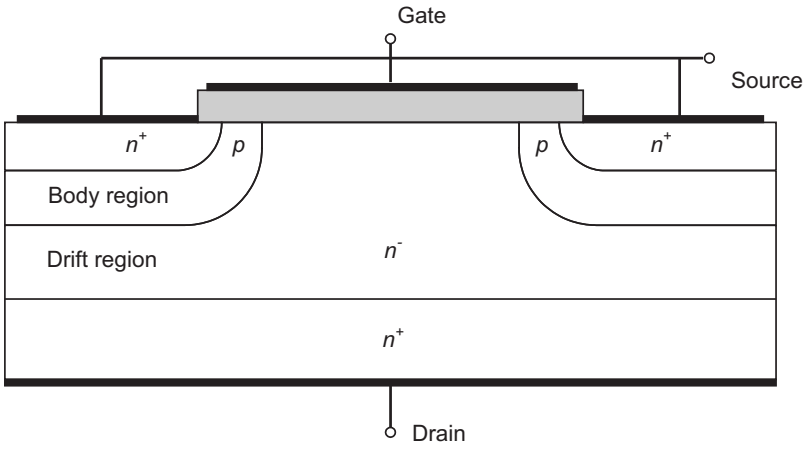

Fig. 3.6 Vertical cross section of a MOSFET.

the applied voltage. There can not be any minority-carriers injected from the gate which is isolated. However, when a positive voltage is applied at the gate, negative charges are attracted to the gate and a n-channel is created that connect the source to the drain. The current flowing in this channel depends on the voltage V_{GS} at the gate where a larger voltage gives a larger current.

The switching of the MOSFET is fast since there are no excess minority carriers that have to be removed or injected at turn-on or turn-off, and principal waveforms are shown in Fig 3.7. However, the lack of excess minority carriers results in a high on-state resistance unlike the IGBT where the large amount of excess carriers injected into the drift region reduce the resistance.

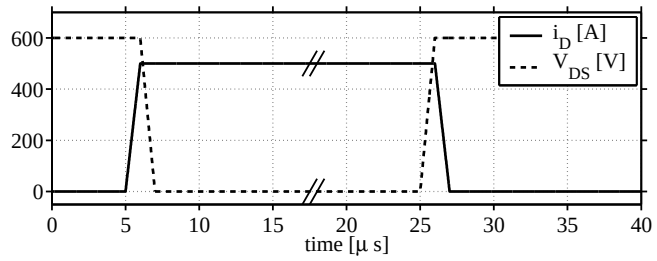

Fig. 3.7 Typical hard switching waveforms of a MOSFET.

3.1.4 IGBTs

The Insulated Gate Bipolar Transistor (IGBT) is the device that is most widely used in new high-power applications. It combines the fast switching of the MOSFET with the

low on-state losses of the BJT (Bipolar Junction Transistor) [12, 44]. The operation of the IGBT is thoroughly described in [12] and will here be explained briefly.

Fundamental IGBT Physics

In Fig. 3.8 the vertical cross section of an IGBT is shown.

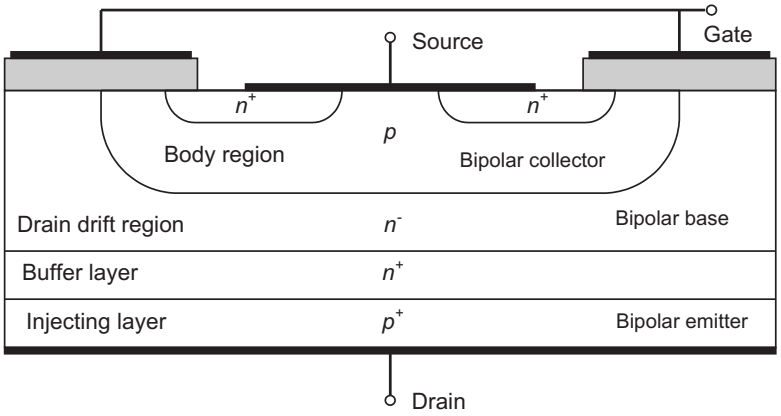

Fig. 3.8 Vertical cross section of an IGBT.

The operation of an IGBT can be explained as a Darlington circuit with a pnp BJT transistor as the main transistor and the MOSFET as the driver device as can be seen in Fig. 3.9.

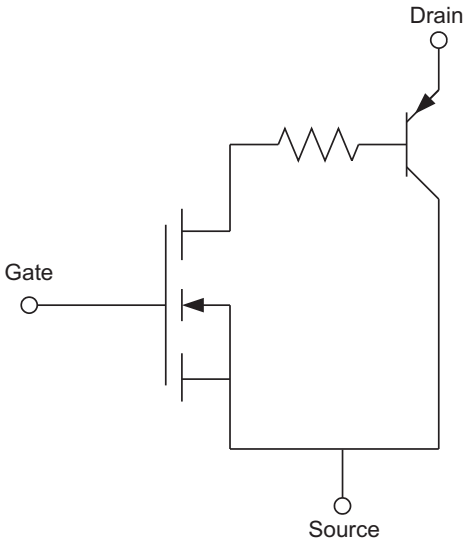

Fig. 3.9 Equivalent circuit for the IGBT.

Combining Figs. 3.8 and 3.9, it can be seen that the MOSFET transistor consists of the n^+-layer, the body region and the drain drift region. When a voltage is applied at the gate,

an inversion channel is created in the body region. An electron current from the source can then flow into the drain drift region, which causes an injection of holes from the p^+ drain contact layer. The BJT is the main transistor in the Darlington circuit in Fig. 3.9 and consists of the body region, the drain drift region and the injecting layer. The buffer layer is optional and will be described later. When the MOSFET has been turned on, the electrons and holes injected into the drain drift region will eventually turn the BJT on. However, the base of the BJT is wide, which gives a low value of β for the BJT. This results in that a significant part of the current flows through the MOSFET transistor.

The IGBT transistor can be seen as a mixture of the MOSFET and the BJT, and its characteristics is a mixture of the characteristics for the MOSFET and the BJT. The most basic differences are that the IGBT has a faster switching than the BJT and a lower on-state voltage than the MOSFET. The presence of conductivity modulation is the reason for the low on-state voltage for the IGBT compared to a comparable power MOSFET. For turn-on and turn-off, the transition is affected both by the MOSFET part and the BJT part. Typically switching waveforms for the IGBT are shown in Fig. 3.10.

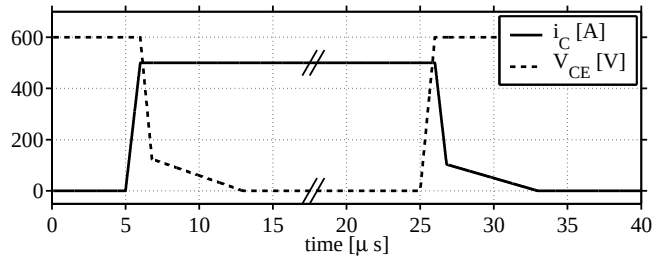

Fig. 3.10 Typical hard switching waveforms of an IGBT.

The basic switching waveforms are similar to the switching of the MOSFET, but the slower BJT-part of the IGBT results in some differences as seen in Fig. 3.10. At turn-on, the difference from the MOSFET is that the fall-time of the voltage is longer since the resistance in the IGBT is lowered due to conductivity modulation in the BJT, and the final on-state voltage is therefore not reached until the BJT has been turned on, which is the ”tail-voltage” seen at turn-on in Fig. 3.10. A similar principle applies for turn-off, where the difference in the waveforms between the MOSFET and the IGBT is the ”tail-current”. For the MOSFET transistor, the current is turned off rapidly but the BJT-current has a slower decrease. A reason for the slow decrease in the BJT current is that there is no possibility for carrier sweep-out and the stored charge in the n^- region must be removed with recombination. It is an open-base turn off process for the bipolar transistor since the MOSFET has been turned off and there is no base current. This tail-current gives a significant part of the turn-off losses, especially for soft-switching operation. To reduce the

tail current the life time of the carriers should be short, but this is a trade-off between the on-state losses that increase with a shorter carrier life time. There are also other ways to reduce the tail-current, where one option is to design the IGBT so the MOSFET carries as large part of the current as possible.

Regarding the n^+ buffer layer, it determines the ability to block reverse voltages. When there is a forward voltage across the IGBT and the MOSFET is turned off, the voltage drop occurs at the junction between the drain drift region and the body region. Since the drain drift region has the lowest doping level, the depletion region will mainly extend into this region. The n region must be large enough to accommodate the depletion region so it does not touch the p^+ layer. This can be done either by having a n^- layer that is large enough or by inserting the n^+ buffer layer. An IGBT without the n^+ layer is called a non-punch-through (npt) IGBT. This option gives the ability to block reverse voltages as large as the maximum blocked voltage in the forward direction. On the other hand, the component will be large. When the n^+ layer is inserted the IGBT is called a punch-through (pt) IGBT. In this case, the drain drift region can be made shorter without extending the depletion region into the p^+ layer for the same forward blocking voltage. However, the maximum reverse blocking voltage is very small due to the high doping on both sides of the junction between the injecting layer and the buffer layer.

3.1.5 Snubber Circuits

In two of the investigated topologies, the fullbridge converter and the single active bridge converter described later in this chapter, the turn-off losses for the IGBT modules are reduced by using snubber capacitors connected across the devices. Fig. 3.11 shows two possible circuit topologies for the turn-off snubber.

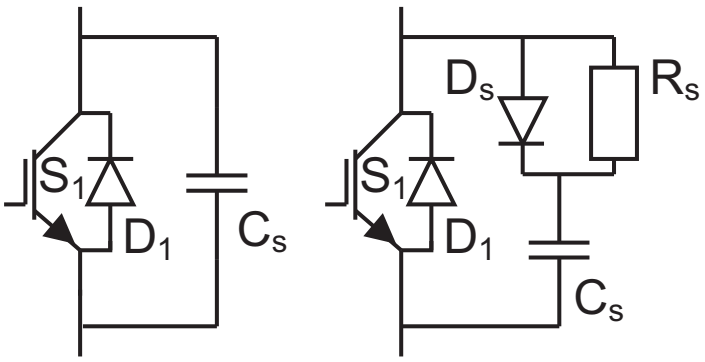

(a) Without limited current at turn-on. (b) With limited current at turn-on.

Fig. 3.11 Snubber circuits to reduce turn-off losses.

The principle of operation of a turn-off snubber is to increase the voltage rise time and thereby avoid high voltage level at the same time as the high current. As seen in Fig. 3.11, there are two different ways to realize the turn-off snubber. The first option is a capacitor connected across the switch as in Fig. 3.11 (a), which is called a lossless snubber. When this snubber circuit is used, the capacitor must be discharged before the switch is turned on. If this is not done, the capacitor will be short circuited through the switch and discharged with a large peak current in the switch. To reduce this current at turn-on, a resistance in parallel with a diode can be connected in series with the capacitor as seen in Fig. 3.11 (b). The resistance will limit the peak current at turn-on and the diode will provide the same characteristics when the capacitor is charging as the pure capacitor. The drawback with this snubber circuit is that there are losses in the resistance when the capacitor is discharged, in contrast to the lossless snubber. However, at turn-off both snubber circuits show the same characteristics since the capacitor is charged and the current will then flow through the diode. The snubber circuits will be studied further in Section 4.1.3 where the reduction of turn-off losses is explained compared to the hard-switching case. Also, the design of the snubber circuits will be studied in Section 5.2.

3.2 Fullbridge Converter

The first possible topology for a high power DC/DC converter described is the fullbridge converter shown in Fig. 3.12.

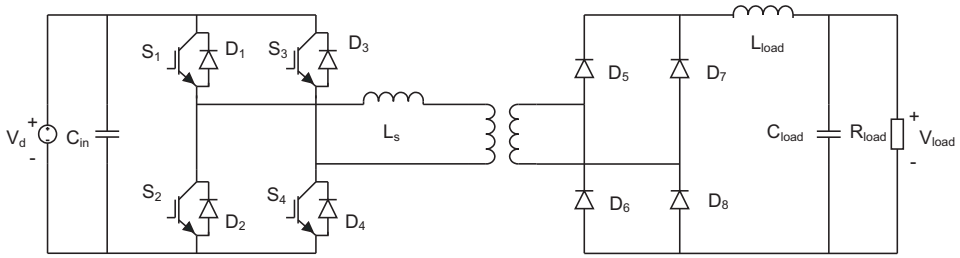

Fig. 3.12 Topology for the fullbridge converter.

In the fullbridge converter, the input bridge creates a high frequency square wave at the transformer, which transforms the voltage to a higher level. On the secondary side of the transformer the high voltage square wave is rectified by the diode bridge and the ripple is reduced to a suitable level by the output filter. Since the output filter is current-stiff, the current in the switches and the transformer is approximately constant during the on-period.

The easiest way to control the fullbridge converter is by duty cycle control, where the output voltage is proportional to the duty cycle. This control gives high switching losses since the switches are turned off at full load voltage. The second way to control the full bridge converter is by phase-shift control. The two switching legs are then controlled individually, where the leading leg changes the converter into the active phase and the lagging leg turns the converter into the passive phase.

3.2.1 Operation of the Fullbridge Converter with Duty Cycle Control

For the fullbridge converter with the topology shown in Fig. 3.12, the resulting currents and voltages for the switches and diodes are shown in Figs. 3.13 and 3.14. The voltage and current for the input to the transformer are shown in Fig. 3.15.

The duty cycle control gives a mean voltage across the transformer that is equal to the output voltage divided by the transformer ratio. This is achieved by an on-state where the switches in two legs are on, applying the input voltage across the transformer. In the off-state, all switches are off and the load current free-wheels through the diodes in the output bridge, which gives zero voltage across the transformer. These voltage variations are eliminated by the filter inductance giving a smooth output current. The operation principle for

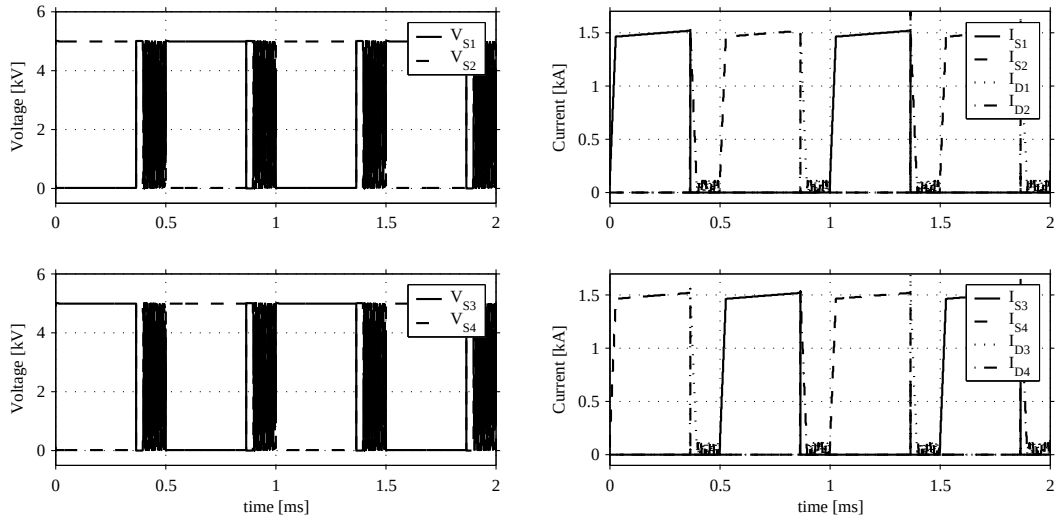

(a) Voltage for the switches.

(b) Current for the switches.

Fig. 3.13 Conditions for the switches in the 5 MW FB duty cycle converter.

the fullbridge converter is explained using the voltages and currents for the diodes and switches in Figs. 3.13 and 3.14 as well as the current and voltage for the transformer in Fig. 3.15 and the conduction paths shown in Fig. 3.16.

In the passive state at $t < t_1$ in Fig. 3.15, the switches in the input bridge are off and the load current flows through the output bridge as shown in Fig. 3.16 (a). In this passive state, there are oscillations between the leakage inductance in the transformer and the capacitance of the switches in the input bridge. These voltage oscillations can be seen in Figs. 3.13 and 3.15 where it also can be seen that the current resulting from these oscillations is small compared to the load current. The active state is initiated at $t = t_1$ when switches S_2 and S_3 are turned on as in Fig. 3.16 (b). Since the output diodes are short circuited, there is a negative voltage across the leakage inductance of the transformer resulting in an increased negative current. When the current has reached the value of the load current at $t = t_2$, the output bridge is not short circuited as in Fig. 3.16 (c) and the current stays constant. At $t = t_3$ switches S_2 and S_3 are turned off, forcing the current to flow through diodes D_1 and D_4. The current is now decreasing and the output bridge is short circuited as shown in Fig. 3.16 (d). When the current has reached zero at $t = t_4$, no switch is turned on and the load current flow through the diodes in the output bridge as shown in Fig. 3.16 (e). The next half period is obtained in the same way, turning on the switches S_1 and S_4 at $t = t_5$. The current is then increasing to the value of the load current and stays constant until the switches are turned off at $t = t_6$. After that, the current flown through the diodes D_2 and D_3 until it has decreased to zero and the passive state has been reached. The next period starts at $t = t_7$ when S_2 and S_3 are turned on.

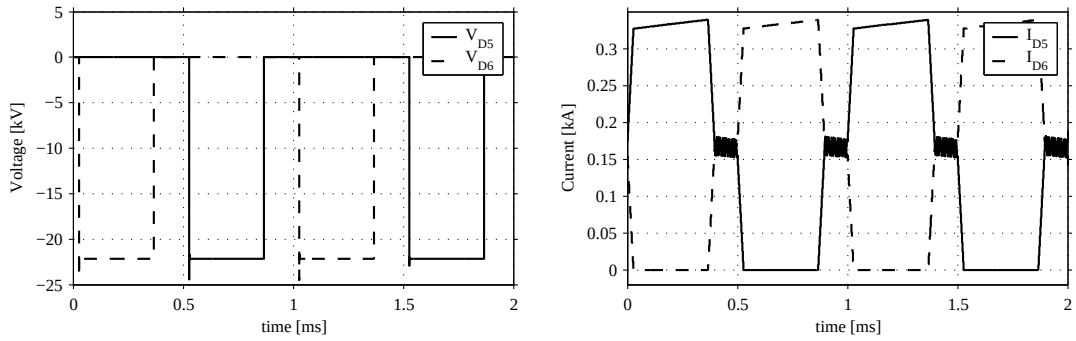

(a) Voltage for the diodes. (b) Current for the diodes.

Fig. 3.14 Conditions for the didoes in the 5 MW FB duty cycle converter.

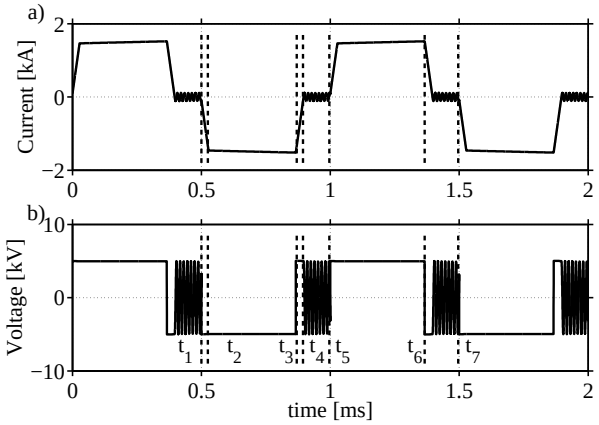

Fig. 3.15 a) current and b) voltage for the primary side of the transformer in the FB duty cycle converter.

From this, it can be seen that there are hard-switching conditions at both turn-on and turn-off for all transistors. This results in considerably high switching losses as will be shown in Section 4.1.

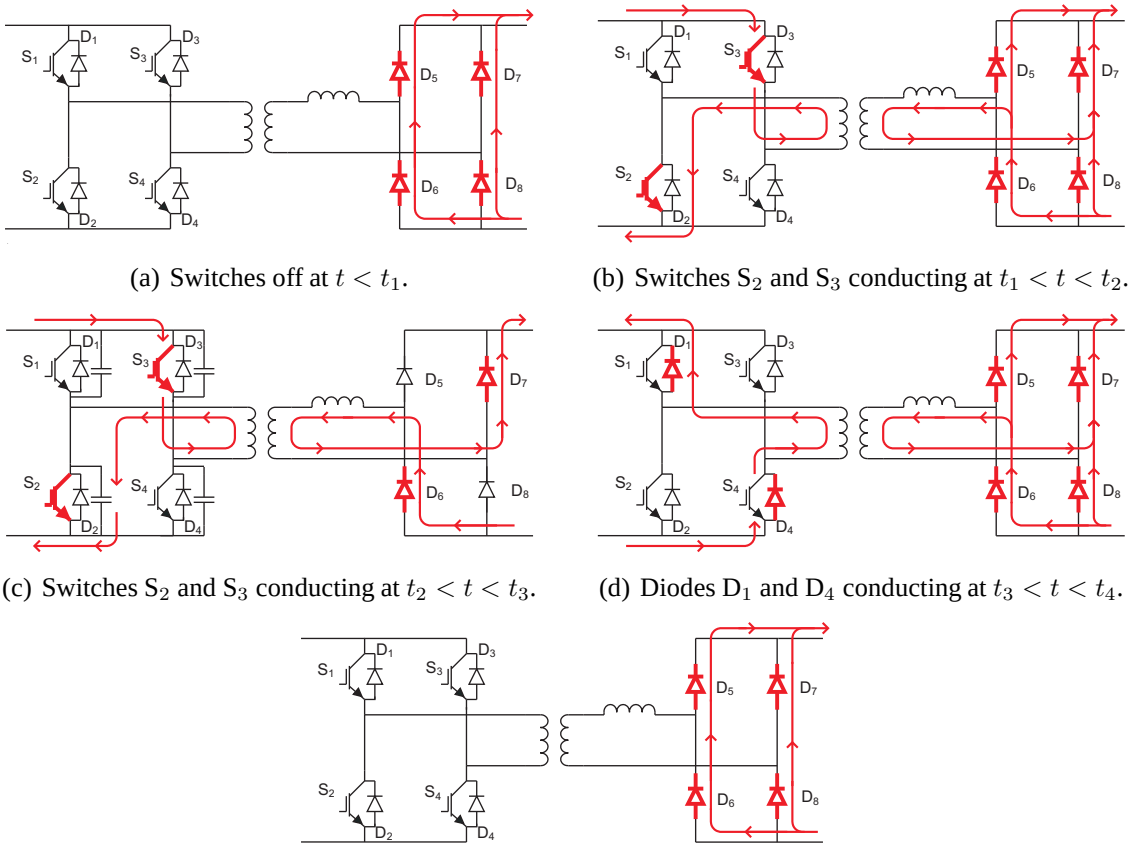

(a) Switches off at $t < t_1$.

(b) Switches S_2 and S_3 conducting at $t_1 < t < t_2$.

(c) Switches S_2 and S_3 conducting at $t_2 < t < t_3$.

(d) Diodes D_1 and D_4 conducting at $t_3 < t < t_4$.

(e) Switches off at $t_4 < t < t_5$.

Fig. 3.16 Conduction paths for the fullbridge converter, operating with duty cycle control.

3.2.2 Operation of the Fullbridge Converter with Phase Shift Control

If there are no snubber circuits across the switches as in the previous section, there would be high switching losses. As mentioned in the introduction, soft switching is often used for reducing the switching losses. This is usually done using the phase-shifted pulse-width modulation technique [6, 7, 8]. In hard-switched converters, a low leakage inductance is desirable for a fast polarity reversal of the current in the transformer which then gives a high maximum duty cycle. However, in a soft-switched converter, a low leakage inductance will result in difficulties to achieve soft-switching of the lagging leg [6, 7]. The switching of the leading leg devices is done using the energy storage in the output filter inductor, and the lagging leg devices are switched using the energy storage in the leakage inductance of the transformer. Unless the leakage inductance of the transformer is very large, the ZVS (Zero Voltage Switching) range is limited and large external capacitors can not be used for the lagging-leg switches [6, 7]. This switching range can be increased by adding an auxiliary circuit to the lagging-leg of the converter. A low leakage inductance of the transformer could lead to larger losses in the lagging-leg switches than in the leading-leg switches. In [8] a control scheme is proposed where one leg behaves as leading leg in one period and the lagging leg in the next period. This does not change the original operation principle of the converter, but, since there can be different losses in the leading leg and the lagging leg, in this case the average losses over two periods will be equal for all switches. In [45], the losses are compared between the hard switching halfbridge, soft switching halfbridge, soft switching fullbridge and semi-soft switching fullbridge converters. It was found that for a 100 kW converter, the semi-soft switching fullbridge converter has slightly higher efficiency than the soft switching fullbridge converter. The reason for this is the circulating currents and duty cycle loss caused by the auxiliary circuit used to obtain soft switching over a wide range of operating conditions.

To lower the switching losses compared to the fullbridge converter with duty cycle control, the converter is controlled by phase-shift control with capacitors connected across the switches in the input bridge as in Fig. 3.17 [5, 7, 37]. This gives lower switching losses but a more complicated control for the input bridge.

The principle of operation for the fullbridge converter with phase shift control is the same as for the converter with traditional duty cycle control. The on-state with the input voltage across the transformer is achieved by turning two switches on. The difference is the switching and the off-state, which is achieved by turning one switch off and let the load current flow through one switch and one diode. With this control method, the switching losses can preferably be lowered by the capacitors across the switches which are charged after turn-off of a device giving zero voltage turn-on switching.

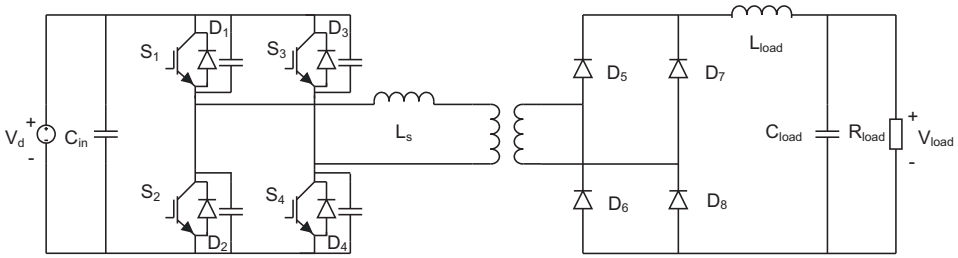

Fig. 3.17 Topology for the FB converter using phase shift control.

The voltages and currents for the switches are plotted in Figs. 3.18- 3.19. The difference between the two control schemes is how the switching is obtained, which is shown in Fig. 3.20.

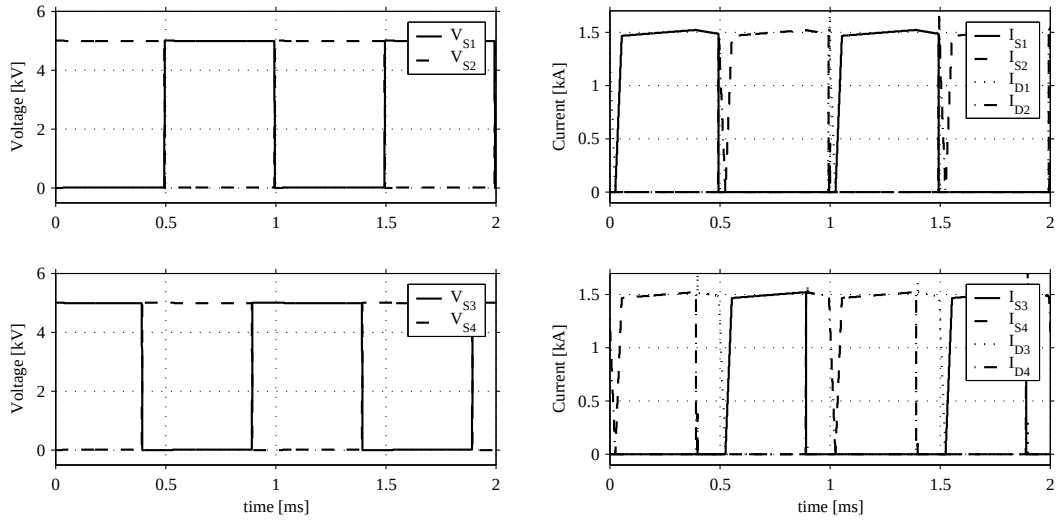

(a) Voltage for the switches.

(b) Current for the switches.

Fig. 3.18 Conditions for the switches in the 5 MW FB phase shift converter.

The switching transitions can be explained from the waveforms in Fig. 3.18- 3.19, Fig. 3.20 and the topology in Fig. 3.17. The voltage and current in the transformer are shown in Fig. 3.21 and the conduction paths during the switching are shown in Fig. 3.22.

In the passive state just before t = t_1, S_1 conducts and the load current is forced to flow through the diode D_3 as shown in Fig. 3.22 (a) since all other switches are turned off. The voltage across the transformer is therefore zero and the converter is in its passive state. Both voltages V_1 across switch S_1 and V_3 across switch S_3 are zero. The active state is initiated at t = t_1 when switch S_1 is turned off. This turn-off occurs at zero voltage since

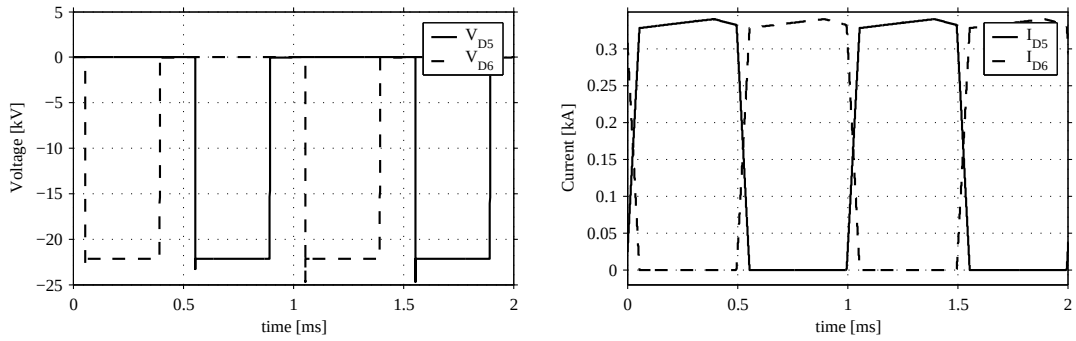

(a) Voltage for the diodes.

(b) Current for the diodes.

Fig. 3.19 Conditions for the didoes in the 5 MW FB phase shift converter.

the diode D_3 is conducting, which can be seen in Fig. 3.17. When S_1 has been turned off, the load current flows in the capacitors as shown in Fig. 3.22 (b), decreasing the voltage V_2 across switch S_2 shown in Fig. 3.20 (a). The decrease in V_2 causes a negative voltage across the leakage inductance, and a large inductance is needed to maintain enough current to charge the capacitors until V_2 = 0 [7]. When D_2 is forward biased, the current starts flowing through D_2 and D_3 which is seen in Fig. 3.22 (c), applying a negative voltage across the leakage inductance L_s. The negative input voltage is then applied across the primary side of the transformer, and there is zero voltage at the secondary side, which gives a negative voltage across the leakage inductance that makes the current in the transformer decrease. When D_2 and D_3 conducts, S_2 and S_3 are turned on at zero voltage and starts conducting when the current in the transformer decreases below zero in the interval between t = t_1 and t = t_2. Since the current in the transformer is lower than the load current, the diodes on the secondary side of the transformer are short circuited. The current in the transformer decreases until it is equal to the negative load current at t = t_2. Then the output bridge is not short circuited as seen in Fig. 3.22 (d). The voltage across the secondary side of the transformer is equal to the negative input voltage and the current stays constant until t = t_3 which is the end of the active state.

The transition from active to passive state is done by switches S_3 and S_4. In Fig. 3.20 (b), the transition from S_3 to D_4 is shown. In the active state before t = t_3, switches S_2 and S_3 are conducting as seen in Fig. 3.22 (d), giving the input voltage across the transformer. The passive state is started when S_3 is turned off at t = t_3. The voltage V_3 across S_3 is then increased until D_4 is forward biased and starts to conduct achieving the passive state shown in Fig. 3.22 (e). The current for the charging of the capacitors is provided by the filter inductance, that adjusts the voltage on the secondary side of the transformer to the same level as for the primary side in order to keep the current constant [7].

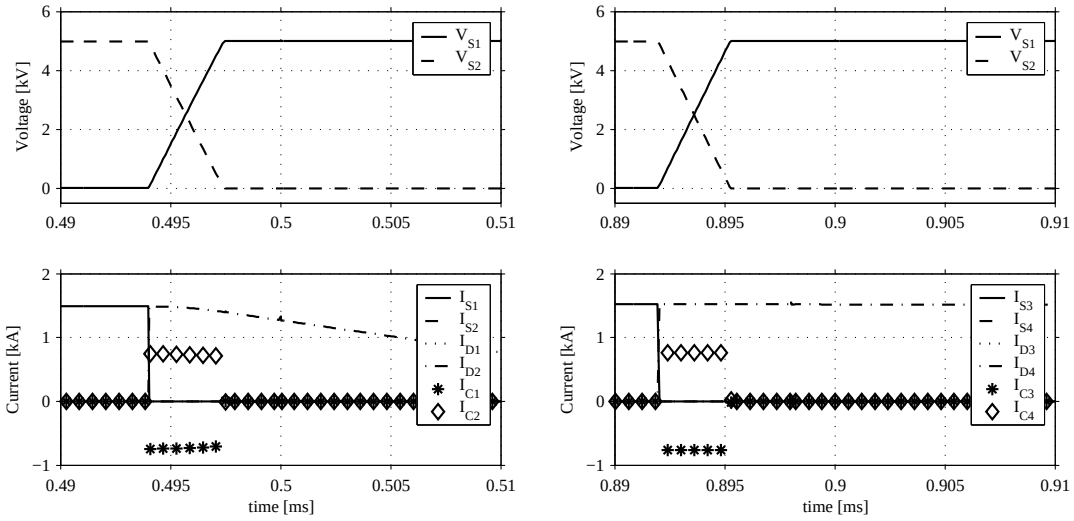

(a) Transistors 1 and 2.

(b) Transistors 3 and 4.

Fig. 3.20 Switching of the transistors in a 5 MW FB phase shift converter.

The passive state lasts until t = t_4 when S_2 is turned off and after charging the capacitor C_2 the diode D_1 starts conducting. Then S_1 and S_4 are turned on and start conducting when the current in the transformer reverses direction. At t = t_5 the current in the transformer equals the load current and the output bridge is not short circuited. At t = t_6 the active state is ended by turning S_4 off. After charging capacitor C_4, D_3 starts conducting and the passive state is achieved, which is the same as just before t = t_0.

From the transitions, it can be seen that all switching occur at soft-switching conditions. At turn-off the snubber capacitors result in a slower rise of the voltage and thereby lower losses as is shown in Section 4.1. At turn-on, the soft switching is based on that the current in the leakage inductance is large enough to charge the capacitors to the input voltage before the switch is turned on. A lower current would require a smaller capacitance or a longer delay before the switch is turned on. It can therefore be turn-on losses if the current is too low to charge the capacitors before the switches are turned on.

The output voltage for the ideal fullbridge converter using phase shift control can be calculated in the same way as for the fullbridge converter using duty cycle control where the output voltage is the input voltage multiplied with the duty cycle. Using phase shift control with a transformer with ratio 1:n, the output voltage V_{load} for an ideal converter can be calculated as

$$V_{load} = nV_d\phi, \tag{3.34}$$

where V_d is the input voltage and ϕ is the phase shift variable calculated as

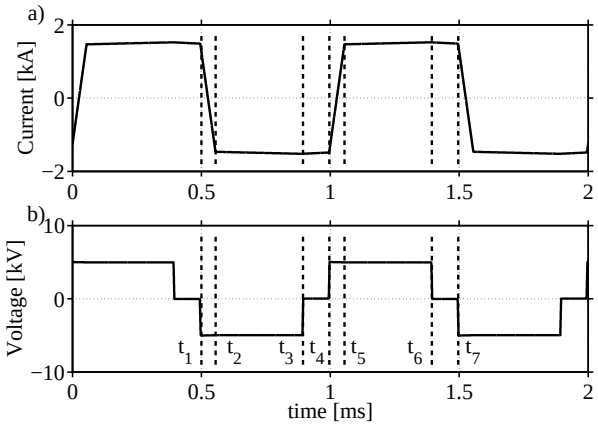

Fig. 3.21 a) current and b) voltage for the primary side of the transformer in the FB converter.

$$\phi = \frac{t_3 - t_1}{T_s/2}, \tag{3.35}$$

which basically is the time of the active phase $t_3 - t_1$ divided by the time of a half period $T_s/2$. The phase-shift variable ϕ varies between 0 and 1 and is the same as the duty cycle for the duty cycle control.

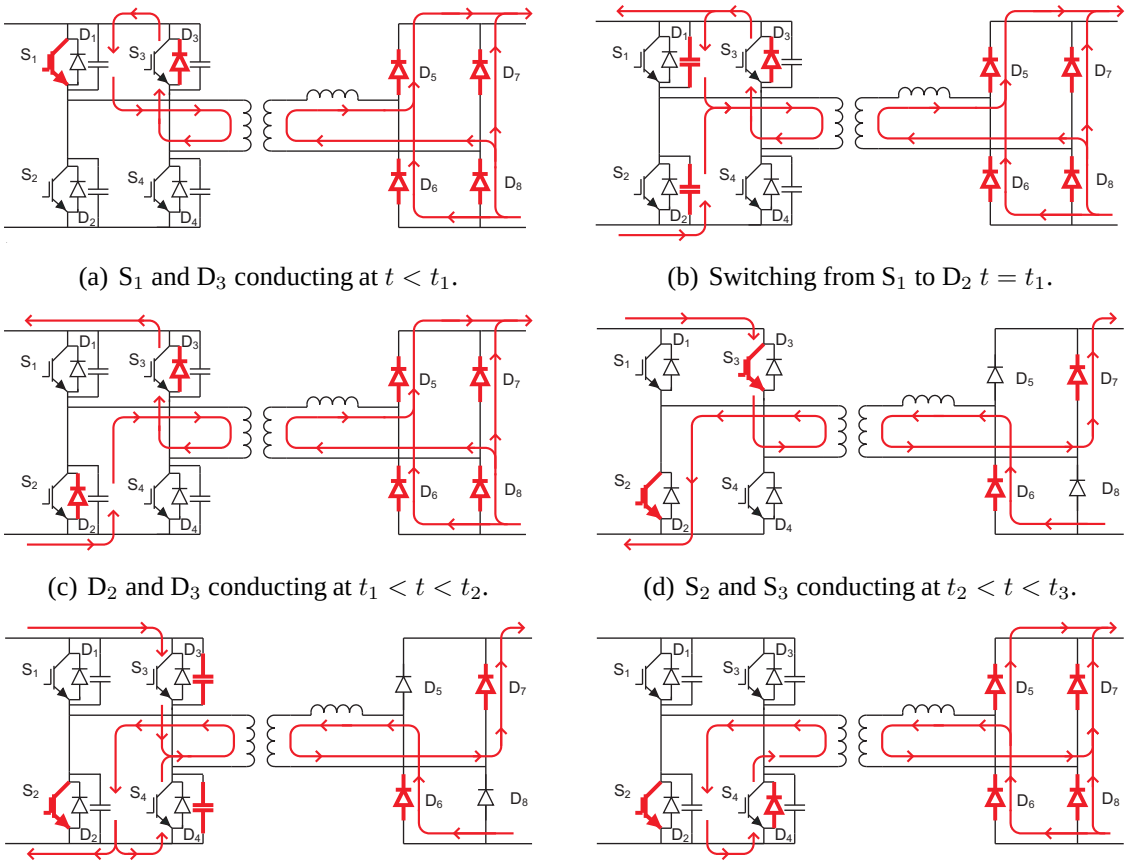

(a) S_1 and D_3 conducting at $t < t_1$.

(b) Switching from S_1 to D_2 $t = t_1$.

(c) D_2 and D_3 conducting at $t_1 < t < t_2$.

(d) S_2 and S_3 conducting at $t_2 < t < t_3$.

(e) Switching from S_3 to D_4 $t = t_3$.

(f) S_2 and D_4 conducting at $t_3 < t < t_4$.

Fig. 3.22 Conduction paths for the fullbridge converter, operating with phase shift control.

3.3 Single Active Bridge Converter

The single active bridge (SAB) converter in Fig. 3.23 looks similar to the fullbridge converter but due to the voltage stiff output it behaves differently and accordingly it is controlled in a different way [10].

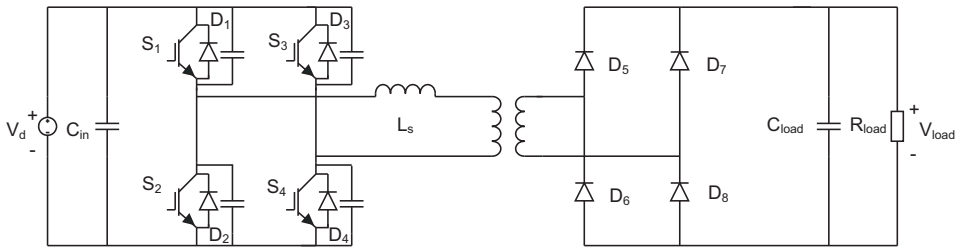

Fig. 3.23 Topology for the SAB converter.

3.3.1 Operation of the Single Active Bridge Converter

For the single active bridge converter, the output filter creates a voltage stiff output and the current waveforms in the converter are dependent on the voltage across the leakage inductance L_s of the transformer [10]. The operation of the converter is explained using the voltage and current waveforms for the switches and diodes in Figs. 3.24 and 3.25 as well as the waveforms for the transformer in Fig. 3.26 and the conduction paths in Fig. 3.27

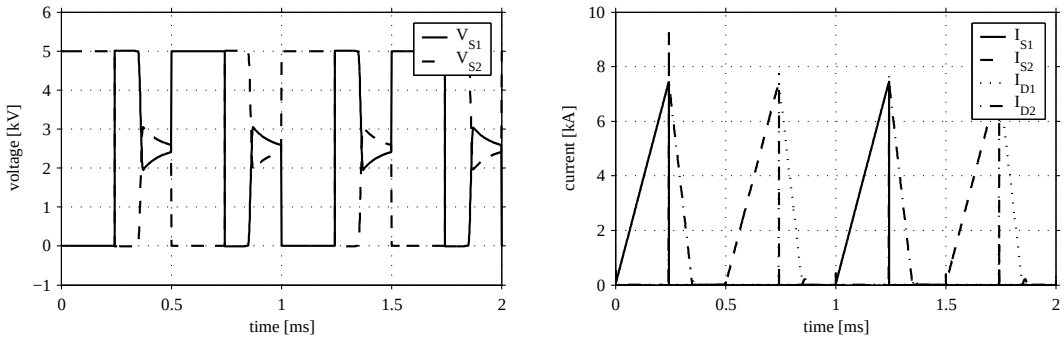

(a) Voltage for the switches.

(b) Current for the switches.

Fig. 3.24 Conditions for the switches in the 5 MW SAB converter.

In the passive state at $t < t_1$, the switches are turned off as seen in Fig. 3.27 (a) and the load current is given by the output capacitor. It can be seen in Figs. 3.24 (b) and 3.25 (b) that there is no current in the diodes or switches. The switches S_2 and S_3 in the input bridge are turned on at zero current at time $t = t_1$ which is shown in Fig. 3.27 (b). Then

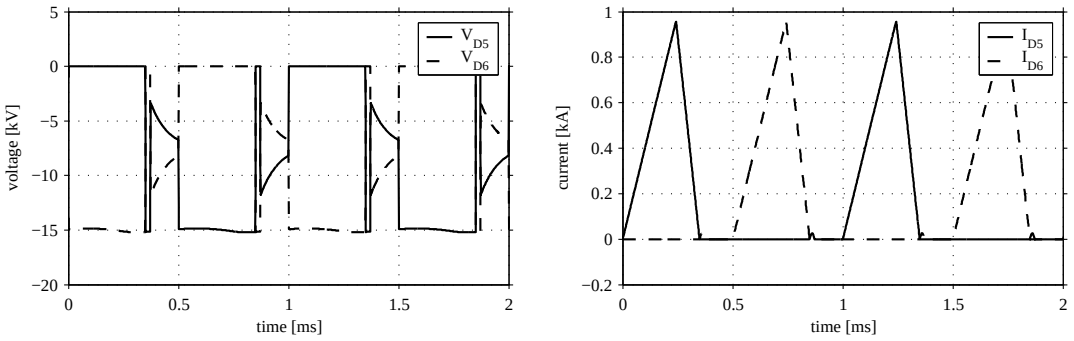

(a) Voltage for the diodes. (b) Current for the diodes.

Fig. 3.25 Conditions for the diodes in the 5 MW SAB converter.

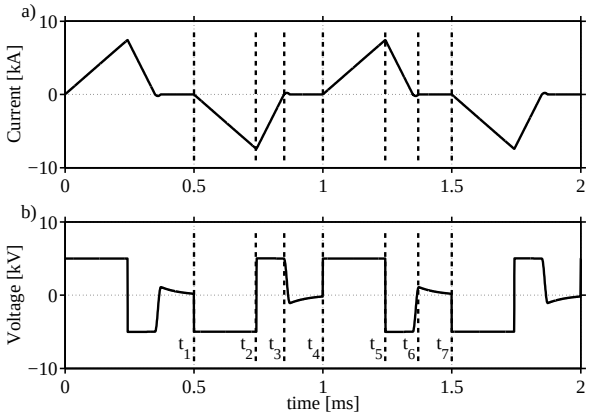

Fig. 3.26 Current and voltage for the primary side of the transformer in the SAB converter.

the transformer input voltage minus the output voltage is applied across the leakage inductance which gives an increasing current. When the current has reached its maximum value, the switches S_2 and S_3 are turned off at a high current at t = t_2. After the switches have been turned off, D_1 and D_4 starts conducting as in Fig. 3.27 (c) and the input voltage across the transformer changes polarity. This gives a reverse voltage across the leakage inductance equal to the sum of the input voltage and the output voltage. This drives the current in the leakage inductance to decrease quickly to zero at t = t_3 where the diodes stops conducting. Then there is an off-time as seen in Fig. 3.27 (d) between the current has reaches zero at t = t_3 and switches S_1 and S_4 are turned on at t = t_4. As a result, the current is increasing until S_1 and S_4 are turned off at t = t_5 and the diodes D_2 and D_3 start conducting. The current is decreased to zero at t = t_6 and is off until the next period starts at t = t_7.

For the single active bridge converter, the turn off occurs at a high current leading to

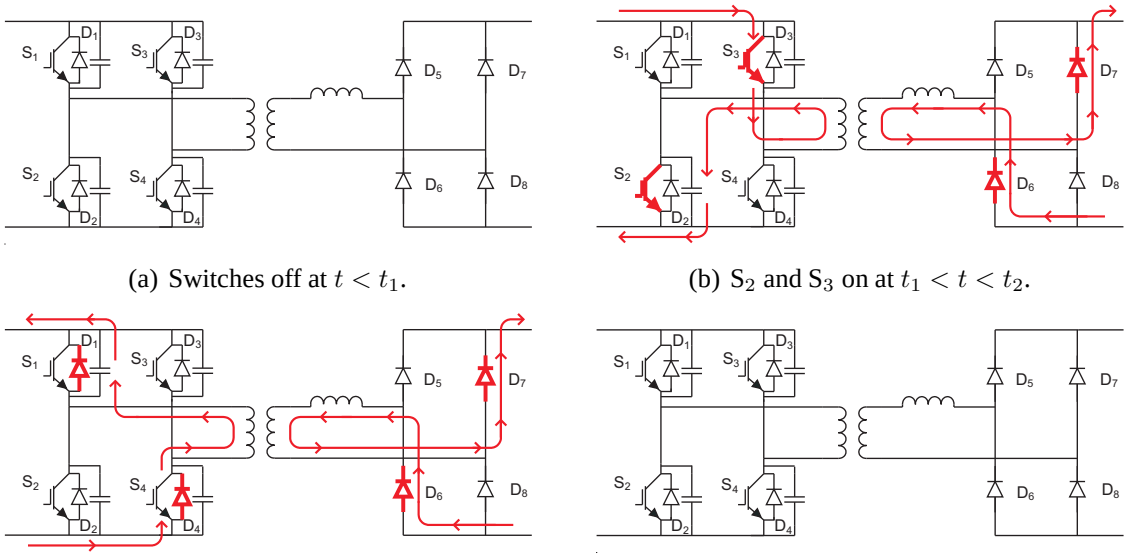

(a) Switches off at $t < t_1$.

(b) S_2 and S_3 on at $t_1 < t < t_2$.

(c) D_1 and D_4 on at $t_2 < t < t_3$.

(d) Switches off at $t_3 < t < t_4$.

Fig. 3.27 Conduction paths for the single active bridge converter.

large losses. However, a snubber capacitor is connected across the switch to lower the turn-off losses as seen in Section 4.1. At turn-on the current is zero but there is a turn-on loss resulting from the snubber capacitors if the transistor is not turned on while the freewheeling diode is conducting.

3.4 Series Parallel Resonant Converter

Another possible topology for the DC/DC converter is the series parallel resonant (LCC) converter seen in Fig. 3.28. This topology is the preferred load resonant topology since it takes advantage of the best characteristics of the parallel and series resonant converters [38].

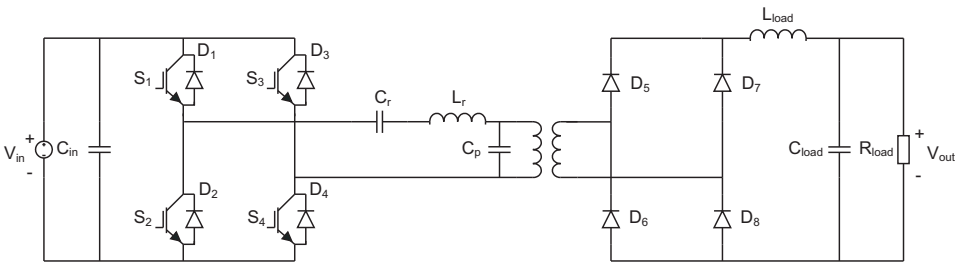

Fig. 3.28 Topology for the LCC converter.

The purpose of the resonant converter is to reduce the switching losses by switching at zero current and/or zero voltage. This is achieved by the resonant tank consisting of the inductance L_r and the capacitances C_r and C_p as shown in detail in [12]. However, there are some disadvantages with the load resonant converters. The need of a wide frequency range has made the dimensioning of passive components difficult [8], and resonant converters also have the disadvantage of a large resonant inductance and capacitance [5]. In [38], the series resonant, the parallel resonant and the series parallel resonant converters were compared. It is also stated that operation above resonance is preferred since there are no turn-on losses for the switches and no diode switching losses. The series resonant converter has a series resonant capacitor on the primary side that acts like a dc blocking capacitor and the current on the devices decrease when the load decreases. The drawbacks is that the output voltage can not be regulated for the no-load case and the output filter capacitor must carry high ripple current. The parallel resonant converter is able to control the voltage at no load by switching above resonance frequency. The main disadvantage is that the current in the switches are independent of the load and it is not suited for a converter with wide input voltage range. The series parallel converter takes advantage of the best characteristics of the series resonant and the parallel resonant converters and eliminate their main disadvantages.

3.4.1 Operation of the Series Parallel Resonant Converter

In the series parallel resonant converter, a resonant operation is created by the resonant tank resulting is a current pulse. The switches can then be turned off at zero current and

zero voltage. In this converter, the shape of the current pulse is determined by the input voltage, the output voltage and the components in the resonant tank. The amplitude and duration of the current pulse can therefore not be controlled, instead the only way to control the output is by changing the off-time between two current pulses. This resulting frequency control makes the filtering of the input and output current difficult. When the output voltage and power are high, there is a short off-time between the pulses and for this case an ”effective” filter could more easily be designed. There is a high peak-value in the output current but there is an almost continuous current. When the power level is low, there is a long off-time between the pulses as shown in Fig. 3.30, which complicates the filter design. This is an obvious disadvantage for the resonant converter at low output power. Another disadvantage is the high peak voltage across the transformer in Fig. 3.29 b), which is a result of the high peak voltage across the leakage inductance in the transformer which is a part of the resonant tank.

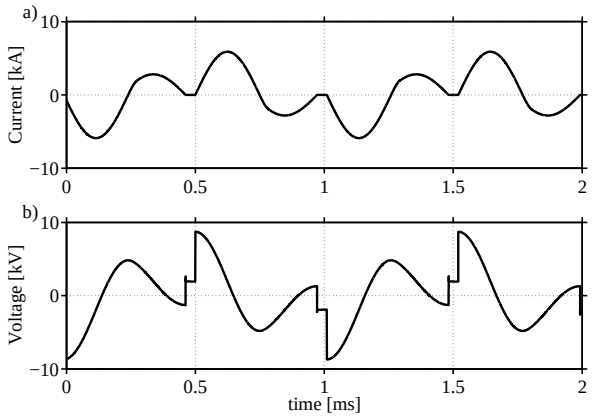

Fig. 3.29 Current and voltage for the primary side in the LCC converter.

The resonant operation starts when switches S_1 and S_4 are turned on at time $t = t_1$ as shown in Fig. 3.34 (a). The resonant tank will then create a resonant pulse that makes the current in the switches decrease to zero at $t = t_2$. In the second half of the resonant pulse, diodes D_1 and D_4 conduct as in Fig. 3.34 (b) until the current goes back to zero at $t = t_3$. There is then an off-time due to the frequency control until the second half-period starts at $t = t_4$ by turning switches S_2 and S_3 on. At $t = t_5$ the current reverses direction and D_2 and D_3 starts conducting. Then there is an off period from $t = t_6$ until $t = t_7$ where the next period starts by turning on switches S_1 and S_4.

For the resonant converter, the switches are turned of while the freewheeling diode is conducting which results in zero turn-off losses. Also the turn on losses are small due to the slow increase in the current in the resonant tank as shown in Section 4.1.

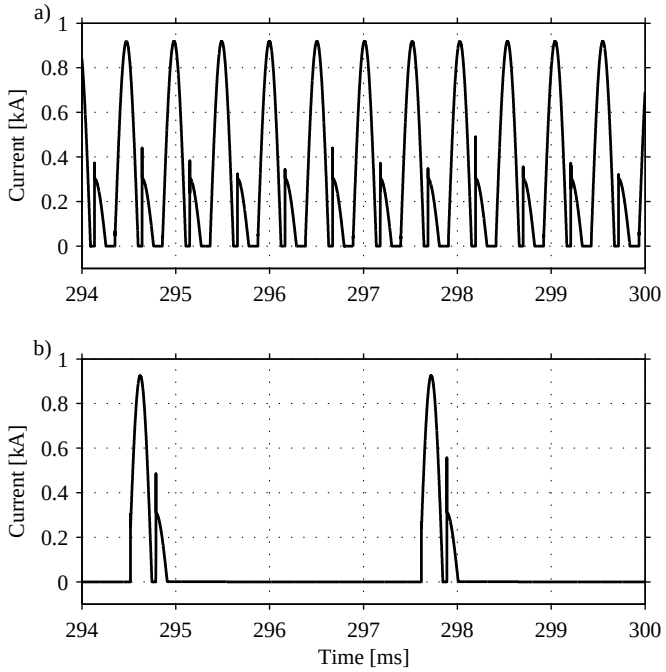

Fig. 3.30 Current to the output filter for LCC converter for position 1b for a) 12 m/s and b) 6 m/s.

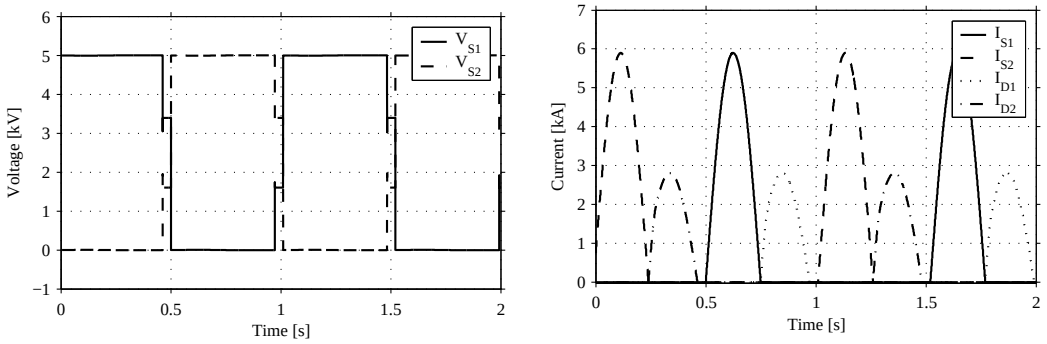

(a) Voltage for the switches.

(b) Current for the switches.

Fig. 3.31 Conditions for the switches in the 5 MW LCC converter.

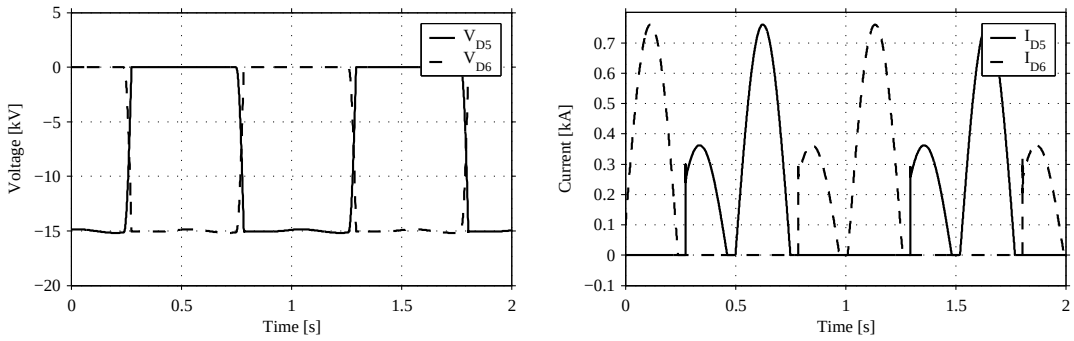

(a) Voltage for the diodes. (b) Current for the diodes.

Fig. 3.32 Conditions for the diodes in the 5 MW LCC converter.

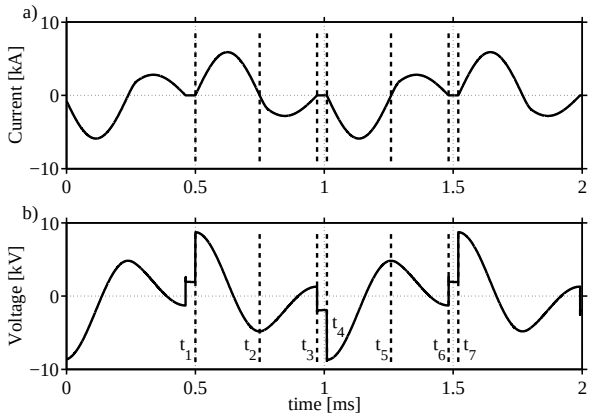

Fig. 3.33 Current and voltage for the primary side in the LCC converter.

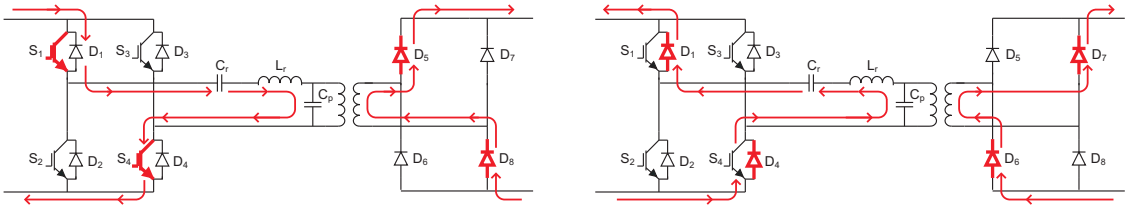

(a) S_1 and S_4 on at $t_1 < t < t_2$. (b) D_1 and D_4 on at $t_2 < t < t_3$.

Fig. 3.34 Conduction paths for the series parallel resonant converter.

Chapter 4

Loss Determination

In the previous chapter, the converters have been introduced with simulations using models with ideal switches and an ideal transformer giving basic current and voltage waveforms. These waveforms are used both for designing the components of the converter and to calculate the losses. In this chapter, the origins of the losses in the different parts of the converter are explained. The methods of loss calculations are presented in this chapter and are used in Chapter 5, where the converters are designed aiming for lowest possible total losses.

In this thesis, the focus will be on the comparison of three different topologies, and therefore the losses will be treated that vary between the topologies. The losses for the transformer and the semiconductor components are strongly dependent on the voltage and current waveforms and will be different for the three topologies. However, additional losses as losses for cooling and losses in the drive circuits will be similar for all topologies and are not included in the loss calculations. It will be shown from the experimental circuit in Chapter 6 that the main sources of the losses are the semiconductor components and the transformer.

For the semiconductor components, there are basically two ways to simulate the losses that are known and published [46, 47]. The first way is to use physics-based simulation models, which is suitable for designing new power electronics devices and converters. This procedure requires implicit integration methods, leading to increased simulation times and requires detailed knowledge of the physical dimensions of the device [48, 49]. The second way, that is used in this thesis, is to simulate the power electronic system with ideal switches and to obtain the current and voltage for these devices. Knowing the voltage and current waveforms as well as the switch design, the conduction and switching losses for the semiconductor components can be calculated using the information found either in data sheets for the components or in look-up tables based on experimental results.

4.1 Semiconductor Losses

For the semiconductor devices, all losses are calculated for a single module from the known switching conditions. Since the switches consists of a number of modules connected in series and parallel, the current and voltage are distributed to the modules. Knowing the voltage and current for one module, the losses can be obtained either from calculations or from a look-up table using measured results. The losses are then added for all modules in a switch giving the losses for the switch. The total switching losses are then obtained by multiplying the energy loss for one duty cycle with the switching frequency.

4.1.1 Conduction Losses

The conduction losses can be calculated using the on-state characteristics for the components found in the data sheets, which is the relation between the on-state voltage and current. Knowing the current in the components, the conduction losses can be calculated as the voltage multiplied with the current.

The diode Conduction Losses

The semiconductor components used in the converters are diode modules and IGBT modules. In the IGBT modules, there is a freewheeling diode connected in parallel with the IGBT, which can be seen in Fig. 4.1.

Fig. 4.1 Connection of an IGBT and a diode in a press-pack module

In the data sheet for a diode, the forward voltage V_F is shown in a graph as a function of the forward current I_F. The forward voltage V_F in the diode can be approximated as

$$V_F = A_F + B_F I_F + C_F I_F^2. \tag{4.1}$$

The power losses, P_{FC} due to the conduction in the diode are then given by

$$P_{FC} = V_F I_F = A_F I_F + B_F I_F^2 + C_F I_F^3. \tag{4.2}$$

The values for the constants A_F, B_F and C_F can be obtained from the data sheet for the diode.

The IGBT Conduction Losses

In the same way as for the diode, the on-state voltage for the IGBT, V_{CE}, can be expressed as a function of the on-state current I_C as

$$V_{CE} = A_C + B_C I_C + C_C I_C^2. \tag{4.3}$$

The conduction losses, P_{IC}, for the IGBT can be obtained by multiplying the on-state voltage and current, giving

$$P_{IC} = V_{CE} I_C = A_C I_C + B_C I_C^2 + C_C I_C^3. \tag{4.4}$$

As for the diode, the values for the constants A_C, B_C and C_C can be obtained from the data sheet for the IGBT. The mean value of the conduction losses in the IGBT as well as in the diode is given by the average of the instantaneous conduction losses over a switching cycle.

4.1.2 Diode Switching Losses

The switching losses of a pn-diode are approximately the same as the turn-off losses since the turn-on losses are negligible in comparison with the turn-off losses [43]. The energy dissipation at turn-off is depending on the charge stored during the forward conduction of the diode. At diode turn-off a part of the stored charge in the diode is removed by a reverse current I_{rr} as shown in Figs. 4.2 and 4.3, and not lost to internal recombination [12, 50]. This charge is called the recovered charge, Q_{rr}. During the reverse recovery, a negative current flows in the diode while the diode remains forward biased, which results in a high instantaneous power loss in the transistor [50].

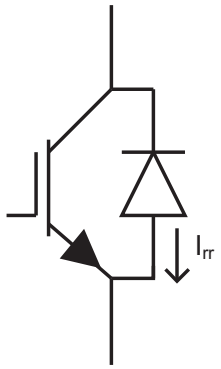

Fig. 4.2 Reverse recovery current for the diode at turn-off.

Just as the switching losses for the IGBT, the turn-off losses in the diode due to the reverse recovery can be calculated using the linearized model [47]

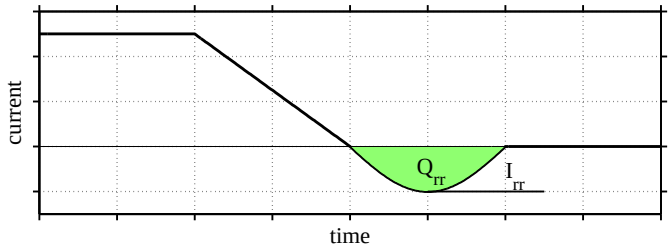

Fig. 4.3 Reverse recovery current for the diode at turn-off.

$$E_{rr} = E_{DR}\frac{V_F}{V_{ref}}\frac{i_F}{i_{ref}}. \tag{4.5}$$

For the a diode, the turn-off losses can be calculated using the information in the data sheets which gives [51]

$$E_{rr} = E_{DR}\frac{V_R}{V_{ref}}\left(\frac{A_R}{A_R + B_R} + \frac{B_R}{A_R + B_R}\frac{i_F}{i_{ref}}\right). \tag{4.6}$$

Here, E_{DR} is the switching loss at V_{ref} and i_{ref} and the values for the constants A_R and B_R can be obtained from information in the data sheet for the diode. This equation results from a linearization assuming that the diode turn-off losses are proportional to the voltage across the diode. For the diodes just as for the IGBTs, the loss calculations are done for a single module and then multiplicated to obtain the losses for the whole switch.

The losses at turn-off of the diode is depending on the charge that is not dissipated due to internal recombination but removed with the reverse recovery current. Resulting from this, a fast decrease in the forward current gives a shorter time for the charges to recombine and a large part of the charge must be removed due to reverse recovery current. On the other hand, a slower decrease in the forward current gives the charges more time to recombine leading to a lower reverse recovery current and thereby lower losses. In the data sheet for the diode [51], it can be seen that the diode switching losses decrease with a decreasing di_F/dt. A linear dependence on the derivative of the forward current is then inserted in (4.6) resulting in

$$E_{rr} = E_{DR}\frac{V_R}{V_{ref}}\left(\frac{A_R}{A_R + B_R} + \frac{B_R}{A_R + B_R}\frac{i_F}{i_{ref}}\right)\frac{di_F/dt}{di_{ref}/dt}. \tag{4.7}$$

Consequently, to calculate the turn-off losses for a diode the forward current i_F, the time rate of change of the forward current di_F/dt as well as the reverse voltage V_R must be known.

4.1.3 IGBT Switching Losses

The IGBT switching losses are calculated based on the known switching conditions obtained from the simulations. After that, the switching losses can either be calculated using a linearized equation or using values from a look-up table based on measurements. When switching an IGBT, losses occur during the switching when both the voltage and current are high. To reduce these losses, soft switching can be achieved either by a load resonant tank as for the resonant converter or by adding a snubber capacitor across the device.

Hard Switching

For the hard-switching case, the losses are known and well documented in the data sheet for the components. In Fig. 4.4, typical hard switching waveforms for an IGBT in the input bridge for a converter shown in Fig. 4.5.

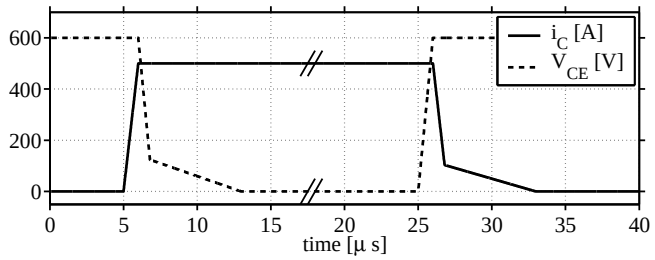

Fig. 4.4 Typical hard switching waveforms of an IGBT.

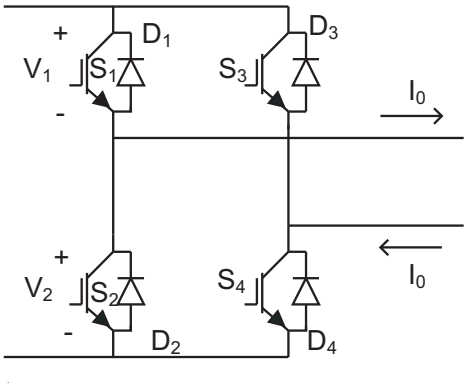

Fig. 4.5 Input bridge for a converter without snubber circuits.

Assume that the waveforms in Fig. 4.4 is for the IGBT S_1 in the input bridge in Fig. 4.5. The collector-emitter voltage V_{CE} for S_1 is equal to the voltage V_1 in Fig. 4.5. At t = 0,

S_1 is off with zero current flowing in the device. The load current I_0 is assumed to be constant and is then flowing through the diode D_2. At t = 5 μs, the device is turned on and the current is thereby increased in the device. However, since the load current is constant, the diode D_2 stays on until S_1 has taken over the entire load current. As a result, the voltage does not start to decrease until the current has reached its maximum value. This results in a high current and a high voltage at the same time and thereby a high instantaneous power loss during the switching cycle. When the device is on, the full load current flows in S_1. For turn-off, the voltage across S_1 must increase in order to lower the voltage across S_2 and forward bias the diode D_2. When D_2 is forward biased the current in S_1 start to decrease. As seen in Fig. 4.4, there is also a high instantaneous power loss at turn-off.

In the data sheet for the IGBT [52, 53], the switching losses are given as a function of gate resistance, collector current I_C and voltage V_{CE}. The calculation of the switching losses can be done with a linearized model as in [47] using

$$E_s = E_{SR}\frac{V_V}{V_{ref}}\frac{i_V}{i_{ref}}. \tag{4.8}$$

Here, E_s is the actual switching loss at current i_V and voltage V_V, and E_{SR} is the rated switching loss at the current i_{ref} and voltage V_{ref}. The total switching energy for a duty cycle is then given by

$$E_s = E_{SRon}\frac{V_V}{V_{ref}}\frac{i_V}{i_{ref}} + E_{SRoff}\frac{V_V}{V_{ref}}\frac{i_V}{i_{ref}}. \tag{4.9}$$

The reference values used in (4.8) and (4.9) are found in the data sheet for the IGBT module.

Soft Switching Using a Snubber Circuit

To lower the switching losses at turn off, a snubber circuit can be connected across the switches as in Fig. 4.6. These snubber circuits are used to lower the turn-off losses in the fullbridge converter with phase shift control and the single active bridge converter which were introduced in sections 3.2 and 3.3.

The current i_C and the voltage V_{CE} for the switch are shown in Fig. 4.7 with and without the turn-off snubber. The resulting power loss during the turn-off is shown in Fig. 4.8.

For the hard switching case, the current in the switch S_1 must reach the maximum value before the diode D_2 stops conducting and the voltage across S_1 starts to decrease. This results in high instantaneous power losses which can be seen in Fig. 4.8. In the case with snubber capacitors connected across the switches as in Fig. 4.6, the current and voltage waveforms during switching change as seen in Fig. 4.7 and it also results in a lower power

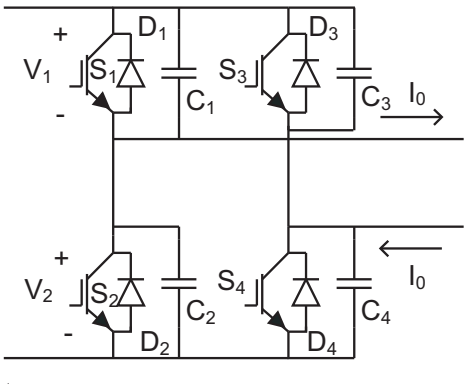

Fig. 4.6 Input bridge for a converter with snubber circuits.

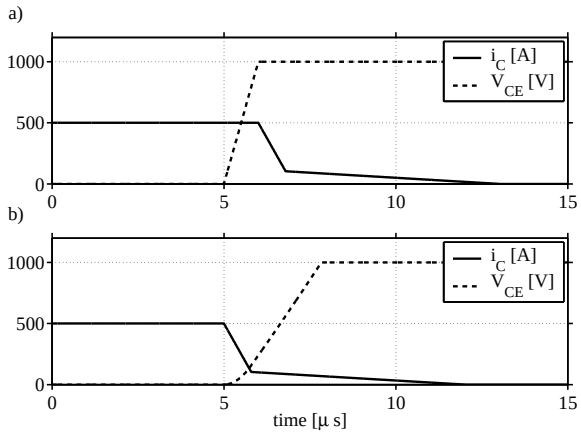

Fig. 4.7 Current and voltage during switching of an IGBT a) without snubber capacitor and b) with snubber capacitor.

dissipated in the switch at turn-off which in shown in Fig. 4.8.

When switch S_1 is turned off, the current in the device starts to decrease immediately since it can flow through capacitors C_1 and C_2. The increase of the voltage is a result of the current flowing in the capacitors. This current is the difference between the constant load current I_0 and the current in S_1. Capacitor C_1 is then charged and capacitor C_2 is then discharged until the voltage V_{CE} has reached its maximum value and the diode D_2 is forward biased and starts conducting. In Fig. 4.8 it can be seen that the maximum instantaneous power dissipation is substantially reduced. However, the total energy dissipated is still a significant part of the energy dissipated without a snubber. This is due to the tail current in the IGBT, and in the example in Fig. 4.8 the energy dissipated in the IGBT with the snubber is 30 % of the energy dissipated without the snubber.

The lossless snubber shown in Fig. 4.6 can only be used when the switch is turned on at

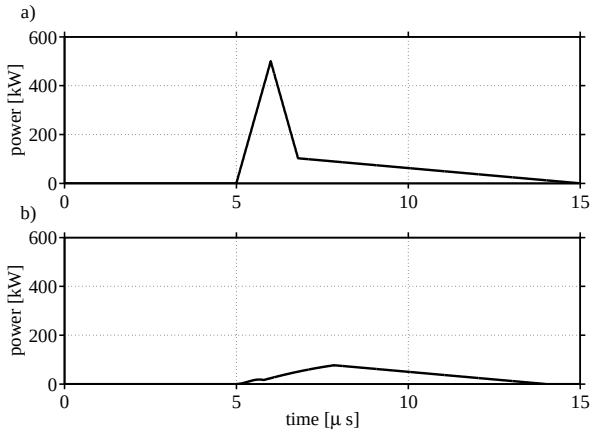

Fig. 4.8 Power loss during switching of an IGBT a) without snubber capacitor and b) with snubber capacitor.

zero voltage. If the switch is turned on at a finite voltage, the capacitor will be discharged through the switch with a very high peak current. This case requires a resistor that is connected in parallel with the diode as shown in Fig. 3.11.

Switching Losses for the Resonant Converter

In the resonant converter, the load resonant tank achieves turn-on at zero current as was described in Section 3.4. In this converter, the waveform of the current after turn-on is determined by the resonant tank seen in Fig 4.9. In Fig. 4.10, the voltage and current at turn-on of the resonant tank is shown, where the resonant current pulse has a maximum value of 1 kA and a frequency of 2 kHz.

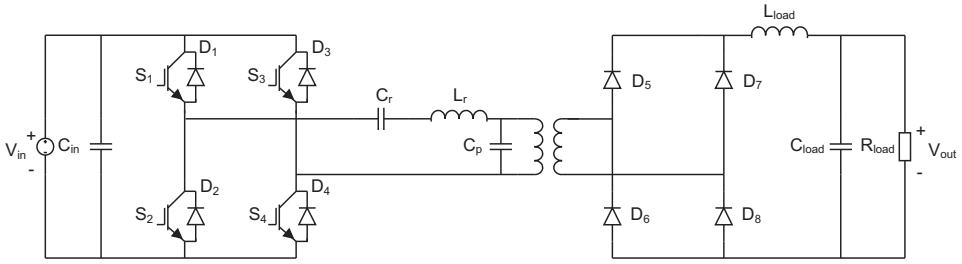

Fig. 4.9 Topology for the LCC converter.

It can be seen that the current rise time is long due to the low resonant frequency compared to the fast fall time of the voltage. These turn-on losses can be calculated by making an analytical model based on the current and voltage waveforms as presented in [54]. Starting with the turn-on losses for the transistors, the fall time of the voltage must be known as

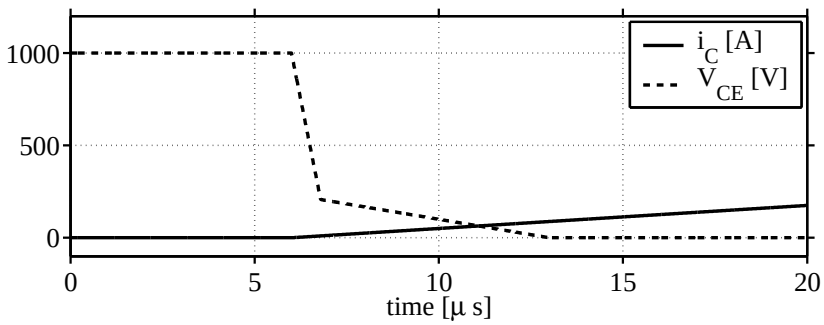

Fig. 4.10 Current and voltage during turn-on of an IGBT in a resonant converter.

well as the waveform for the current. The turn-on losses occur during the fall-time of the voltage, where the voltage across the transistor can be expressed as

$$V_{CE}(t) \approx V_d \left(1 - \frac{t}{t_{fv}}\right), \quad t < t_{fv}. \tag{4.10}$$

Where V_d is the off-state voltage across the transistor and t_{fv} is the fall time of the voltage. The current during this time interval is the start of the resonant operation that can be described by

$$I_C(t) = I_{C,peak} \sin \omega_0 t. \tag{4.11}$$

Where $I_{C,peak}$ is the peak value of the current during the resonant operation and ω_0 is the resonant frequency. The energy loss during turn-on is obtained by integrating the power loss during the fall time of the voltage, and the expression is derived in (4.12)-(4.16).

$$E_{on} = \int_0^{t_{fv}} V_d \left(1 - \frac{t}{t_{fv}}\right) I_{C,peak} \sin \omega_0 t dt = V_d I_{C,peak} \int_0^{t_{fv}} \left(1 - \frac{t}{t_{fv}}\right) \sin \omega_0 t dt \tag{4.12}$$

$$E_{on} = V_d I_{C,peak} \int_0^{t_{fv}} \sin \omega_0 t - \frac{t}{t_{fv}} \sin \omega_0 t dt \tag{4.13}$$

$$E_{on} = V_d I_{C,peak} \left[-\frac{\cos \omega_0 t}{\omega_0} - \frac{t}{t_{fv}} \frac{\sin \omega_0 t}{\omega_0^2} + \frac{t}{t_{fv}} \frac{\cos \omega_0 t}{\omega_0} \right]_{t=0}^{t=t_{fv}} \tag{4.14}$$

$$\begin{aligned} E_{on} = {} & V_d I_{C,peak} \left[-\frac{\cos \omega_0 t_{fv}}{\omega_0} - \frac{t_{fv}}{t_{fv}} \frac{\sin \omega_0 t_{fv}}{\omega_0^2} + \frac{t_{fv}}{t_{fv}} \frac{\cos \omega_0 t_{fv}}{\omega_0} \right] \\ & + V_d I_{C,peak} \left[\frac{\cos \omega_0 0}{\omega_0} + \frac{0}{t_{fv}} \frac{\sin \omega_0 0}{\omega_0^2} - \frac{0}{t_{fv}} \frac{\cos \omega_0 0}{\omega_0} \right] \end{aligned} \tag{4.15}$$

$$E_{on} = V_d I_{C,peak} \left[\frac{1}{\omega_0} - \frac{\sin \omega_0 t_{fv}}{t_{fv} \omega_0^2} \right] \tag{4.16}$$

As can be seen in (4.16), the turn-on energy in the IGBT-modules can be expressed as a function of the off-state voltage V_d, the peak resonant current $I_{C,peak}$, the fall time of the voltage t_{fv} and the resonant frequency ω_0. This equation is used to get an estimation of the switching losses in the resonant converter.

4.1.4 IGBT Properties at Soft-Switching Conditions

In a large number of high-power applications, soft switching conditions are used to reduce the switching losses either by load resonant operation or by adding snubber circuits. The behavior of the IGBT under soft switching conditions is significantly different from the behavior under hard-switching conditions [54, 55]. Most commercially available IGBTs are designed for hard-switching conditions, and the data sheets contain information about the characteristics under hard-switching conditions. However, unexpected characteristics have been found when the IGBTs are operated in a soft switching mode. Detailed investigations have shown that IGBT devices do not operate according to the data sheets under zero voltage switching (ZVS) and zero current switching (ZCS) conditions [54, 55].

Losses at Zero Voltage Turn-on

To reduce the power loss at turn on, circuits can be designed using zero voltage switching (ZVS). There is no voltage applied across the device before it is turned on, and according to the hard switched operation the switching losses should be negligible. However, at ZVS the voltage and current waveforms differ from the waveforms at hard switching conditions. Typical waveforms for ZVS turn-on are shown in Fig. 4.11. In the figure, a spike in the forward voltage drop is observed at turn-on as described in [56] and [44].

At zero voltage turn on the current initially flows in the anti-parallel diode with a certain di/dt and then transfers to the IGBT under ZVS conditions. Due to the external circuit, the current will then rise with a constant di/dt until it is turned off or kept at a constant level. When the device begins to conduct at time t_0, there is a voltage spike across the device, with an amplitude increasing with an increasing di/dt. This is due to the build up of charges in the drift region as explained in [44]. When the MOSFET has just been turned on, an electron current begins to flow into the drift region. This region is initially in low-level injection and is therefore resistive. Since the current flows through a resistive bulk, the voltage will increase linearly with the current giving the voltage spike as seen at point a in Fig. 4.11. When a current flows in the device, charges build up in the drift region until the entire drift region is in high-level injection at point b. After this point, the resistance decreases dramatically and the forward voltage falls even though the current is

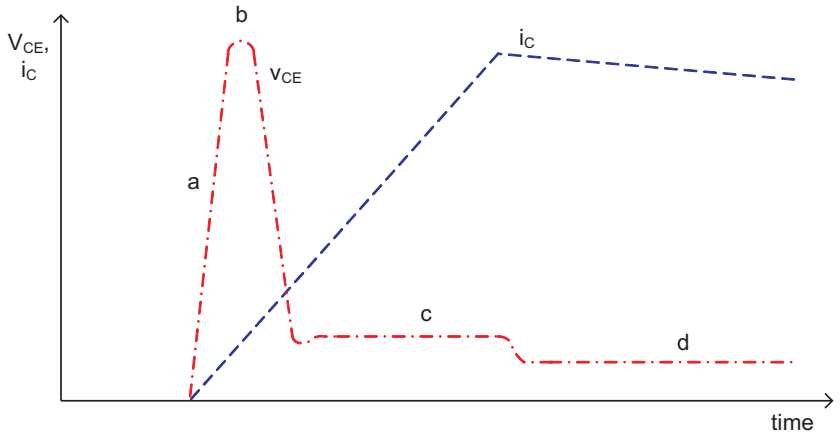

Fig. 4.11 Typical turn-on voltage and current for ZVS of an IGBT

still increasing. Finally, the voltage settles at a value needed to maintain the charge build-up in the drift region and the device is in dynamic saturation. The peak of the overshoot is dependent on di/dt, but the time to reach the peak of the over-shoot does not change significantly [44]. When the current increases further after high-level injection has been reached at c, additional charges are provided with a finite time delay associated with the life time τ_c. This is called the conductivity modulation lag and is the difference between the dynamic saturation voltage when the current is increasing and the voltage at d corresponding to the same current in the static I-V characteristics. The overshoot for the voltage at turn-on can then be divided into two parts. The first part is the voltage spike that occur before high-level injection has been reached and the voltage drop is due to the resistive drift region. The second part is the increase in voltage due to the conductivity modulation lag, when there is a high-level injection and the current is increasing.

For hard-switching, the entire off-state voltage appears across the device when it has just been turned on. As high-level injection builds up in the drift region, the voltage decays exponentially. In this hard-switching case, the turn-on time is much shorter than for the soft-switching [44].

Losses at Turn-off

During hard switching turn-off, a large power spike occur when the voltage increases rapidly while the device is carrying a significant current. When the snubber capacitor is added, the voltage is forced to increase slowly so that high voltage and high current do not occur at the same time. This gives significantly lower switching losses [56], and the resulting waveforms for the current and voltage are shown in Fig. 4.12.

On the other hand, there are some unwanted results from the snubber capacitor described

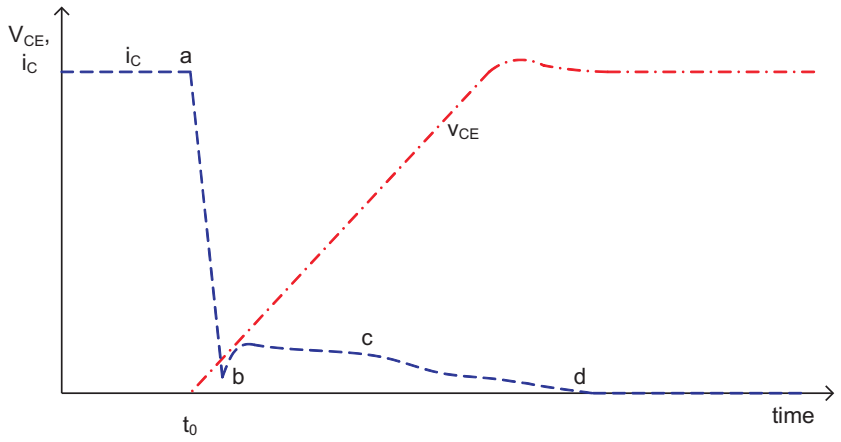

Fig. 4.12 Typical turn-off voltage and current for an IGBT with a snubber capacitor.

in [56, 44]. During turn-off, the current waveform shows a tail current ”bump”. That is a result of inadequate charge removal from the drift-region, where the carriers are not swept out but have to recombine. At soft-switching conditions, the turn-off losses occur mostly due to this tail current. It is shown that a device with shorter carrier life time will have lower turn-off losses since the excess carriers will recombine faster and thereby the current will decrease faster.

The reason for the tail current ”bump” is described in detail in [44]. At hard-switched turn-off, the gate voltage is cut off when a current is flowing in the device. To support the current, the voltage across the device rises and the current is still flowing in the device until the diode has been turned on. This results in a large power loss that can be controlled by connecting a snubber capacitor across the device. Also, the capacitor provides an alternative path for the current when the device current drops. The capacitor provides a ramping up of the voltage while turning off.

At point a in Fig. 4.12, which is the start of the transition, the device is operating in its on-state. When the device is on, the emitter and base of the BJT are shorted, resulting in a voltage drop across the junction between the bipolar base and the emitter. When the device is turned off, the MOS channel shuts off resulting in zero base current for the bipolar transistor. The current is then rapidly decreased to point b where the current in the MOSFET is zero as well as the base current for the BJT. In the high-level injection region, the current is dominated by diffusion at the ends and drift in the central region where the electric field is maximum. When the MOS channel has been turned off, all applied voltage appears across the MOSFET and thereby will the base-emitter bias for the BJT be reduced, the current in the emitter will also drop to zero and the rest of the current will flow in the snubber capacitor. When current flows in the snubber capacitor, the voltage across the device will rise. This voltage increase will cause an electric field to build up in

the wide base. A current will then start to flow with electrons flowing towards the IGBT drain and holes towards the IGBT source. The current together with the recombination of holes and electrons will cause the concentration of excess carriers to decrease, which is given by the continuity equation. At the same time as the excess carriers decrease, the voltage across the device increases and thereby also the electric field. This results in two conflicting mechanisms, the rising electric field and the reduction of the excess carrier concentration. As a result, there is a maximum in the product of carrier concentration and electric field giving the tail current "bump" at point c. After the maximum value the tail current falls to zero with time until point d. The charge in the tail current changes with the value of the snubber capacitor. If the value of the capacitor is large, it takes longer time for the electric field to build up in the device and therefore more excess carriers recombine and do not leave the device in the tail current.

For hard-switching conditions, the dv/dt is larger resulting in an increased electric field. Then the excess electrons and holes are swept out more rapidly into the collector and emitter contacts, and the tail current "bump" is lower.

On-state Losses

The forward conduction voltage drop can be changed by varying the carrier life time τ_c, where an increase in τ_c results in a decrease in V_{CE} as well as the resistivity of the drift-region [56]. Also, the buffer layer affects the conductivity of the IGBT. The increased built-in junction potential due to the n^+ buffer layer results in a less efficient hole injection.

4.2 Transformer Losses

For the transformer losses, the losses include both losses P_w in the winding and losses P_{core} in the core. The losses in the windings are calculated from the rms-currents I_{pri} in the primary winding and I_{sec} in the secondary winding and the resistances R_{pri} and R_{sec} of the transformer windings together with the ac resistance coefficients $K_{ac,pri}$ and $K_{ac,sec}$ shown in (3.10)-(3.12) using

$$P_w = P_{w,pri} + P_{w,sec} = R_{pri}K_{ac,pri}I_{pri}^2 + R_{sec}K_{ac,sec}I_{sec}^2. \tag{4.17}$$

The iron losses are obtained from the volume of the core V_{core}, the switching frequency f_{tr} and the peak value of the magnetic flux B_{max} using (4.18)

$$P_{core} = K_1 f_{tr}^{K_2} B_{max}^{K_3} V_{core}. \tag{4.18}$$

The constants K_1, K_2 and K_3 are obtained from the material in the core. As an example, for the POWERLITE® inductor core from Metglas®, the losses in the core can be calculated as

$$P_{core} = 6.5 f_{tr}^{1.51} B_{max}^{1.74} m_{core}. \tag{4.19}$$

The losses P_{core} are in [W], the frequency f_s in [kHz], the flux B in [T] and the weight m_{core} of the core in [kg] [57]. For non-sinusoidal current and voltage waveforms, the core losses are given by using the equivalent frequency f_{eq}

$$P_{core} = \frac{1}{\tau} K_1 f_{eq}^{K_2 - 1} (B_{max})^{K_3} V_{core}, \tag{4.20}$$

as shown in Section 3.1.1.

Chapter 5

Design for the DC/DC Converters as Wind Farm Components

For the design of the DC/DC converters as wind farm components, the operating conditions must be known for the converters in the DC-based wind farm. In this chapter, a local wind turbine grid with five wind turbines is introduced which can be seen as a part of a large wind farm. Starting from the output from a single wind turbine, the operating conditions for the converters are lined out using different control strategies for the voltage levels in the local grid.

For all three topologies introduced in Chapter 3, a converter is designed for each position in the local wind turbine grid as specified in Table 5.1. The switching frequency is set to 1 kHz, and suitable modules for semiconductor components are chosen that are connected in series and parallel to reach the needed current and voltage ratings. The design considerations for these converters will be discussed and a suitable design will be chosen and used for the loss calculations. As a result, the losses for the different topologies will be presented both as a function of the wind speed and as a mean value for different average wind speeds. Further, the different control strategies will be compared both regarding the energy efficiency and the contribution to the energy production cost.

5.1 Operating Conditions in the DC-based Wind Farm

As stated above, the operating conditions must be known for the investigation of DC/DC converters in a DC wind farm. The level of the DC output voltage from a wind turbine depends on the rectifier. If a diode rectifier is used, the voltage varies with the wind speed while if an IGBT rectifier is used the voltage can be constant for all wind speeds as seen in Fig. 5.2 b). For all cases, the output voltage of the DC wind farm should be constant, which is obtained by adjusting the voltage levels with the DC/DC converters if needed in the DC grid system. In addition, the power flowing through the converters varies strongly

with the varying wind speed.

5.1.1 Wind Turbine with a DC-Output

The wind turbine with a DC-output differs only in the electrical system compared to the standard full power converter variable speed wind turbine with an AC-output, as can be seen in Fig. 5.1, where the block diagram for the wind turbine with a DC-output is shown. Compared to the standard system the inverter towards an internal AC-network has been removed and replaced with a DC/DC converter. The mechanical system consists of the main shaft and a gear box or only the main shaft if a low speed generator is used. The generator is here assumed to be a synchronous generator, since the rectifier is assumed to be a diode rectifier. If instead an IGBT rectifier is used, it would be possible to use an asynchronous generator and then achieve a constant output voltage from the rectifier for all wind speeds. The DC/DC converter in the wind turbine is used as a DC transformer to increase the rectified voltage to a level suitable for the local wind turbine grid.

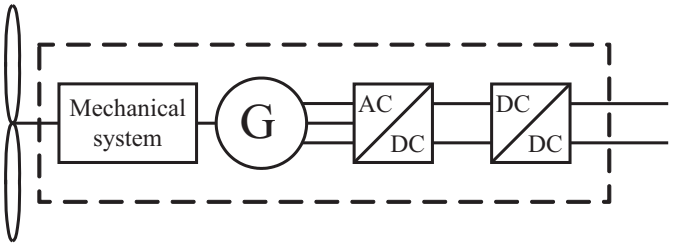

Fig. 5.1 Block diagram of the wind turbine with a DC-output.

Rectifier Output

The output from the rectifier depends on the wind speed, the type of generator and the control strategy. In this thesis it is assumed that the turbine is operated as a variable speed wind turbine. This means that for low wind speeds, the ratio between the wind speed and the rotational speed of the turbine is kept constant. The ratio is kept constant until rated speed of the turbine is reached, after this the speed is kept constant. The rotational speed is adjusted according to the wind conditions to convert as much wind energy into mechanical (shaft) energy as possible. In Fig. 5.2 a) the output power from the rectifier is shown. For this turbine, the cut-in wind speed is 4 m/s and the rated rotational speed is reached at 10 m/s.

Since the synchronous generator is connected to a diode rectifier in Fig. 5.2 a), it is assumed that the output voltage of the rectifier is proportional to the speed of the generator. The voltage is assumed to be 2 kV at 4 m/s and 5 kV at 10 m/s which can be seen in

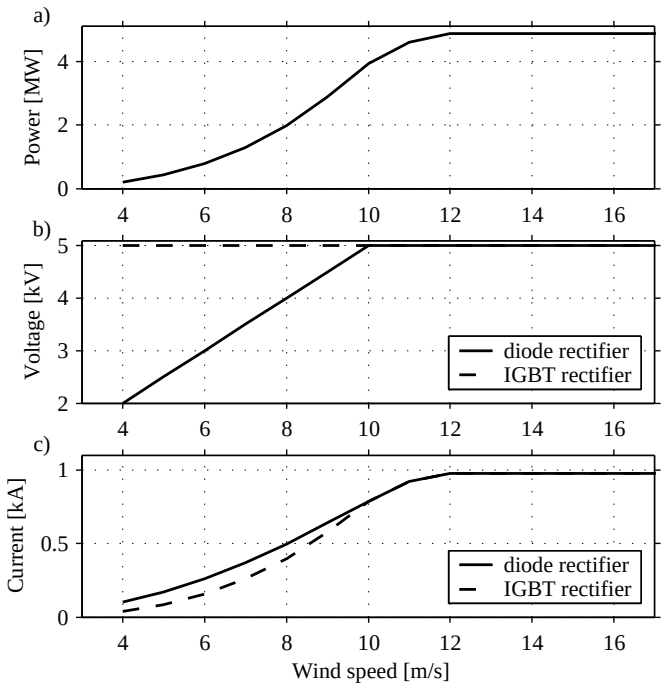

Fig. 5.2 Output from the wind turbine rectifier. a) power, b) voltage and c) current.

Fig. 5.2 b). In the case of a rectifier using IGBTs, the output voltage level can be adjusted by the rectifier to be constant 5 kV instead of the varying level, which is shown in Fig. 5.2 b).

Average Power Loss Calculation

For the evaluation of the different DC/DC converters and control strategies, the average power loss for the systems will be used. The average power losses or the expected power losses can be calculated as

$$P_{loss,avg} = \int_0^\infty f(\omega_w) P_{loss}(\omega_w) \mathrm{d}\omega_w \tag{5.1}$$

where $f(\omega_w)$ is the probability density function for the wind speed and $P_{loss}(\omega_w)$ is the losses as function of the wind speed, ω_w. As shown in Chapter 2, the probability distribution is then given by the average wind speed as

$$f(w) = \frac{\pi \omega_w}{2\bar{\omega}_w^2} \exp\left[-\frac{\pi \omega_w^2}{4\bar{\omega}_w^2}\right]. \tag{5.2}$$

The average wind speed varies between different locations, average values of 7.2 m/s and 5.4 m/s have been measured at two different sites in Sweden [24], which here are considered to be a medium and low wind speed sites. At the wind farm Horns Rev at

the Danish west coast, the average wind speed is as high as 10 m/s [25]. The probability distributions for these different average wind speeds are shown in Fig. 5.3.

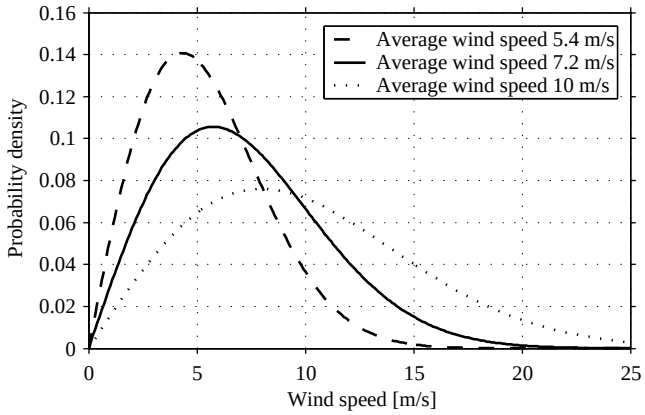

Fig. 5.3 Probability distribution for the wind speed.

5.1.2 Design Considerations for the Local Wind Turbine Grid

In Fig. 1.1, it was seen that the turbines are connected in different steps. First a group of turbines are connected to a DC/DC converter, then this group is connected to other groups and further until all turbines have been connected and the transmission voltage has been achieved.

Starting from a single wind turbine, the output from the rectifier is a relatively low DC voltage which varies with the wind speed. In a wind farm, the wind speed can vary between the turbines, resulting in different output voltages from the rectifiers. In the turbine itself, the DC voltage is transformed to a higher voltage level by the DC/DC converter in the wind turbine. The wind turbine is connected in parallel with other turbines, resulting in the same output voltage for all wind turbines in the group. The voltage for the group is then transformed to a higher level by the next DC/DC converter. From there, the last DC/DC converter raises the voltage to the transmission level for the HVDC connection.

The output voltage of the rectifiers in the turbines, which vary with the wind speed and thus varies between wind turbines, should be adjusted to one common level for the HVDC transmission. This could be done in a number of ways, resulting in different demands for the DC/DC converters. In this thesis two different control strategies are evaluated for the generating system consisting of a synchronous generator with a diode rectifier, control strategy 1 and 2. In control strategy 1 the DC/DC converters in the wind turbines handles all voltage variations. In control strategy 2 the DC/DC converters in the wind turbines only handles the variations between the wind turbines in the same group and the group DC/DC

converter handles the variations between the groups. Further, the case with an IGBT rectifier with a constant output voltage is also investigated, here called control strategy 3.

Another option could be to remove the DC/DC converter in the wind turbine and thereby force the output voltages from the wind turbine rectifiers within a group to have the same voltage. The voltage variations then have to be handled by the upstream DC/DC converters.

Control Strategy 1

The first control strategy is that each wind turbine will give a constant output voltage independent of the wind conditions. All voltage variations will be taken up by the first converter, and the group DC/DC converter can then have a fixed input and output voltages. In Fig. 5.4 one group of wind turbines is shown together with the voltage and power levels.

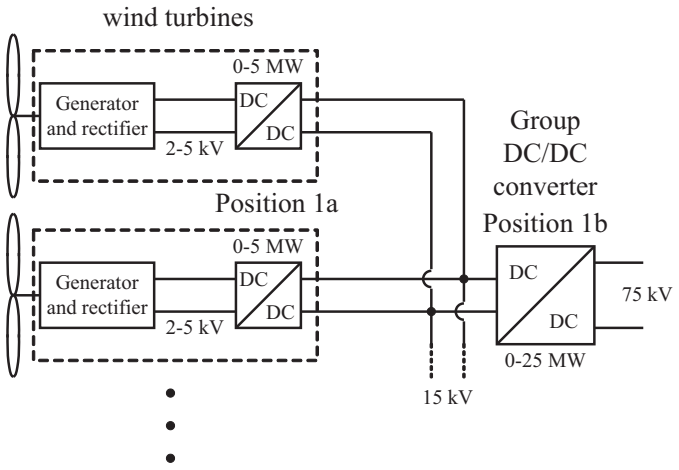

Fig. 5.4 One group of wind turbines and the voltage and power levels for control strategy 1.

From the figure it can be seen that the voltage from the rectifier varies between 2 and 5 kV. In this case, all voltage variations should be handled by the first DC/DC converter. Assuming that the DC/DC converter can just be used as a step-down converter apart from the fixed voltage ratio in the high-frequency transformer, the transformer must be designed for the minimum input voltage and the maximum output voltage. For higher input voltages, the DC/DC converter lowers the transformation ratio. The range of voltage transformations, apart from the transformer ratio, for the wind turbine DC/DC converter is 1:1 to 1:0.4 and for the group DC/DC converter 1:1. Since all voltage variations are taken care of for each individual turbine, there is no need to consider the variations in wind conditions between the turbines. As can be noted, this control strategy needs a DC/DC converter

with a wide transformation range for the wind turbine, and one with fixed transformation range for the group converter.

Control Strategy 2

The second strategy is to adjust the voltage level of the turbines to a common variable voltage level, which then is adjusted by the group DC/DC converter to the fixed output voltage. In Fig. 5.5 one group of wind turbines is shown as well as the voltage and power levels used.

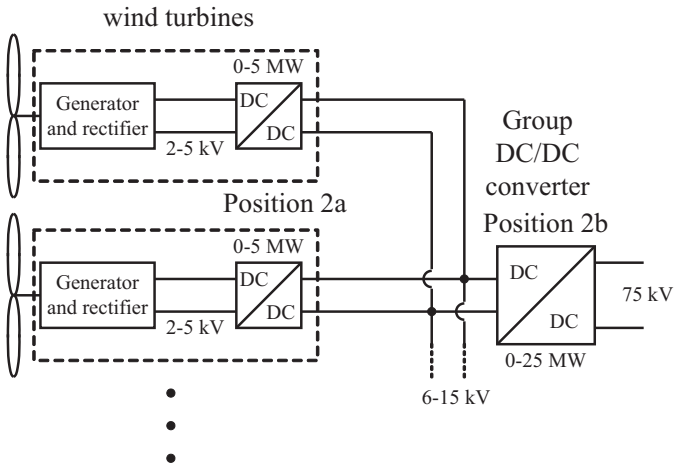

Fig. 5.5 One group of wind turbines and the voltage and power levels for control strategy 2.

In this control strategy, the first converter has constant ratio between in the input voltage and the output voltage except for the adjustment in the case of different wind speeds for the different turbines. The adjustment of the voltage levels from the different turbines does not need any special design considerations for the DC/DC converter in the wind turbine. The output voltage is proportional to the input voltage and the ratio of the converter is 1:1 excluding the transformer ratio. If the voltage levels are different for the different turbines, the duty cycle can be lowered for the turbines with highest output voltage. For the group DC/DC converter, the voltage variations that must be handled is the same as for the wind turbine DC/DC converter in the previous control strategy, which is between 1:0.4 and 1:1. As can be noted this control strategy needs a DC/DC converter with a lower transformation range for the wind turbine DC/DC converter, but a wide range group DC/DC converter.

Control Strategy 3

The third control strategy is when a wind turbine with a constant output voltage is used as shown in Fig. 5.5.

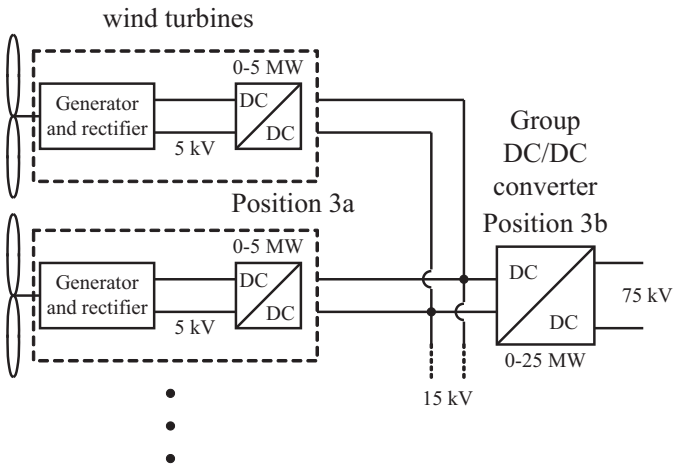

Fig. 5.6 One group of wind turbines and the voltage and power levels for control strategy 3.

As seen in the figure, all DC/DC converters have fixed voltage levels in control strategy 3, and the range of voltage transformations, apart from the transformer ratio, is 1:1 for both the wind turbine converter and the group converter.

Summary of the Control Strategies

For the three control strategies shown in Figs. 5.4, 5.5 and 5.6, the resulting demands for the DC/DC converters in different positions are summarized in Table 5.1. Position 1a is in the wind turbine and position 1b is for the group of turbines in control strategy 1. Similarly, positions 2a and 2b are in the turbine and for the group of turbines in control strategy 2 and the same applies for control strategy 3.

Table 5.1: Operating conditions for the converters.

Converter	Input voltage	Output voltage	Input power
Position 1a	2-5 kV	15 kV	0.2-5 MW
Position 1b	15 kV	75 kV	1-25 MW
Position 2a	2-5 kV	6-15 kV	0.2-5 MW
Position 2b	6-15 kV	75 kV	1-25 MW
Position 3a	5 kV	15 kV	0.2-5 MW
Position 3b	15 kV	75 kV	1-25 MW

Note that the operating conditions for positions 1b and 3b are identical and the converters will therefore have the same design. Further, it can be noted that the output voltage from the local wind turbine grid is not high enough to be used in an HVDC transmission. To achieve a complete grid system for a wind farm, an additional step is needed with a DC/DC converter to achieve the transmission voltage as seen in Fig. 1.1. This DC/DC converter could be an up-scaled version of the DC/DC converters studied in this thesis.

5.2 Choice of Material and Components

In the design and loss calculations of the converters, the properties of all the components have to be known. In Chapter 4, the calculation of the losses for the converters are presented. However, for obtaining results, specific materials and components must be chosen. In this section, the choice of components and materials used in this thesis will be presented along with its characteristics and parameters.

5.2.1 Choice of IGBT and Diode Modules

As a part of the converter design, the switches must be designed including the number of series- and parallel connected modules as well as the design of snubber circuits. Since the voltage level will be high for the switches in the input bridge, 5 kV for the converter for a wind turbine and 15 kV for the group converter, a number of IGBT modules must be connected in series. Also the current is high, which then requires a number of IGBT modules connected in parallel. This could be done with the StakPak^{TM} modules from ABB, where the chosen IGBT module 5SNR 20H2500 has a rated voltage of 2500 V and a rated current of 2000 A [52]. For the hard-switching case loss data is available, but unfortunately there is no loss data available for this IGBT during soft-switching conditions.

Another option for the IGBT switches is an IGBT from Eupec, the FF200R33KF2C IGBT module with rated voltage 3300 V and rated current 200 A. For this component, data for losses during hard-switching is found in the data sheet [53] and data for switching losses during soft-switching conditions are found in [58]. Further, it is assumed that it is possible to make a single module of 10 parallel connected Eupec IGBT, which then has the same rated current as the ABB module.

A comparison of the two IGBT modules are found in Table 5.2. Here, the ABB module is the 5SNR 20H2500 StakPak^{TM} and the Eupec module is a module of 10 parallel connected FF200R33KF2C IGBT.

As seen in the comparison in Table 5.2, there is a difference between the losses for the two IGBT modules. The ABB module has higher switching losses than the Eupec module but

Table 5.2: Comparison between the ABB and Eupec IGBT modules.

Value	ABB module	Eupec module
$V_{CE,max}$	2.5 kV	3.3 kV
$I_{C,max}$	2 kA	2 kA
E_{on}, 1.25 kV, 2 kA	4.0 J	2.53 J
E_{off}, 1.25 kV, 2 kA	3.6 J	1.77 J
P_c, 2 kA	4.4 kW	8 kW
P_c, 1 kA	1.8 kW	3 kW

has lower conduction losses. Therefore, the ABB module is preferred for lower switching frequencies while the lower switching losses of the Eupec module is advantageous for high switching frequencies.

For the rectifying diode bridge, the ABB StakPak$^{\mathrm{TM}}$ diode module 5SNF 20H2500 is used with maximum voltage 2.5 kV and rated current 2 kA.

5.2.2 Losses for the IGBT and Diode Modules

The conduction losses P_C for both the IGBTs and the diodes are given by

$$P_C = V_C I_C = A_C I_C + B_C I_C^2 + C_C I_C^3 \tag{5.3}$$

as shown in Chapter 4. The conduction losses is a function of the current I_C in the device and the constants A_C, B_C and C_C obtained from the relation between V_C and I_C in the data sheets for the components [52, 51, 53]. The values for the constants are presented in Table 5.3 for the ABB IGBT module 5SNR 20H2500 (”ABB diode in” and ”ABB IGBT”), for the ABB diode module 5SNF 20H2500 (”ABB diode out”) and for the Eupec IGBT module FF200R33KF2C (”Eupec diode in” and ”Eupec IGBT”). Note that the conduction losses for the Eupec diode and IGBT should be calculated for the assumed module with 10 FF200R33KF2C components connected in parallel.

For the switching losses, is was shown in Chapter 3 that the turn-on losses are negligible compared to the turn-off losses for the fullbridge converter and the single active bridge converter. For these converters, the turn-off losses for the IGBT modules are reduced by using snubber capacitors connected across the devices as shown in sections 3.2 and 3.3, using the topology of the snubber circuit shown in Section 3.1.5. On the other hand, these capacitors must be discharged before the device is turned on. If this is not done, the ca-

Table 5.3: Constants for calculations of conduction losses in the semiconductor devices.

Component	A_C	B_C	C_C
ABB diode in	1.047	$4.94 \cdot 10^{-4}$	$-3.64 \cdot 10^{-8}$
ABB IGBT	1.030	$9.13 \cdot 10^{-4}$	$-3.70 \cdot 10^{-8}$
Eupec diode in	0.860	$1.25 \cdot 10^{-3}$	$-1.30 \cdot 10^{-7}$
Eupec IGBT	1.140	$1.68 \cdot 10^{-3}$	$-1.38 \cdot 10^{-7}$
ABB diode out	1.047	$4.94 \cdot 10^{-4}$	$-3.64 \cdot 10^{-8}$

pacitor is discharged through the IGBT and adds losses to that component. For the series parallel resonant converter, the switching losses are negligible if all switchings occur under zero voltage and/or zero current conditions. For the hard-switching turn-off losses, the values in the data sheet for the component can be used for the loss calculations. However, the calculation of turn-off losses when a turn-off snubber capacitor is used to reduce the losses, needs to be investigated more carefully.

The basic principle of the snubber capacitor to increase the rise time of the voltage at turn-off was shown in Sections 4.1.3. However, as mentioned in Section 4.1.4, the switching losses for soft-switching conditions are hard to predict. Therefore, the most accurate way for calculating these losses is to use data from measurements of losses during soft switching of the IGBT. Results from such measurements are available in [58]. From the measured data, it was assumed that the switching losses are proportional to both current and voltage, but the constant is different for the different snubber values. From Section 4.1, the equation to calculate the turn-off losses during hard-switching is given by

$$E_{s,off} = E_{SRoff} \frac{V_V}{V_{ref}} \frac{i_V}{i_{ref}}, \tag{5.4}$$

where the energy dissipated at turn-off $E_{s,off}$ is a function of the voltage V_V and the current i_V at turn-off. The reference values E_{SRoff}, V_{ref} and i_{ref} are given in the data sheet of the component. In this case, the same equation is assumed to be valid for snubbered turn-off, even though the value of E_{SRoff} changes with the value of the snubber capacitor. From the measured results presented in [58], the values of E_{SRoff} are presented in Table 5.4 for V_{ref} = 1800 V and i_{ref} = 2000 A.

In the simulations and loss calculations of the converter topologies, the Eupec IGBT module with rated current 2 kA consisting of 10 FF200R33KF2C modules connected in parallel is used as shown in Table 5.4.

Table 5.4: Reference value E_{SRoff} for turn off losses for 10 parallel connected EUPEC FF200R33KF2C IGBT modules at 1800 V and 2000 A as a function of the snubber capacitor.

Capacitor value	E_{SRoff}
C_s = 0	2360 mJ
C_s = 1.0 μ F	1750 mJ
C_s = 2.2 μ F	1560 mJ
C_s = 4.7 μ F	1320 mJ

For the switch that consists of several IGBT modules, the value for the snubber capacitor must be adjusted according to the number of modules connected in series and parallel. The voltage V_{sw}, the current I_{sw} and the capacitor C_{sw} for a switch are distributed to the voltage V_{mod}, the current I_{mod} and the capacitor C_{mod} for a single IGBT module assuming n_s modules in series and n_p modules in parallel as

$$V_{mod} = \frac{V_{tot}}{n_s}, \;\; I_{mod} = \frac{I_{tot}}{n_p} \;\text{ and }\; C_{mod} = C_{tot}\frac{n_s}{n_p}. \tag{5.5}$$

The total stored energy W_{cap} in the snubber capacitors for the single modules can then be calculated as

$$W_{cap} = n_s n_p \frac{1}{2} C_{mod} V_{mod}^2 = n_s n_p \frac{1}{2} C_{tot} \frac{n_s}{n_p} \frac{V_{tot}^2}{n_s^2} = \frac{1}{2} C_{tot} V_{tot}^2, \tag{5.6}$$

which shows that the turn-on losses due to the energy stored in the capacitors can be calculated for the whole switch.

5.2.3 Core Material for the Transformers

In the design of the transformer and the inductors shown in Chapter 3 and the calculation of losses as shown in Chapter 4, the characteristics of the core material must be known. Here, two different core materials are chosen. The first material is laminated steel NO12 with a thickness of 0.12 mm [59], and the second material is a Metglas® POWERLITE® core [57]. For both materials, the core losses are given by

$$P_{core} = K_1 f_{tr}^{K_2} B_{max}^{K_3} V_{core} \tag{5.7}$$

as stated in Chapters 3 and 4. P_{core} is here given in kW, the transformer frequency f_{tr} in kHz, the peak flux density B_{max} in T and the core volume V_{core} in m^3. The values of

the constants K_1, K_2 and K_3 as well as some other characteristics of the materials are summarized in Table 5.5.

Table 5.5: Characteristics of the core materials for transformer and inductor design.

Parameter	Steel core	Metglas® core
K_1	298	46.7
K_2	1.19	1.51
K_3	1.65	1.74
Saturation flux	$\approx$ 1.4 T	1.56 T
Density	7.65 g/cm^3	7.18 g/cm^3

As seen in Table 5.5, the steel core has higher losses than the Metglas® core. On the other hand, the steel core is less expensive and can be available in a larger number of shapes. In the loss calculations for the converters, the results using the Metglas® core will be presented. If the steel core is used, the transformer losses will be higher but the cost for the transformer will be lower.

5.2.4 Design Considerations of the Transformer

For the design of the transformer, the design procedure is shown in detail in Chapter 3. However, there is a large number of possible designs that fulfill the requirements for a specified converter. These different designs have different sizes and losses for the specified operating conditions. For the operation in a DC-based wind farm, the converters are going to be situated in a wind turbine or on an offshore platform. This location makes a small and less heavy transformer preferable since that is lowering the cost of the material and the costs for the mechanical as well as the costs for transporting the transformer to its final location and it makes the design of the mechanical structure easier.

Also a rough estimation was made of the cost of the material compared to the cost of the losses in the transformer during its lifetime. The cost of the material was then multiplied several times to also count for the manufacturing costs, the cost for transportation and other factors. The result was that the transformer with the lowest weight for specified ratings of voltage, current, transformer ratio and leakage inductance was the most suitable choice.

5.3 The Fullbridge Converter

For the fullbridge converter, the design conditions are considered and suitable designs are obtained for the positions in the wind farm presented in Section 5.1.2. The designs should have as low losses as possible and also low complexity and weight. To limit the complexity of the converter, no auxiliary circuits except a turn-off snubber are considered.

5.3.1 Design Criteria

The fullbridge converter has a current-stiff output filter, as seen in Fig. 5.7, resulting in that the output voltage depends on the input voltage, the duty cycle and also the loss of duty cycle caused by the switching-time as explained in Section 3.2.2.

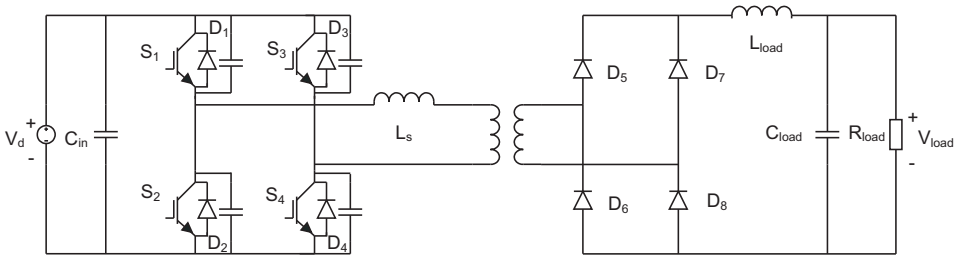

Fig. 5.7 Topology for the FB converter using phase shift control.

There are some design considerations common for all positions in the wind farm, that are lined up for the fullbridge converter. The first design criteria is the transformer ratio that is determined by the highest demanded transformation ratio for the converter. Since the fullbridge converter just can operate as a step-down converter apart from the transformer ratio, the transformer ratio is determined by the highest ratio between the output voltage and the input voltage. Further, the leakage inductance of the transformer is determined by the soft-switching requirements of the converter. If the lagging-leg should be soft-switched, the energy stored in the leakage inductance of the transformer must be larger than the energy stored in the snubber capacitors in the lagging leg. Further, the input and output filters should be designed.

Leakage Inductance and Snubber Capacitors

For investigating the leakage inductance needed for achieving soft-switching of the transistors, calculations are performed for an ideal converter. First, the ratio of the transformer n is determined as the largest step-up ratio of the converter. Then, the duty cycle D is calculated

$$D = \frac{V_{load}}{V_d n}. \tag{5.8}$$

After this, the current for the conducting devices in the input bridge is calculated as

$$i_{in} = \frac{P_{in}}{V_d D}, \tag{5.9}$$

where the current i_{in} is assumed to be constant during the on-state. Further, the leakage inductance L_s required for soft-switching of the lagging-leg devices is calculated as

$$\frac{1}{2} L_s i_{in}^2 = 2 \frac{1}{2} C_s V_d^2, \tag{5.10}$$

giving

$$L_s = \frac{2 C_s V_d^2}{i_{in}^2}. \tag{5.11}$$

The energy required for charging the snubber capacitors in (5.10) is twice the energy required for one snubber capacitor. This is due to the series connection of two snubber capacitors (one across each switch) where one capacitor has to be charged and the other has to be discharged.

The resulting leakage inductance values required for soft-switching are shown in Fig. 5.8 for (a) position 1a, (b) position 2a and (c) position 3a and in Fig. 5.9 for (a) position 1b and (b) position 2b, where the positions in the local wind turbine grid are shown in Table 5.1. Note that the value for the snubber capacitor shown in the figures is the value for the snubber capacitor for one IGBT module. The total snubber capacitor across one switch is calculated using (5.5).

In Fig. 5.8 it is shown that a large leakage inductance of the transformer is required to achieve soft-switching for the lagging leg devices in a large range of operating conditions. However, there are also drawbacks with a large leakage inductance since there is a loss of duty cycle for the converter when the current in the transformer reverses direction as shown in Section 3.2.2. The time Δt for reversing the current from i_{in} to $-i_{in}$ when the voltage V_d is applied across the leakage inductance L_s is calculated using

$$\Delta t = L_s \frac{2 i_{in}}{V_d}, \tag{5.12}$$

and the resulting time Δt is shown in Fig. 5.10 for (a) position 1a, (b) position 2a and (c) position 3a and in Fig. 5.11 for (a) position 1b and (b) position 2b for different wind speeds.

The resulting time Δt should be compared with the time for one period that is 1000 μs. It is then obvious that it is not reasonable to have a leakage inductance that can achieve soft-switching over the whole operating range for any of the converters as shown in Figs. 5.8 and 5.9. Since there are two current reversals in each period, a value of Δt of more than

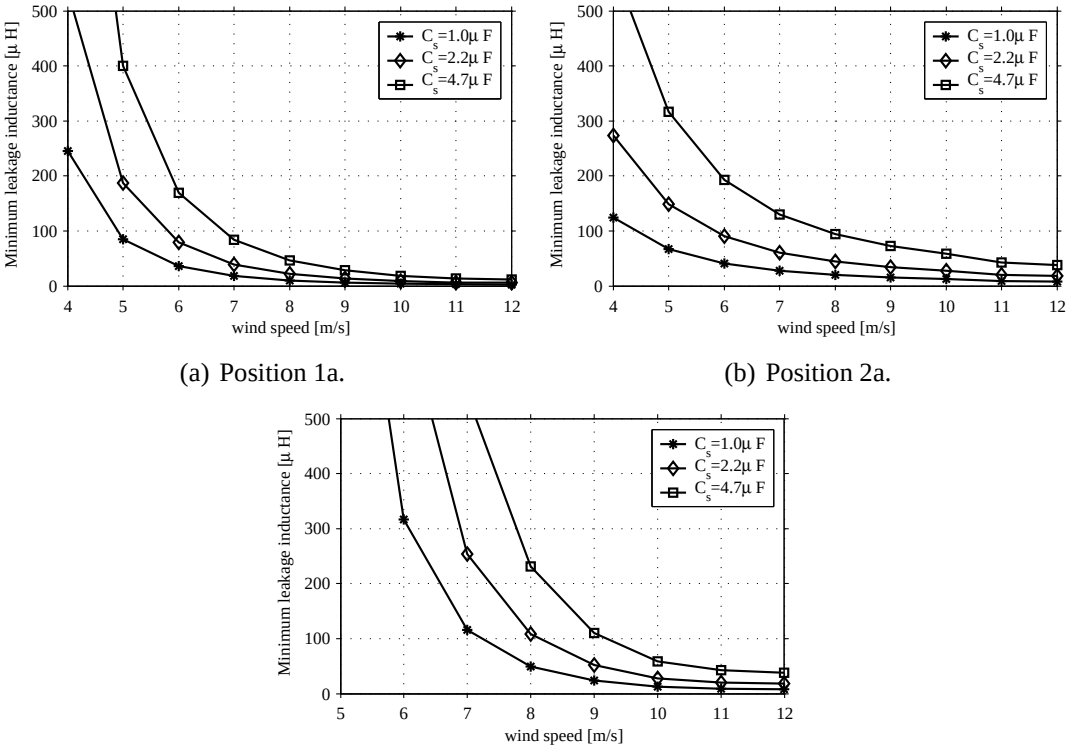

(a) Position 1a.

(b) Position 2a.

(c) Position 3a.

Fig. 5.8 Leakage inductance required for soft-switching of the lagging leg in the fullbridge converter.

100 μs is not reasonable since it would give more than 20 % loss of duty cycle. The value of the leakage inductance that gives a Δt of 100 μs is 230 μH for positions 2a and 3 a and 100 μH for position 1a. With these values of the leakage inductance, soft switching can just be achieved in a few operating points at high wind speeds. At lower wind speeds, the lagging leg switches are forced to turn on at a finite voltage resulting in large losses due to the discharge of the snubber capacitors. Therefore, a more suitable option would be to have the lagging leg hard-switched without snubber capacitors and chose a leakage inductance below 50 μH for a low loss of duty cycle. The same principle applies for converters 1b and 2b as seen in Figs. 5.9 and 5.11.

Another design issue for the fullbridge converter is the time for charging and discharging the snubber capacitors for the leading leg. Even though there is enough energy in the filter inductance to charge the capacitors, the time for charging can be a considerable fraction of the switching period. The time Δt_c for charging the capacitors of the leading leg is calculated using

$$\Delta t_c = C_s \frac{\Delta V}{i_{in}/2}. \tag{5.13}$$

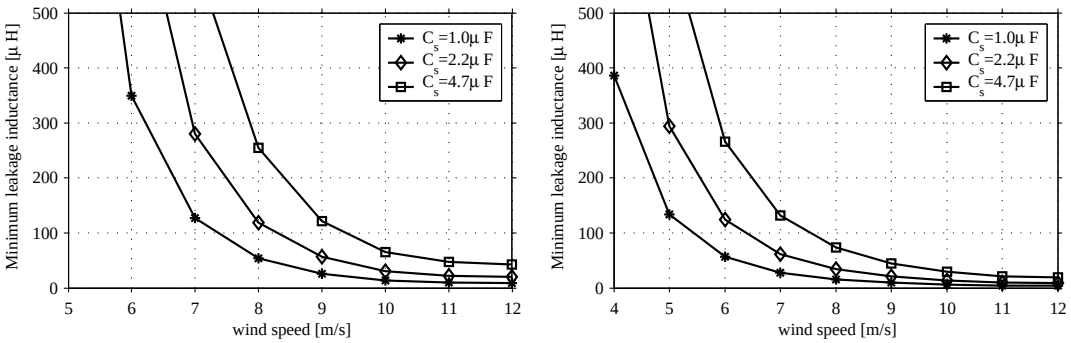

(a) Position 1b. (b) Position 2b.

Fig. 5.9 Leakage inductance required for soft-switching of the lagging leg in the fullbridge converter.

The resulting time Δt_c for charging the leading-leg snubber capacitors are shown in Fig. 5.12 for (a) position 1a, (b) position 2a and (c) position 3a and in Fig. 5.13 for (a) position 1b and (b) position 2b for different wind speeds.

To evaluate the results from Fig. 5.12, it should be noted that a time of 10 μs for charging the capacitors corresponds to 2 % of the switching cycle. Thereby, an assumption is made that the maximum time allowed for charging the capacitors is 20 μs, equal to 4 % of the switching cycle. This will then result in turn-on losses at low wind speeds where the snubber capacitor is not discharged before the switch is turned on.

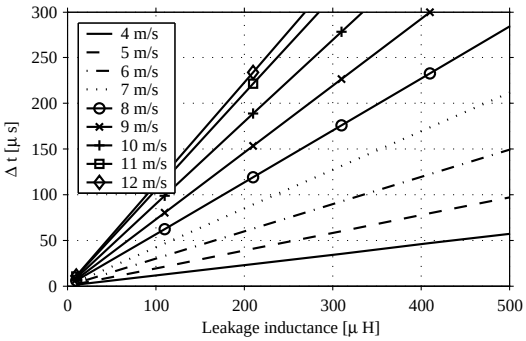

(a) Position 1a.

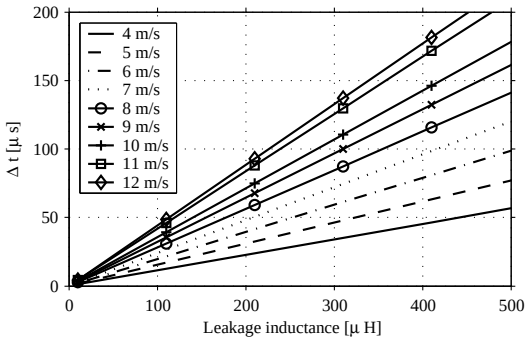

(b) Position 2a.

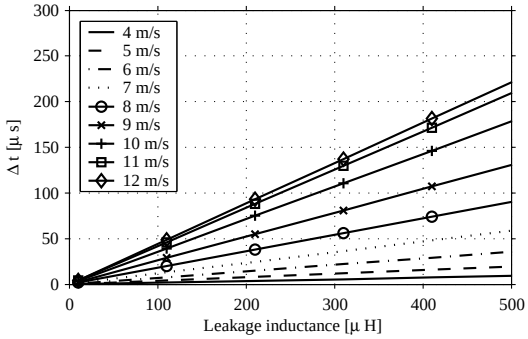

(c) Position 3a.

Fig. 5.10 Time Δt for current reversal as a function of the leakage inductance.

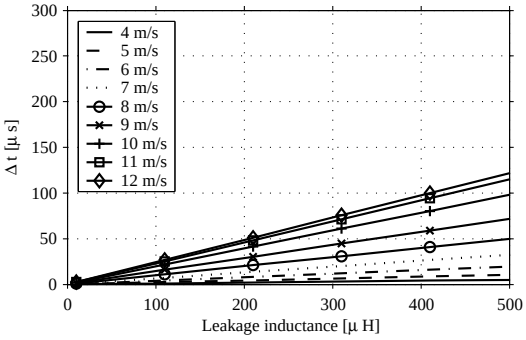

(a) Position 1b.

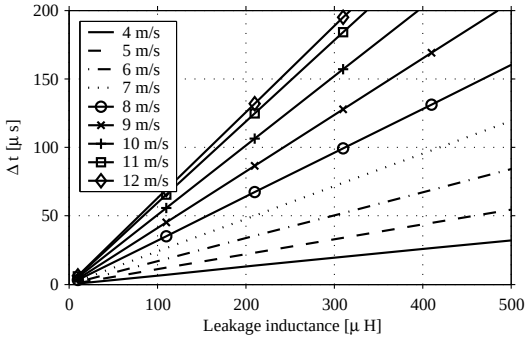

(b) Position 2b.

Fig. 5.11 Time Δt for current reversal as a function of the leakage inductance.

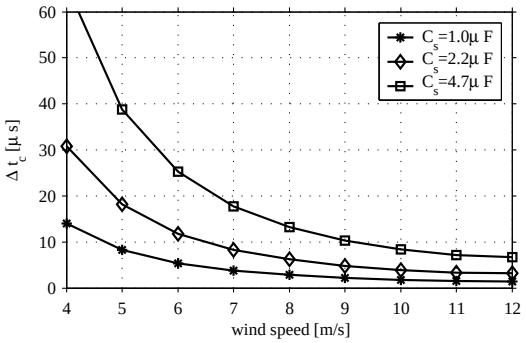

(a) Position 1a.

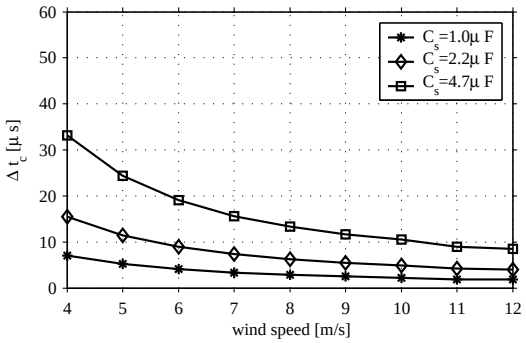

(b) Position 2a.

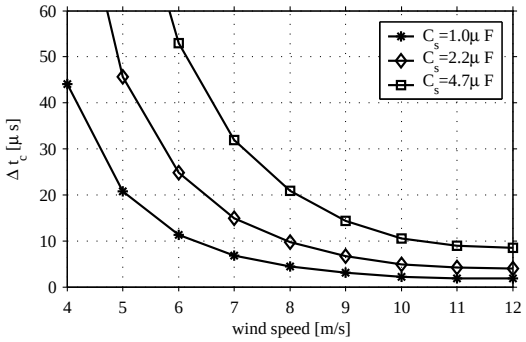

(c) Position 3a.

Fig. 5.12 Time Δt_c for charging the lagging-leg capacitors.

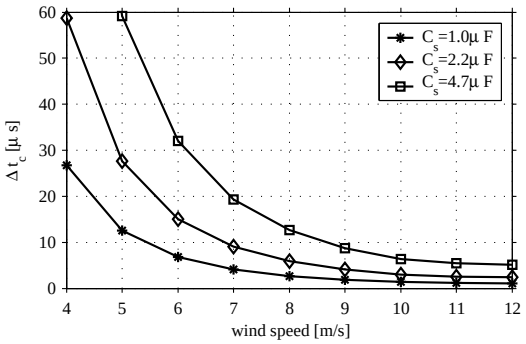

(a) Position 1b.

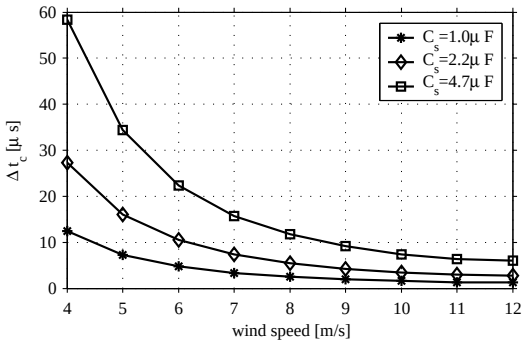

(b) Position 2b.

Fig. 5.13 Time Δt_c for charging the lagging-leg capacitors.

Filter design

For the operation of the converter both input and output filters are needed. The input filter is simplified as a large capacitor which provides a constant input voltage to the IGBT bridge even if the input current is not constant. Assuming that the peak-to-peak ripple in the input voltage ΔV_{in} is expressed as

$$\Delta V_{in} = \frac{1}{C_{in}} \left(I_{load} n - I_{in} \right) \frac{T_s}{2} \frac{V_{load}}{V_{in} n}, \tag{5.14}$$

where I_{in} is the average of the input current, I_{load} is the average output current, V_{in} is the input voltage, V_{load} is the output voltage, C_{in} is the value of the input capacitor, n is the transformer ratio and T_s is the switching period. The minimum value of C_{in} is then given by

$$C_{in} = 5 \frac{T_s V_{load}}{V_{in}^2 n} \left(I_{load} n - I_{in} \right). \tag{5.15}$$

The resulting values for the input capacitor is summarized for the different positions in Table 5.6.

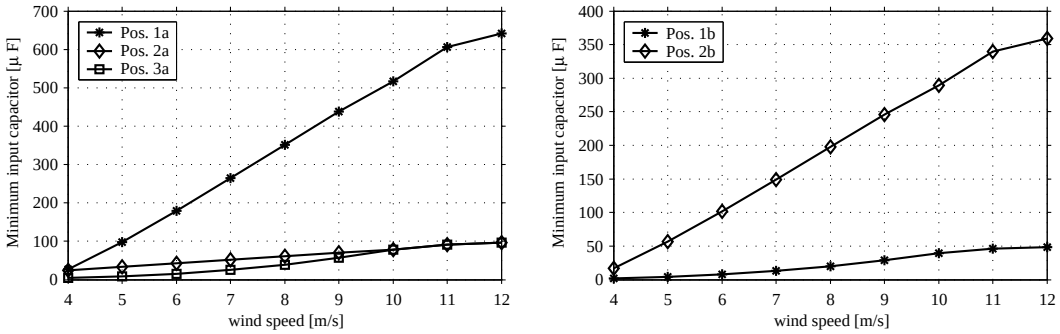

(a) Positions 1a, 2a and 3a.

(b) Positions 1b and 2b.

Fig. 5.14 Minimum input capacitor C_{in} for the FB converter.

It can be seen that the converters with varying ratio between the input voltage and the output voltage have the highest requirements for the input capacitor. The converters with constant voltage ratio can have a almost full duty cycle at all wind speeds and the the stresses for the input filter will then be low.

The output filter for the fullbridge converter will be simplified to a larger filter inductance due to its current stiff characteristics. To calculate this inductance L_{load}, the peak-to-peak ripple in the output current is calculated as

$$\Delta I_{load} = (V_{in}n - V_{out})\,\frac{T_s}{2}\,\frac{V_{out}}{V_{in}n}\,\frac{1}{L_{load}}. \tag{5.16}$$

Assuming that the maximum current ripple $\Delta I_{load} = 0.1 I_{load}$, the minimum value for the filter inductance can be calculated as

$$L_{load} = \frac{T_s}{0.2 I_{load}} \left(V_{load} - \frac{V_{out}^2}{V_{in}n} \right), \tag{5.17}$$

and the results are shown in Fig. 5.15.

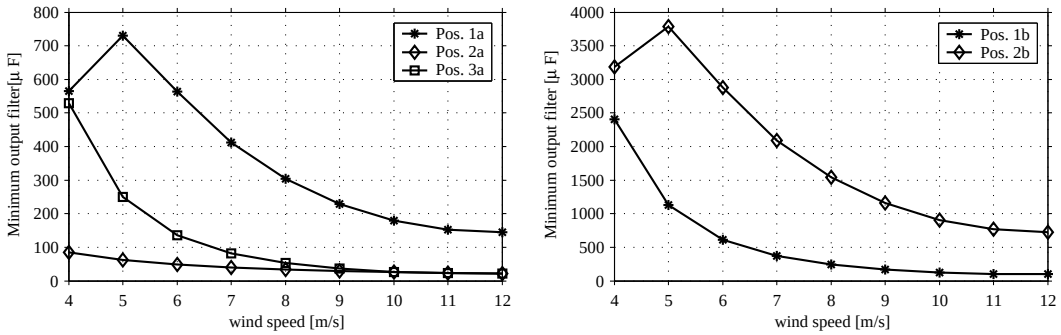

(a) Positions 1a, 2a and 3a.

(b) Positions 1b and 2b.

Fig. 5.15 Minimum output inductance L_{load} for the FB converter.

From the results, it can be seen that the largest value of the inductance needed to maintain the current ripple ΔI_{load} below 10 % of the output current occurs at low power levels. Since the value of the inductance is large, the converter would be both less heavy and less expensive if the value of the inductance can be decreased. In Table 5.6 both the value of the inductance needed to limit the current ripple at all wind speeds is presented as well as the value needed for limiting the current ripple below 10 % at wind speeds above 8 m/s. Also, just as for the input capacitor, a larger value is needed for the converters with a varying voltage ratio.

Table 5.6: Minimum values for the filter components for the FB converters.

	Pos. 1a	Pos. 2a	Pos. 3a	Pos. 1b	Pos. 2b
C_{in}	641 μF	97 μF	97 μF	49 μF	360 μF
L_{load}	700 mH	90 mH	530 mH	2400 mH	3800 mH
$L_{load}, > 8m/s$	305 mH	35 mH	55 mH	240 mH	1540 mH

5.3.2 Losses in the Fullbridge Converter

In this section, the losses in the fullbridge converter are plotted for different values of the snubber capacitor. Assuming that the snubber capacitor across a single IGBT module is given by the values used in [58], the total snubber capacitor for a switch is determined by the number of modules connected in series and parallel. The formula for calculating the total snubber capacitor C_{sw} is

$$C_{sw} = C_{mod}\frac{n_p}{n_s}, \tag{5.18}$$

where C_{mod} is the snubber capacitor for one module and n_p and n_s are the numbers of modules connected in parallel and series. In the resulting losses, the value of the snubber capacitor is the value of the snubber capacitor for one module.

The results from the loss calculations are shown for the different positions for different values of the snubber capacitor in Fig. 5.16 for positions 1a, 2a and 3a and in Fig. 5.17 for positions 1b and 2b. The loss distribution for the converters using snubber capacitor C_s = 1 μF are then shown in Figs. 5.18 and 5.19 and the losses are summarized in Tables 5.7 and 5.8 for an average wind speed of 7.2 m/s.

Table 5.7: Losses for different values of the snubber capacitor C_s for positions 1a, 2a and 3a.

Position	C_s = 0	C_s = 1 μF	C_s = 2.2 μF	C_s = 4.7 μF
Pos. 1a	57 kW	55 kW	55 kW	54 kW
Pos. 2a	29 kW	28 kW	28 kW	27 kW
Pos. 3a	29 kW	28 kW	31 kW	47 kW

Table 5.8: Losses for different values of the snubber capacitor C_s for positions 1b and 2b.

Position	C_s = 0	C_s = 1 μF	C_s = 2.2 μF	C_s = 4.7 μF
Pos. 1b	195 kW	192 kW	192 kW	214 kW
Pos. 2b	321 kW	312 kW	310 kW	317 kW

For each position in the local wind turbine grid, a suitable snubber capacitor should be chosen. From Table 5.7 it can be seen that the converter for both position 3a has the lowest

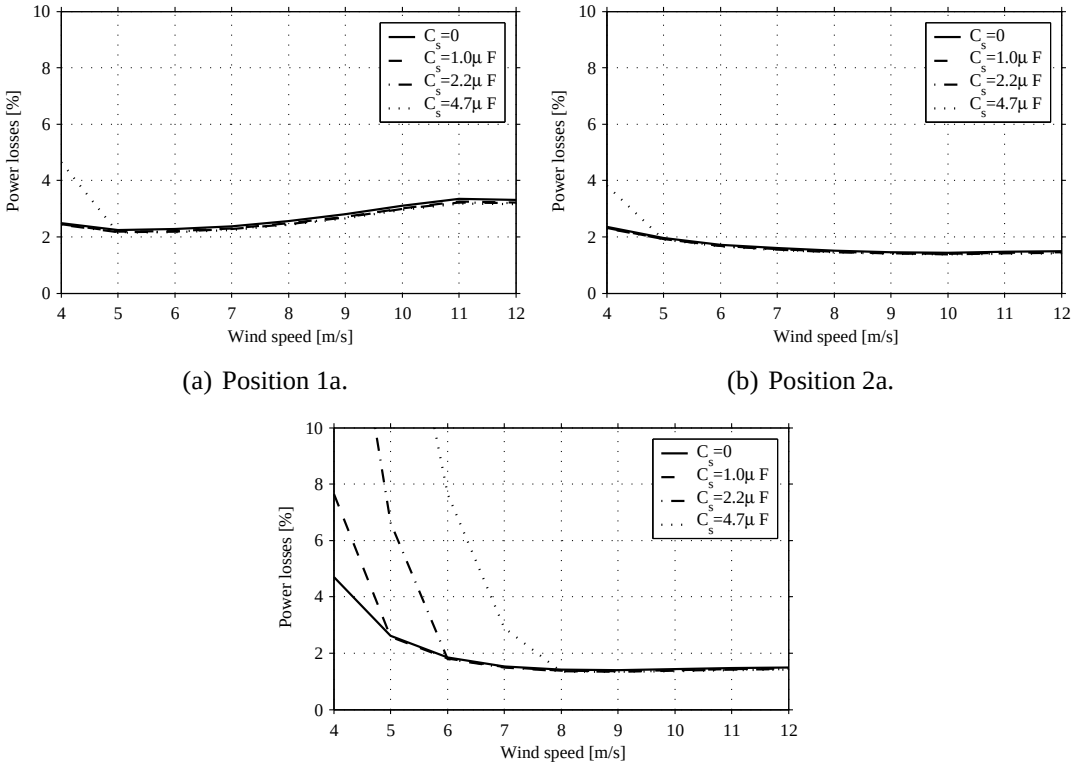

(a) Position 1a.

(b) Position 2a.

(c) Position 3a.

Fig. 5.16 Losses as a fraction of input power for the FB converter for positions 1a, 2a and 3a.

losses using the snubber capacitor C_s = 1 μF, while the converters for positions 1a and 3a have the lowest losses with the snubber capacitor C_s = 4.7 μF. For position 1b, as seen in Table 5.8, the lowest losses are achieved with snubber capacitor C_s = 1 μF or C_s = 2.2 μF and for position 2b, the lowest losses are achieved with snubber capacitor C_s = 2.2 μF. In the cases where the losses are similar for different snubber capacitors, the capacitor with the lowest value is chosen to reduce the cost and increase the switching speed.

The resulting losses for the fullbridge converter shows clearly that a constant ratio between the input and output voltage reduces the losses for the converter. Since the output voltage basically is the input voltage times the duty ratio, the duty ratio can be kept constant at a high value. For positions 2a, 3a and 1b, the converter has a constant transformation ratio which results in low losses, especially at high wind speeds as shown in Figs. 5.16 and 5.17. If the ratio between the input and the output voltage varies as for positions 1a and 2b, the converter has to be designed for the highest transformation ratio leading to a higher ratio of the transformer. This results in a decrease in the duty cycle at high wind speeds where the ratio of the transformer is considerably higher than the desired transformation ratio and the voltage levels are the same for all converters. Since the ratio of the transformer is higher, the current at turn-off in the switches will be higher than

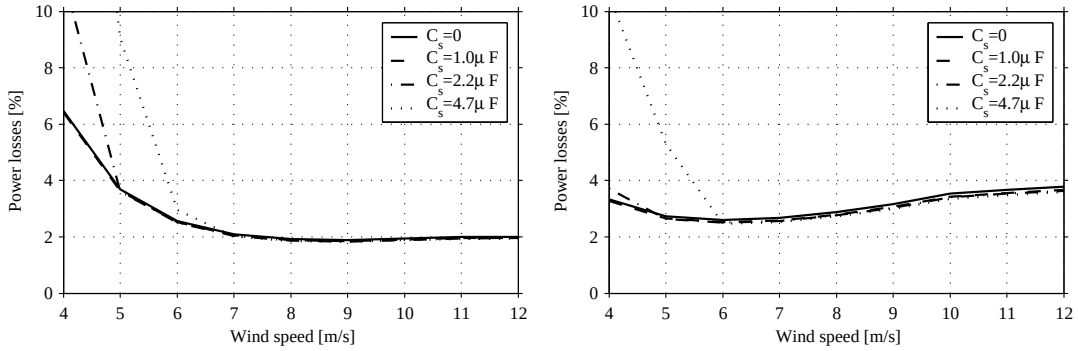

(a) Position 1b. (b) Position 2b.

Fig. 5.17 Losses as a fraction of input power for the FB converter for positions 1b and 2b.

for the converters with constant voltage ratio and thereby a lower ratio of the transformer. A higher current at turn-off gives higher turn-off losses and thereby higher losses for the converters. Also, the high current will flow in the semiconductor components even in the off-state, giving high conduction losses.

Another source of increased losses due to the wide range of operating conditions is the limited design of the snubber capacitors. The complexity of the converters should be kept as low as possible whereby no additional circuits apart from the turn-off snubbers are allowed. Due to this, the value of the snubber capacitor is limited due to the high voltage and low current at low wind speeds, where the time for discharging the capacitors is longer than the allowed delay between turn-on and turn-off. A large snubber capacitor will then cause large turn-on losses at low wind speeds while a smaller snubber capacitor not leading to any turn-on losses will not give any significant reduction in turn-off losses. The lowest losses are obtained by the converter at position 2a that has constant voltage ratio and also lower voltage levels at lower power levels. Also, the leakage inductance in the transformer required for discharging the capacitors in the lagging leg at low wind speeds is too large whereby that leg will be hard-switched. For all converters the efficiency at the lowest wind speed is low since the transferred power is as low as 4 % of the maximum power and the converter is drastically over-rated.

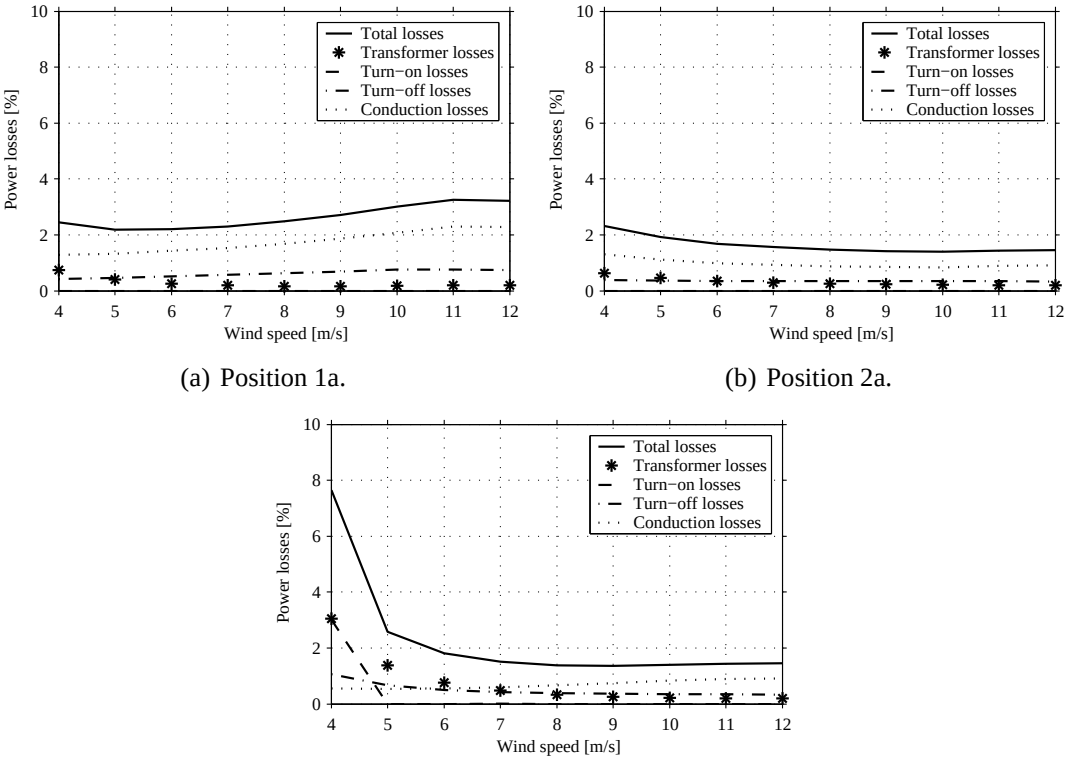

(a) Position 1a.

(b) Position 2a.

(c) Position 3a.

Fig. 5.18 Loss distribution for the FB converter for positions 1a, 2a and 3a with snubber capacitor C_s = 1 μF.

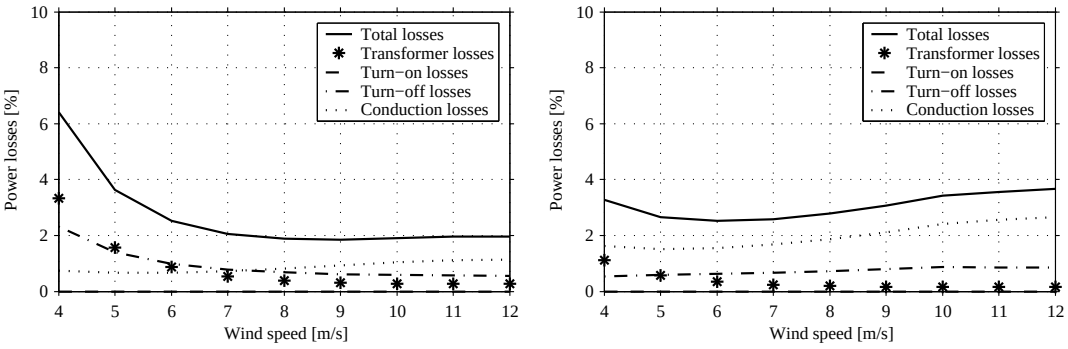

(a) Position 1b.

(b) Position 2b.

Fig. 5.19 Loss distribution for the FB converter for positions 1b and 2b with snubber capacitor C_s = 1 μF.

5.4 The Single Active Bridge Converter

For the single active bridge converter, design conditions have been presented in [10] as well as different control methods for the converter. Here, the control methods used in this thesis will be presented and, just as for the fullbridge converter, designs will be made for each position in the local wind turbine grid. Then the losses will be evaluated for each position using both control methods.

5.4.1 Control Methods

In [10], the control of the single active bridge converter is discussed and here two of the control methods are presented that will be used in this thesis.

Turn-off Time Control Operating at DCM

The first control method used for the single active bridge converter is called turn-off time control operating at discontinuous conduction mode (DCM) described in [10]. The switching frequency is constant for this control method, and the power flow is instead limited by lowering the duty cycle for the transistors. As a result of this there will be an off-time between the time-point when the current through the diodes has decreased to zero and the time instant when the transistors starts conducting. Since the switching frequency is constant, the designs of the transformer and the filters are easier to optimize. On the other hand, the power flow will be interrupted in the discontinuous conduction mode and there will be turn-on losses when the snubber capacitors are discharged at turn-on after an off-period.

Variable Frequency Control

The second control method is the variable switching frequency control [10]. For this control method, there is no off-time between the current through the diodes has decreased to zero and the transistors starts conducting. Consequently, the transistors can be turned on while the freewheeling diodes are conducting and there are no turn-on losses. The control is achieved by varying the switching frequency, where an increase in the frequency increases the impedance of the leakage inductance and thereby limits the transferred power. However, this control method will give large frequency variations for the wide range of operating conditions for a wind turbine. Thereby, it is hard to find designs for both the transformer and the filters suitable for all operating points.

5.4.2 Design Criteria

For the single active bridge converter seen in Fig. 5.20, the design of the converter is basically the choice of the leakage inductance of the transformer and the transformer ratio,

which determines the operation of the converter as shown in Section 3.3.

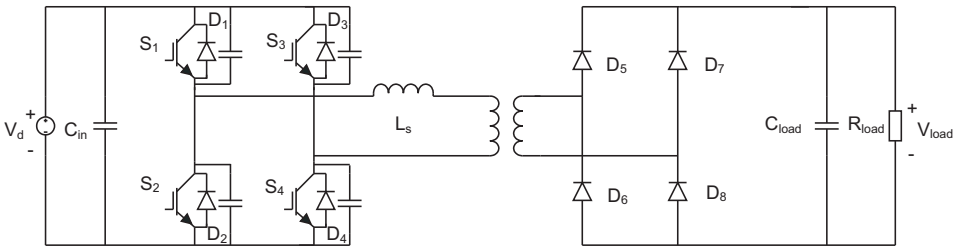

Fig. 5.20 Topology for the SAB converter.

For the single active bridge converter, sources for increased losses compared the the full-bridge converter are the turn-on losses due to the discharge of the snubber capacitors and the larger turn-off losses due to the triangular current waveform. The turn-on losses can only be reduced by turning the switch on while the freewheeling diode is conducting as in the variable frequency control. However, that results in an increased frequency which gives larger turn-off losses whereby this frequency variations should be limited as much as possible. Also, for the constant frequency control, the turn-off losses increase if the duty cycle is low since the current at turn-off is higher than in the case of a higher duty cycle with the same operating conditions. Consequently, both control strategies would benefit from a converter design that is operating as close to the desired frequency or the desired duty cycle as possible for all operating points. For the design of the converter, the case with constant frequency control which results in the current waveform in the transformer as shown in Fig. 5.21 will now be considered.

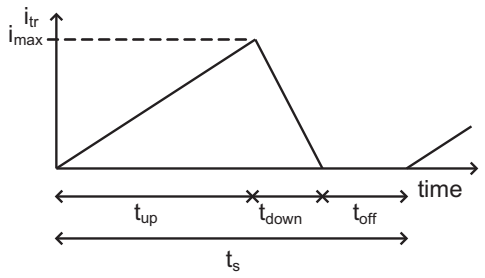

Fig. 5.21 Principal current waveform in the transformer for the single active bridge with constant frequency control.

Using these waveforms, the design of the converter can be investigated using ideal components. Assume an input voltage V_{in} on the input of the transformer, and an output voltage V_{out} on the secondary side of the transformer. To simplify the calculations, V_{out} is down scaled to the primary side of the transformer. Further, the leakage inductance of the transformer seen from the primary side is L_s, the peak current is i_{max} and the transferred power

is P_{tr}. The rise time t_{up}, the fall time t_{down} and the off time t_{off} of the transformer current can be calculated using

$$t_{up} = \frac{L_s}{V_{in} - V_{out}} i_{max}, \tag{5.19}$$

$$t_{down} = \frac{L_s}{V_{in} + V_{out}} i_{max} \tag{5.20}$$

and

$$t_{off} = t_s - t_{up} - t_{down}. \tag{5.21}$$

Further, the transferred power P_{tp} can be expressed as

$$P_{tp} = \frac{t_{up} - t_{down}}{t_s} \frac{V_{in} i_{max}}{2}. \tag{5.22}$$

Using (5.19)-(5.22), the peak current i_{max} can be expressed as

$$i_{max} = \sqrt{\frac{P_{tp} t_s (V_{in}^2 - V_{out}^2)}{V_{in} V_{out} L_s}}. \tag{5.23}$$

Knowing the peak current, t_{off} can be calculated using (5.21). The aim of the design is to minimize the off-time t_{off} as much as possible. Sine the input voltage V_{in}, the transferred power P_{tp} and the cycle period t_s are known, the value of the leakage inductance L_s and the transformer ratio giving V_{out} are varied and t_{off} is plotted in Figs. 5.23 and 5.25. In order to explain the design results, the off-time is eliminated and expressed as

$$t_{off} = t_s - \sqrt{\frac{P_{tp} t_s 4 V_{in} L_s}{(V_{in}^2 - V_{out}^2) V_{out}}}. \tag{5.24}$$

Wind Turbine Converters, Positions 1a, 2a and 3a

Using (5.24), the transformer ratio that gives zero off-time can be calculated for different values of the leakage inductance L_s. This is done for all wind speeds for the converters at positions 1a, 2a and 3a and the resulting values are shown in Fig. 5.22.

It should be noted that the conditions for the wind speeds 10, 11 and 12 m/s are the same for all converters. In Fig. 5.22, the values of the transformer ratio and the leakage inductance that give zero off-time are shown. It is obvious that there is no design that gives zero off-time for all operating conditions. From (5.24), it is seen that an increase of the leakage inductance would give a negative off-time, which is not possible. Therefore, the allowed values of the leakage inductance are the values that are lower than the values indicated in the figure. For the single active bridge converter at position 1a as seen in Fig. 5.22 (a),

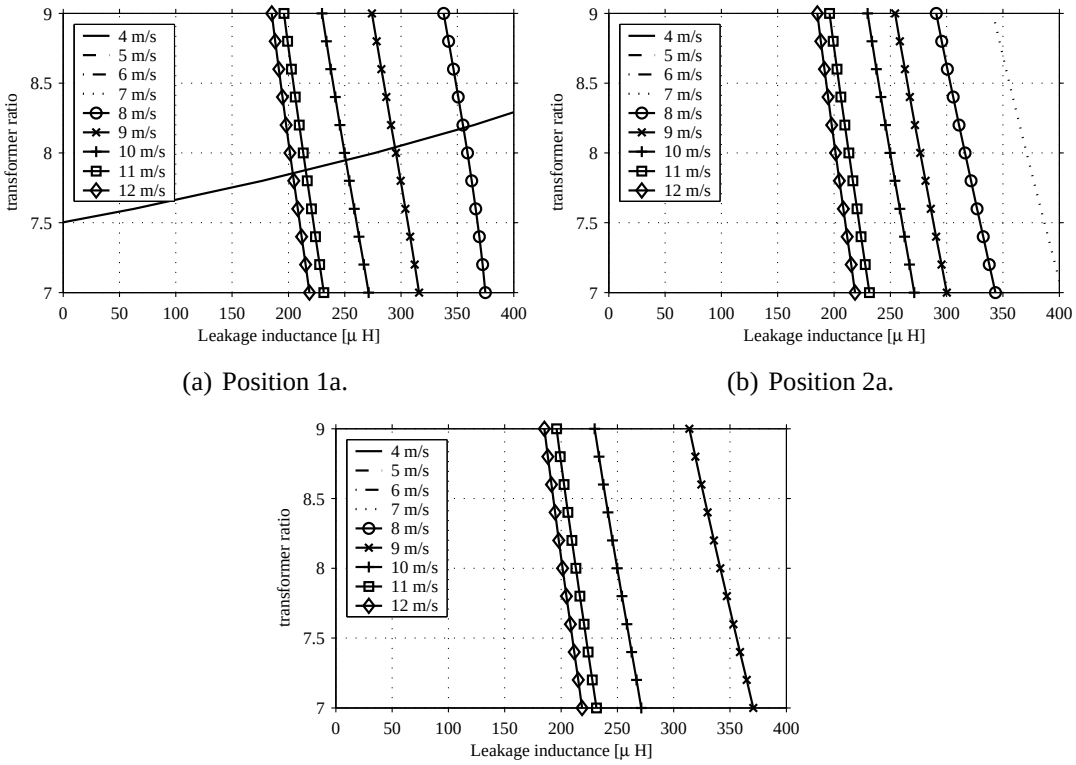

(a) Position 1a.

(b) Position 2a.

(c) Position 3a.

Fig. 5.22 Transformer ratio and leakage inductance for zero off-time for the SAB converter.

there is a crossing point where there is zero off-time for both wind speeds 12 m/s and 4 m/s, and these values are therefore chosen for the design of the converter. For the converters for positions 2a and 3a, any of the designs giving zero off-time for wind speed 12 m/s can be used as shown in Figs. 5.22 (b) and 5.22 (c). Since there is no significant difference between the possible designs for position 2a and 3a, the same design in chosen as for position 1a.

The values for the leakage inductance and the transformer ratio are obtained from approximate calculations and must therefore be slightly adjusted to give zero off-time at 12 m/s in the simulation model. The resulting design values are then a leakage inductance L_s = 200 μH and a transformer ratio of 7.9. The resulting off-time for the different converters are shown in Fig. 5.23, and are compared with the obtained off-times from the simulations.

In Figs. 5.23 (a) and 5.23 (b), it can be seen that the converters for position 1a and 2a have similar off-times except for the operating point where the wind speed is 4 m/s. The converter for position 3a has longer off-time than the other two converters, as seen in Fig. 5.23 (c).

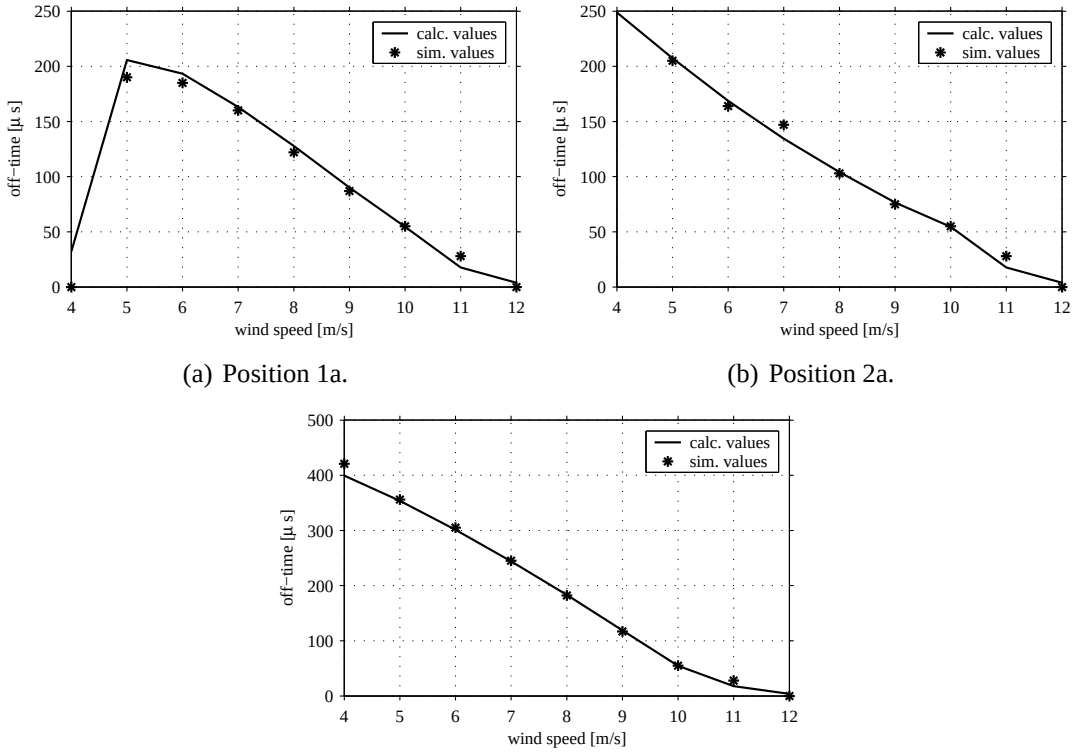

(a) Position 1a.

(b) Position 2a.

(c) Position 3a.

Fig. 5.23 Resulting off-time from the design program for the single active bridge converter.

Group Converters, Positions 1b and 2b

For the single active bridge converters used as group converters, the design is made in the same way as for the converters for one wind turbine. Since the converters for position 1b and 3b are identical, designs are just made for position 1b and 2b. In Fig. 5.24, the transformer ratio that gives zero off-time is presented for positions 1b and 2b as a function of the leakage inductance L_s.

In Fig. 5.24 (b), it can be seen that the design conditions for position 2b are similar as for position 1a in Fig. 5.22 (a). The values for the transformer are then chosen in the same way, namely the values that gives zero off-time for both 4 m/s and 12 m/s, resulting in a leakage inductance L_s = 367 μH and a transformer ratio of 13. For position 1a, the transformer parameters can be chosen more freely in Fig. 5.24 (a), and for simplicity the same transformer is chosen. The resulting off-time for position 1b and 2b are then shown in Fig. 5.25.

In Fig. 5.26, the resulting switching frequency is shown for the converters in the case of variable frequency control.

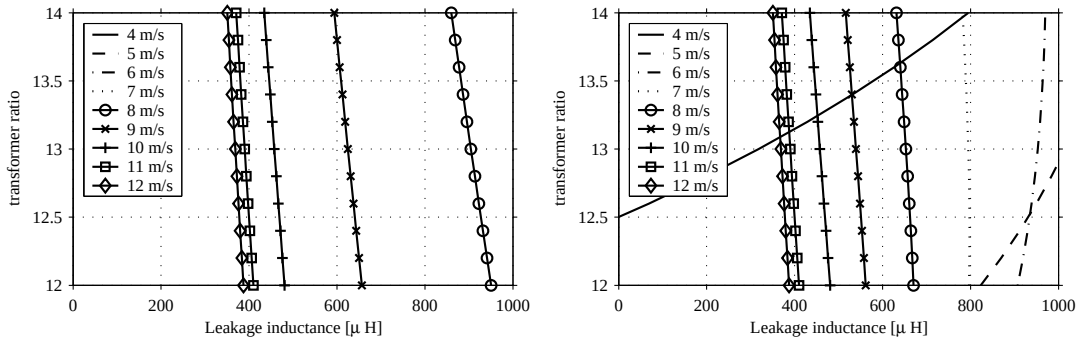

(a) Position 1b. (b) Position 2b.

Fig. 5.24 Transformer ratio and leakage inductance for zero off-time for the SAB converter.

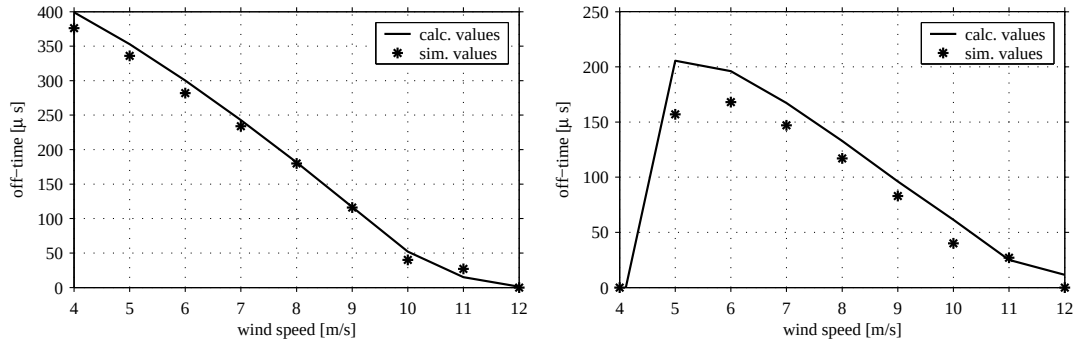

(a) Position 1b. (b) Position 2b.

Fig. 5.25 Resulting off-time from the design program for the single active bridge converter.

It is shown that the switching frequency stays within reasonable values for all converters except for positions 3a and 1b where the resulting switching frequency will be up to 12 kHz for position 1b and 20 kHz for position 3a.

Filter Design

In the single active bridge converter, both the input filter and the output filter are voltage stiff and are therefore simplified as capacitors. Just as for the input filter for the fullbridge converter, the value for the capacitor is calculated that keeps the peak-to-peak voltage ripple within 10 % of the average value of the voltage. Starting with the input capacitor C_{in}, the voltage ripple ΔV_{in} can be expressed as

$$\Delta V_{in} = \frac{1}{C_{in}} \left(\frac{t_{up} i_{max}}{2} - t_{up} I_{in} \left(1 - \frac{1}{2} \frac{I_{in}}{i_{max}} \right) \right), \tag{5.25}$$

where I_{in} is the input current, t_{up} is the rise time of the current as defined in (5.19) and

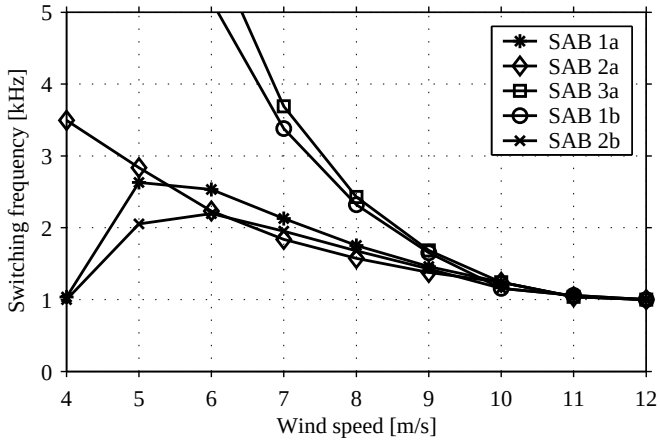

Fig. 5.26 Switching frequency for the SAB converter using variable frequency control.

i_{max} is the peak current as shown in (5.23). Assuming that $\Delta V_{in} = 0.1 V_{in}$ the capacitor value can be expressed as

$$C_{in} = \frac{10}{V_{in}} \left(\frac{t_{up} i_{max}}{2} - t_{up} I_{in} \left(1 - \frac{1}{2} \frac{I_{in}}{i_{max}} \right) \right). \tag{5.26}$$

Similar to the input capacitor, the capacitor for the output filter is calculated as

$$C_{load} = \frac{10}{V_{load}} \left(\frac{(t_{up} + t_{down}) i_{max}/n}{2} - (t_{up} + t_{down}) I_{load} \left(1 - \frac{1}{2} \frac{I_{load}}{i_{max}/n} \right) \right). \tag{5.27}$$

The resulting values for the input capacitor are shown in Fig. 5.27 and the values for the output capacitor are shown in Fig. 5.28. Also, the resulting values are summarized in Table 5.9.

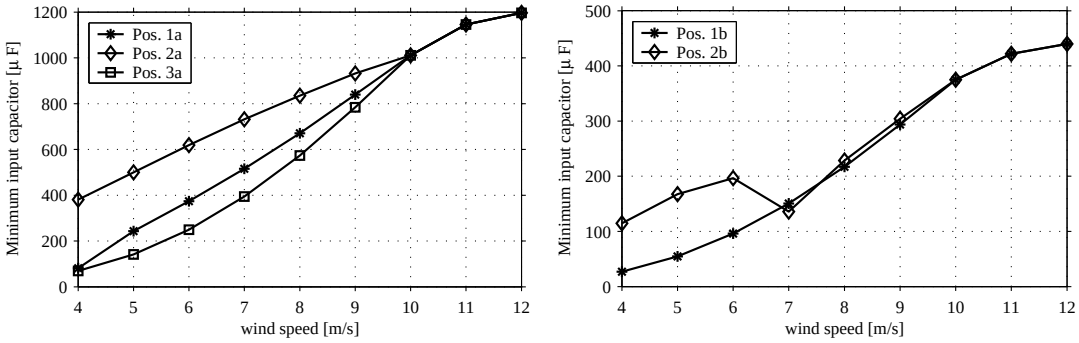

(a) Positions 1a, 2a and 3a.

(b) Positions 1b and 2b.

Fig. 5.27 Minimum input capacitor C_{in} for the SAB converter.

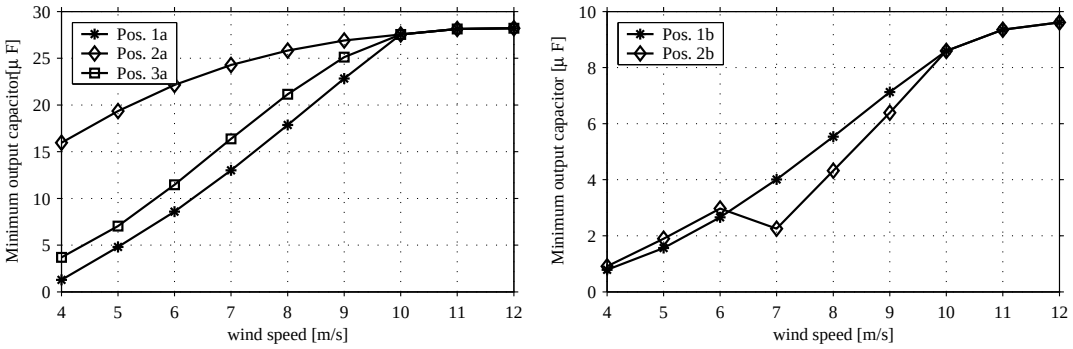

(a) Positions 1a, 2a and 3a.

(b) Positions 1b and 2b.

Fig. 5.28 Minimum output capacitor C_{load} for the SAB converter.

Table 5.9: Minimum values for the filter components for the SAB converters.

	Pos. 1a	Pos. 2a	Pos. 3a	Pos. 1b	Pos. 2b
C_{in}	1200 μF	1200 μF	1200 μF	440 μF	440 μF
C_{load}	28 μF	28 μF	28 μF	10 μF	10 μF

For the single active bridge converter, the designs for the wind turbine converters are the same independent of the control method as shown previous in this section. And since the largest value of the capacitor is required at high wind speeds where the voltage levels also are the same for the different control strategies, the demand for maximum input and output capacitors are the same for the different designs. This also applies for the group converters at positions 1b and 2b.

5.4.3 Losses in the Single Active Bridge Converter

For each position in the local wind turbine grid, the total losses are plotted as a function of wind speed, and there is also an average loss calculation for the average wind speed 7.2 m/s. For each position, the different losses are presented for the constant frequency control as well as for the variable frequency control using different values of the snubber capacitors. The first converters to be considered are the converters for a single wind turbine, i.e. converters for positions 1a, 2a and 3a.

Wind Turbine Converters, Positions 1a, 2a and 3a

Starting with the single active bridge converter operating as a wind turbine converter at positions 1a, 2a and 3a, the resulting losses are plotted as a fraction of the input power in Fig. 5.29 for position 1a, in Fig. 5.30 for position 2a and in Fig. 5.31 for position 3a for a) constant frequency control and b) variable frequency control.

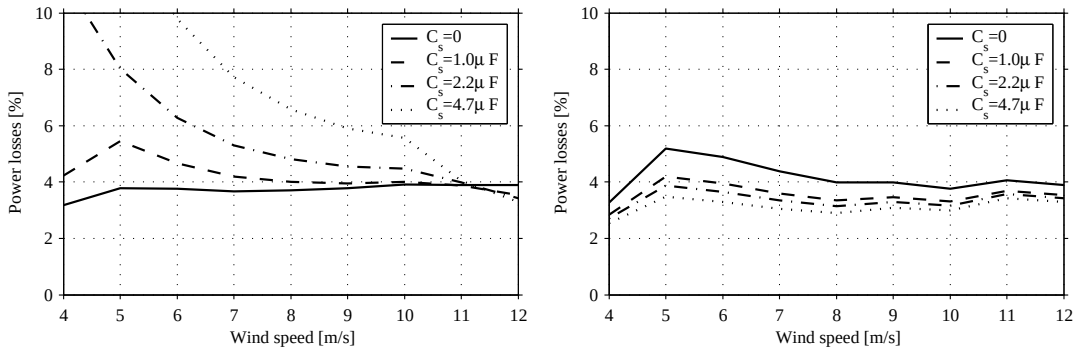

(a) Position 1a with constant frequency control. (b) Position 1a with variable frequency control.

Fig. 5.29 Losses as a fraction of input power for the SAB converter for position 1a.

Also, the losses are divided into different loss components for each converter using the snubber capacitor C_s = 1.0 μF, which is shown in Fig. 5.32 for position 1a, in Fig. 5.33 for position 2a and in Fig. 5.34 for position 3a.

The loss calculations are summarized in Table 5.10, where the mean value of the losses are calculated for an average wind speed of 7.2 m/s.

Starting with position 1a, it can be seen in Fig. 5.29 that the losses increase for increasing snubber value for the constant frequency control due to the high turn-on losses at discharge of the snubber capacitors. For the variable frequency control, a lossless snubber capacitor can be used that lower the turn-off losses but does not give any turn-on losses. However, the switching frequency is higher for the variable frequency control resulting in

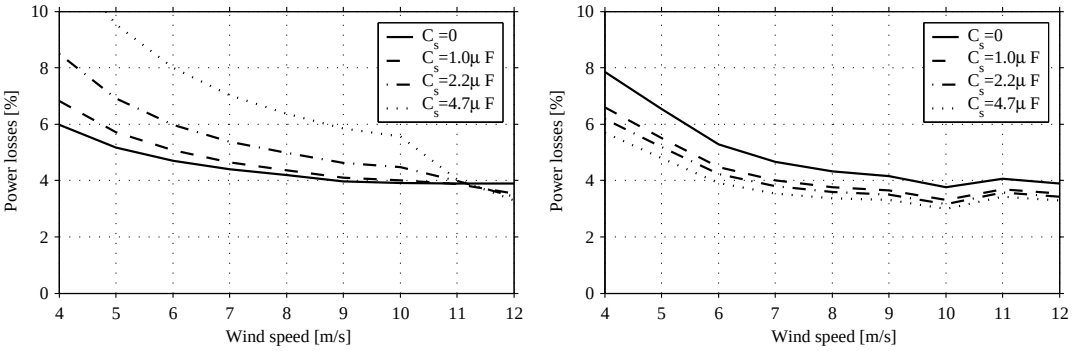

(a) Position 2a with constant frequency control. (b) Position 2a with variable frequency control.

Fig. 5.30 Losses as a fraction of input power for the SAB converter for position 2a.

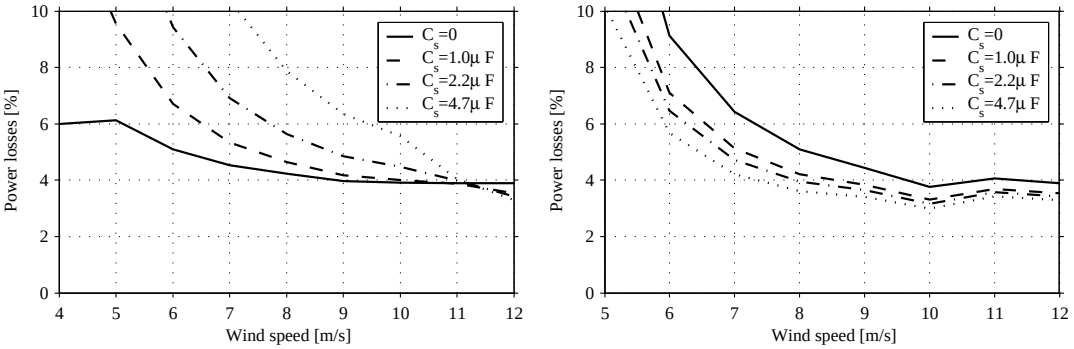

(a) Position 3a with constant frequency control. (b) Position 3a with variable frequency control.

Fig. 5.31 Losses as a fraction of input power for the SAB converter for positions 3a.

higher turn-off losses. The lowest losses are achieved when the variable frequency control is used with snubber capacitor C_s = 4.7 μF. In the loss distribution in Fig. 5.32 it is clearly shown that the turn-on losses is the large difference in losses between the two control strategies. There is a slight increase in turn-off losses for the variable frequency control, but that difference is smaller than the turn-on losses. In Table 5.10 it is shown that the constant frequency control has lower losses than the variable frequency control without the snubber capacitor due to the lower turn-off losses. However, when a snubber capacitor is inserted, the losses are reduced for the variable frequency control while the losses are increased for the constant frequency control. The lowest losses would be achieved with variable frequency control and C_s = 4.7 μF, which also is the chosen design.

Then, the same comparison between different control strategies and capacitor values are made for position 2a. The results for wind speeds 10 to 12 m/s are the same as for position 1a since the voltage levels are constant. For both control methods, the losses are similar as for position 1a except for the lowest wind speeds where the losses are increased due to

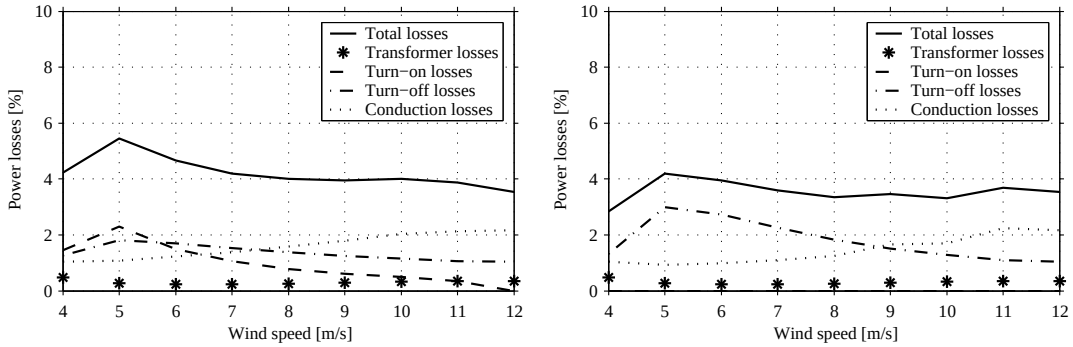

(a) Position 1a with constant frequency control. (b) Position 1a with variable frequency control.

Fig. 5.32 Loss distribution for the SAB converter for position 1a with snubber capacitor C_s = 1.0 μF.

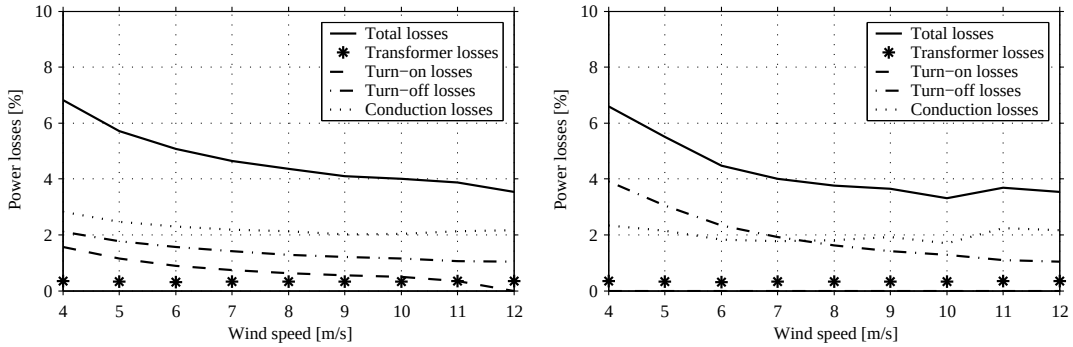

(a) Position 2a with constant frequency control. (b) Position 2a with variable frequency control.

Fig. 5.33 Loss distribution for the SAB converter for position 2a with snubber capacitor C_s = 1.0 μF.

a longer off-time or an increased frequency depending on the control method. The lowest losses for position 2a are obtained using the variable frequency control with snubber capacitor C_s = 4.7 μF as seen in Table 5.10, and this is also the chosen design.

Also for position 3a, the losses at high wind speeds are the same as for position 1a since both the design of the converter and the voltage levels are the same. At lower wind speeds the losses are increased more than for the other positions. This increase in losses is mainly caused by the increased off-time at lower wind speeds as shown in Fig. 5.23 (c). The lowest losses are obtained for variable frequency control and snubber capacitor C_s = 4.7 μF as shown in Table 5.10, and this is the chosen design. However, it should be noted that the maximum switching frequency is 20 kHz instead of the rated 1 kHz and if this is a problem the constant frequency control without a snubber capacitor should be used.

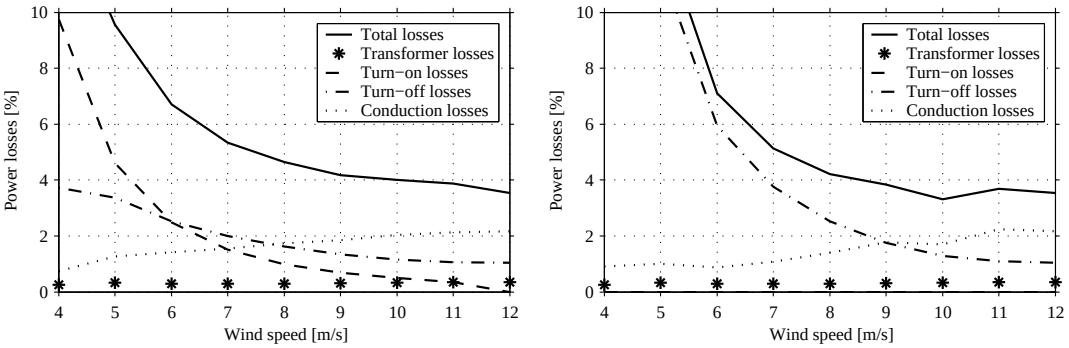

(a) Position 3a with constant frequency control. (b) Position 3a with variable frequency control.

Fig. 5.34 Loss distribution for the SAB converter for position 3a with snubber capacitor C_s = 1.0 μF.

Table 5.10: Losses for different values of the snubber capacitor C_s for positions 1a, 2a and 3a at the average wind speed 7.2 m/s.

Position	Control	$C_s = 0$	$C_s = 1\ \mu$F	$C_s = 2.2\ \mu$F	$C_s = 4.7\ \mu$F
Pos. 1a	Const. freq.	73 kW	75 kW	84 kW	108 kW
Pos. 1a	Var. freq	76 kW	67 kW	64 kW	60 kW
Pos. 2a	Const. freq.	77 kW	77 kW	84 kW	101 kW
Pos. 2a	Var. freq	79 kW	70 kW	67 kW	64 kW
Pos. 3a	Const. freq.	78 kW	82 kW	96 kW	128 kW
Pos. 3a	Var. freq	94 kW	81 kW	76 kW	71 kW

Group Converters, Positions 1b and 2b

For the single active bridge converter as a group converter at positions 1b, 2b and 3b, the resulting losses are plotted as a fraction of the input power in Fig. 5.35 for position 1b and in Fig. 5.36 for position 2b for a) constant frequency control and b) variable frequency control. The converter for position 3b is the same as the converter for position 1b.

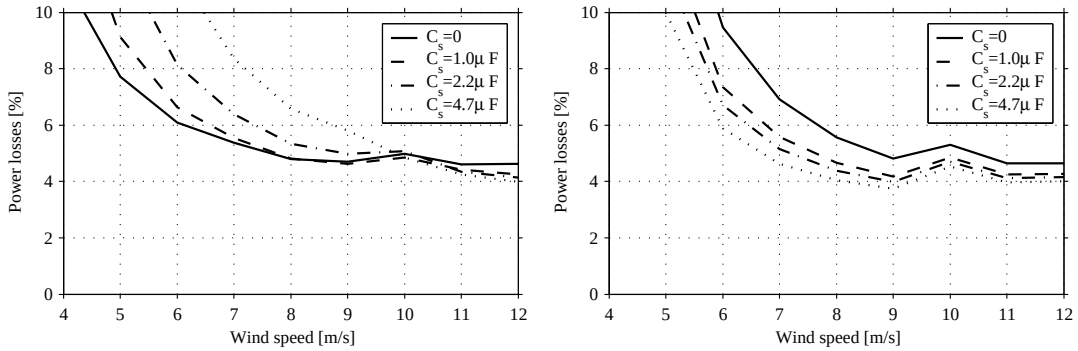

(a) Position 1b with constant frequency control. (b) Position 1b with variable frequency control.

Fig. 5.35 Losses as a fraction of input power for the SAB converter for positions 1b and 3b.

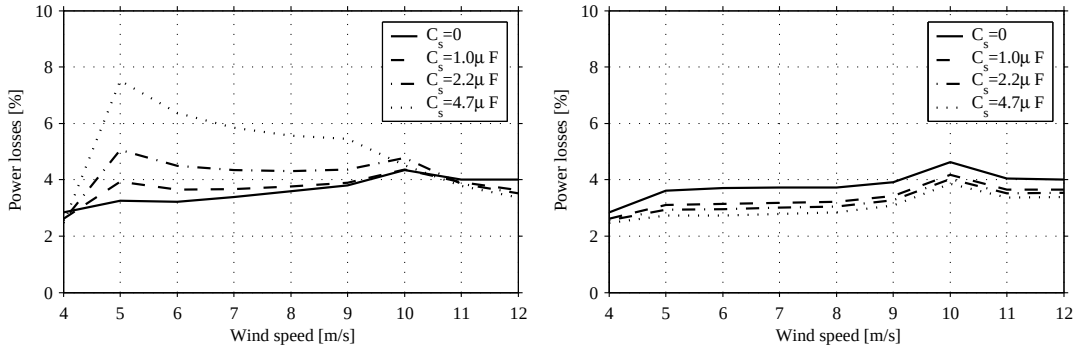

(a) Position 2b with constant frequency control. (b) Position 2b with variable frequency control.

Fig. 5.36 Losses as a fraction of input power for the SAB converter for position 2b.

In the same way as for the wind turbine converters, the losses are divided into different loss components for each converter using the snubber capacitor C_s = 1.0 μF, which is shown in Fig. 5.37 for position 1b and in Fig. 5.38 for position 2b.

The summary of the loss calculations is done in Table 5.11, with the mean value of the losses for an average wind speed of 7.2 m/s.

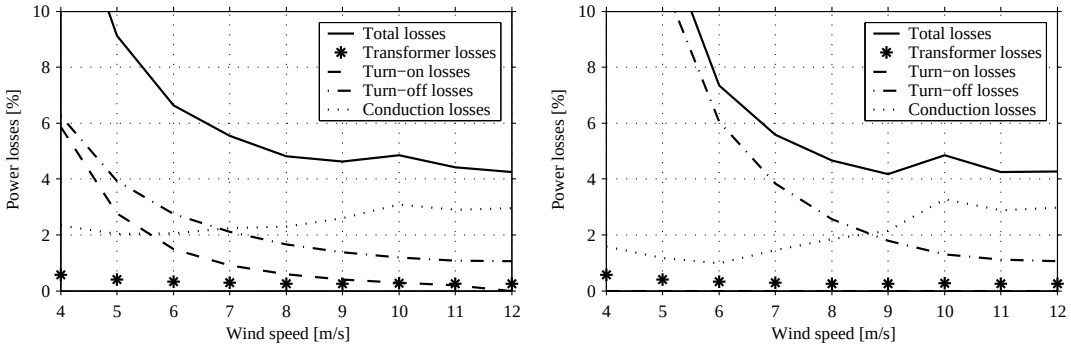

(a) Position 1b with constant frequency control. (b) Position 1b with variable frequency control.

Fig. 5.37 Loss distribution for the SAB converter for position 1b and 3b with snubber capacitor C_s = 1.0 μF.

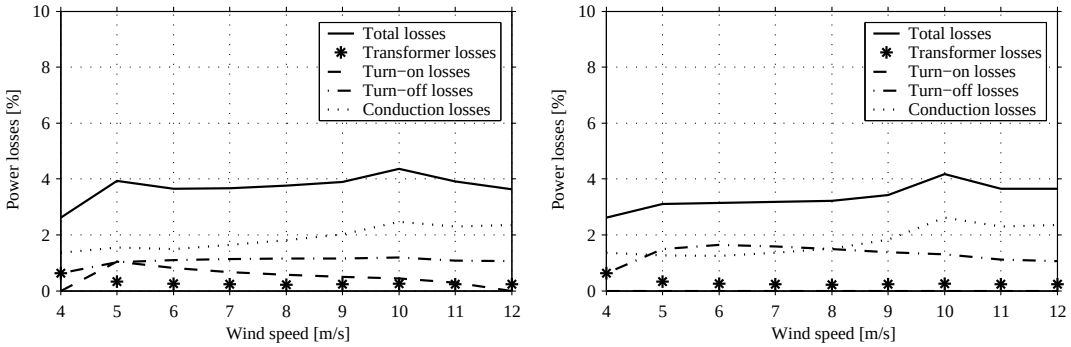

(a) Position 2b with constant frequency control. (b) Position 2b with variable frequency control.

Fig. 5.38 Loss distribution for the SAB converter for position 2b with snubber capacitor C_s = 1.0 μF.

For the converter for positions 1b and 3b, there are high losses for low wind speeds just as for position 3a due to the long off-time at low wind speeds. There is also higher turn-on losses compared to positions 1a, 2a and 3a due to the higher voltage level at the input for the group converter. The lowest average losses are achieved by variable frequency control and C_s = 4.7 μF as shown in Table 5.11. It should be noted that for the variable frequency control, the switching frequency is as high as 13 kHz at low wind speeds.

For position 2b the loss distribution is similar as for position 1b, but the losses are lower for low wind speeds since the off-time is not as long as for converter 1b. The lowest losses are achieved with variable frequency control and the snubber capacitor C_s = 4.7 μF.

Table 5.11: Losses for different values of the snubber capacitor C_s for positions 1b and 2b at the average wind speed 7.2 m/s.

Position	Control	$C_s = 0$	$C_s = 1\ \mu F$	$C_s = 2.2\ \mu F$	$C_s = 4.7\ \mu F$
Pos. 1b	Const. freq.	466 kW	458 kW	487 kW	548 kW
Pos. 1b	Var. freq	537 kW	467 kW	445 kW	418 kW
Pos. 2b	Const. freq.	367 kW	364 kW	394 kW	430 kW
Pos. 2b	Var. freq	379 kW	338 kW	325 kW	309 kW

5.5 The Series Parallel Resonant Converter

The series parallel converter was introduced in Section 3.4, where it was shown that the only way to control the converter is to change the off-time between the pulses. In this case, the resonant converter is operated in discontinuous conduction mode. It has been shown that the resonant converters has lowest losses when operating in the continuous conduction mode with snubber capacitors across the switches [38]. However, with the wide range of operating conditions shown in the previous section, the converter can not operate in the continuous conduction mode for all operating points. The snubber capacitors would then give large turn-on losses in the other cases, and therefore the converter is operated in discontinuous conduction mode for all operating points.

The design of the resonant converters must be made at the operating point with maximum transferred power. Since the maximum switching frequency should be 1 kHz and the converter should operate in discontinuous conduction mode, the resonant frequency was set to f_0 = 2 kHz. For lower power levels, the off-time between the pulses is increased. Just as in the case with the single active bridge converter, the high peak current results in that the number of modules in the input switches must be increased compared to the fullbridge converter.

5.5.1 Design Criteria

As shown in Section 3.4 and presented in Fig. 5.39, the series parallel resonant converter contains a resonant tank with a series capacitor C_r, a series inductance L_r and a parallel capacitor C_p. This resonant tank has to be designed as well as the input filter and the output filter.

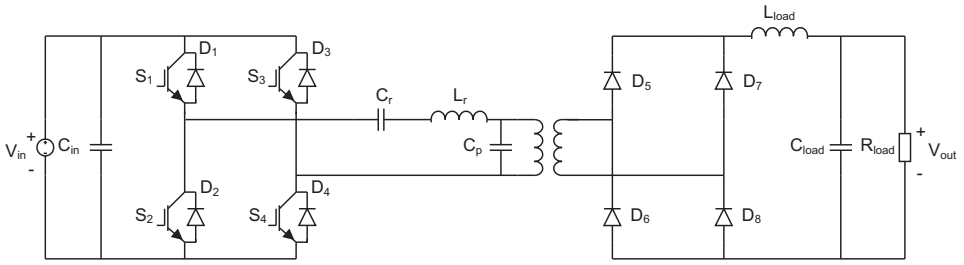

Fig. 5.39 Topology for the LCC converter.

Design of the Resonant Tank

The characteristics of the series parallel resonant converter depends on the operating point of the converter. For a small load resistance, the parallel capacitor can be seen as almost

short circuited by the load resistance and the converter will therefore behave as a series resonant converter. On the other hand, at high values of the load resistance, the characteristics of the converter will become more similar to the parallel resonant converter [38]. The main disadvantage of the series parallel resonant converter is that the output voltage can not be controlled in the no-load case. Since the series parallel resonant converter behaves as a parallel resonant converter at low loads, this disadvantage is eliminated. However, a large value of the parallel capacitor C_p results in a significant current needed for charging and discharging the capacitor once each resonant period. A large increase in the currents in the switches leads to increased conduction losses, which is not desirable. The choice of C_p is then a trade-off between the good operating characteristics of a high value of C_p and the lower conduction losses for a low value of C_p. In [38], a ratio $C_r/C_p = 1$ is stated as a good trade-off. In [9], a design with $C_r/C_p = 0.3$ is preferred since it results in lower stresses for the components and lower conduction losses.

In this design, the main focus is on achieving as low losses as possible and also low stresses for the components whereby a low value of C_p is desirable. Assuming that the value of C_p is low enough for the converter to behave as a series resonant converter at high loads, the converter can be designed as a series resonant converter. The converter is designed for the highest wind speed, which has the highest transferred power, and can then also handle the lower power levels at lower wind speeds by decreasing the switching frequency. First, the angular resonance frequency ω_0 of a series resonant converter is calculated as

$$\omega_0 = \frac{1}{\sqrt{L_r C_r}}, \tag{5.28}$$

and the characteristic impedance is calculated as

$$Z_0 = \sqrt{\frac{L_r}{C_r}}. \tag{5.29}$$

Combining 5.28 and 5.29 the values for the resonant components L_r and C_r are given by

$$C_r = \frac{1}{Z_0 \omega_0} \text{ and } L_r = C_r Z_0^2. \tag{5.30}$$

The angular resonance frequency ω_0 is determined by the desired switching frequency. Assume that the switching frequency f_s for maximum power is 1 kHz, the resonance frequency f_0 should be $f_0 = 2f_s = 2kHz$. The characteristic impedance Z_0 for a series resonant converter depends on the input voltage and the current as [12]

$$Z_0 = \frac{V_d}{I_{base}}. \tag{5.31}$$

Further, the base current I_{base} can be approximated as $I_{base} \approx 2I_{load}$, where I_{load} is the average value of the load current. Note that the transformer ratio must be taken into account.

Since the calculated value of Z_0 applies for a series resonant converter and no losses are considered in the calculations, the value of Z_0 must be slightly modified for the converter to have the desired characteristics in the simulations.

The value of C_p/C_r is chosen to be between 0.12 and 0.19 to limit the current needed for charging the parallel capacitor C_p. For the converters designed for one turbine, positions 1a, 2a and 3a, the same design of the converters can be used. This is due to that the operation conditions are identical for the highest wind speeds, which also determines the design of the converter. For operating at lower wind speeds, the converter achieves the correct output voltage by lowering the switching frequency. For the group DC/DC converter, the design for converter differs between the different control strategies. For position 2b, the transformer must have a minimum ratio of $75/6 = 12.5$ for achieving an output voltage of 75 kV at wind speed 4 m/s since the series resonant converter just can operate as a step-down converter. The converter for position 1b needs a minimum transformer ratio of $75/15 = 5$ and therefore is the design for converter 2b not suitable for converter 1b. Also, the larger transformer ratio for position 2b gives a lower voltage and higher current on the primary side of the transformer. This results in that a smaller amount of the input current is needed to charge the parallel capacitor C_p, and therefore the slightly higher value $C_p/C_r = 0.19$ is chosen in this case. For position 1b, the voltage is higher and the current is lower for the primary side of the transformer and therefore a lower value $C_p/C_r = 0.12$ is chosen. The resulting parameters for the resonant converters are shown in Table 5.12.

Table 5.12: Values for the components in the resonant tank.

Positions		1a, 2a and 3a	1b	2b
Parallel capacitor	C_p	10.0 μF	3.0 μF	8.0 μF
Resonant capacitor	C_r	69.2 μF	24.3 μF	41.9 μF
Resonant inductance	L_r	91.5 μH	310 μH	151 μH
Transformer ratio	n	7.75	7.42	13.42

These values are used for simulating the resonant converters for all positions and for wind speeds between 4 and 12 m/s. The resulting frequencies for the resonant converter are shown in Fig. 5.40.

The converters for positions 1b and 3a have the largest decrease in switching frequency at low wind speeds. This is due to the constant voltage levels and the decreasing power.

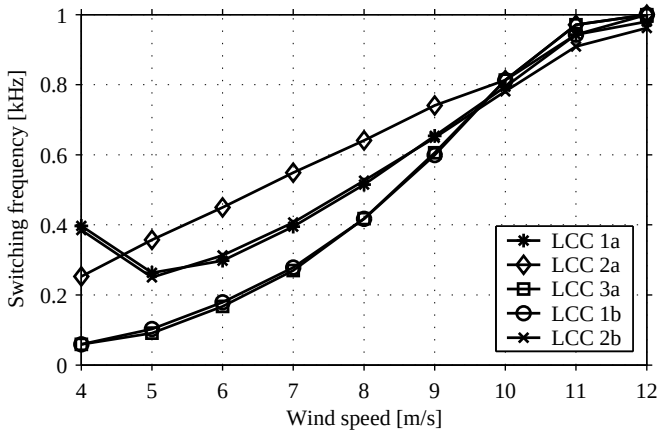

Fig. 5.40 Switching frequency for the resonant converter using variable frequency control.

If the voltage levels are constant, the current pulses are identical and the switching frequency must be roughly proportional to the transferred power. For converter 2a, both the input and output voltages are lower at lower wind speeds giving lower peak current and lower energy contents in each resonant pulse at lower wind speeds. The decrease in the switching frequency is then considerable lower than for the other positions. Finally, for positions 1a and 2b the input voltage is lowered at low wind speeds while the output voltage is constant resulting is a decrease of the frequency in between converter 2a and converters 1b and 3a. At wind speed 4 m/s there is an increase in the frequency since the ratio of the transformer is not much larger than the ratio between the output voltage and the input voltage.

Filter Design

For the resonant converter, as well as for the single active bridge converter, both the input filter and the output filter are voltage stiff and can be simplified as capacitors. Starting with the input filter, the ripple in the input voltage ΔV_{in} can be calculated as

$$\Delta V_{in} = \frac{1}{C_{in}} \left(\frac{2 i_{max}}{\omega_0} - \frac{I_{in}}{\omega_0} \left(\pi - \frac{I_{in}}{\omega_0 i_{max}} \right) \right), \tag{5.32}$$

where i_{max} is the peak current in the resonant pulse on the primary side, I_{in} is the DC input current and C_{in} is the value of the input capacitor. Assuming that the maximum peak-to-peak voltage ripple is $\Delta V_{in} = 0.1 V_{in}$, the minimum value of the input capacitor is calculated as

$$C_{in} = \frac{10}{V_{in}} \left(\frac{2 i_{max}}{\omega_0} - \frac{I_{in}}{\omega_0} \left(\pi - \frac{I_{in}}{\omega_0 i_{max}} \right) \right). \tag{5.33}$$

The resulting values for the input capacitor C_{in} are shown in Fig. 5.41. It can be seen that the value needed for limiting the voltage ripple increases with decreasing wind speed.

This is due to the decreasing frequency resulting in an increasing off-time between the current pulses at low wind speeds. The only exceptions are positions 1a and 2b where the switching frequency increases at the lowest wind speeds and the needed capacitor will therefore increase. Position 2b has a higher demand for the input capacitor since the large transformer ratio requires a large current on the primary side.

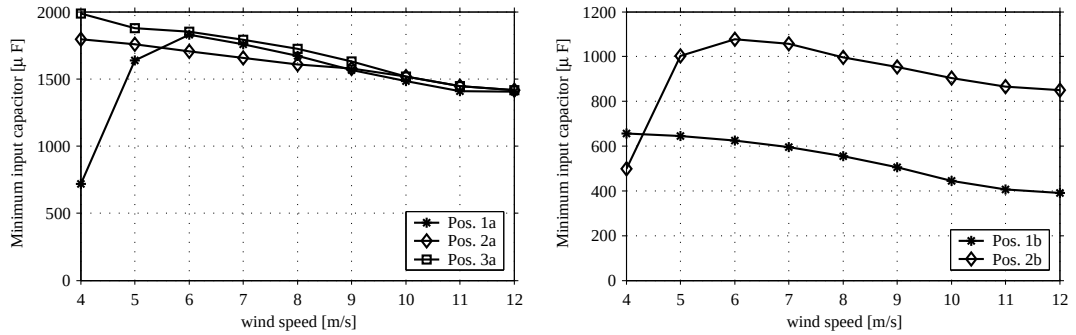

(a) Positions 1a, 2a and 3a.

(b) Positions 1b and 2b.

Fig. 5.41 Minimum input capacitor C_{in} for the LCC converter.

For the output capacitor C_{load}, the value is calculated in two different ways depending on if the output current I_{load} is larger than the peak current i_{max2} of the secondary resonant swing (when the freewheeling diodes are conducting in the input bridge). In the calculations of C_{load}, the peak currents i_{max} and i_{max2} refer to the secondary side of the transformer, as in (5.34) and (5.35). The results for the output capacitor are similar as the results for the input capacitor, a lower wind speeds gives larger off time and a larger capacitor is needed, except for positions 1a and 2b where the switching frequency increases at the lowest wind speeds.

$$C_{load} = \frac{10}{V_{load}} \left(\frac{2i_{max}}{\omega_0} - \frac{I_{load}}{\omega_0} \left(\pi - \frac{I_{load}}{\omega_0 i_{max}} \right) \right) \quad \text{if } I_{load} > i_{max2} \tag{5.34}$$

$$C_{load} = \frac{10}{V_{load}} \left(\frac{2}{\omega_0}(i_{max} + i_{max2}) - \frac{2I_{load}\pi}{\omega_0} + \frac{I_{load}^2}{\omega_0^2} \left(\frac{1}{i_{max}} + \frac{1}{i_{max2}} \right) \right) \quad \text{if } I_{load} < i_{max2} \tag{5.35}$$

The resulting values for C_{load} are shown in Fig. 5.42 and the maximum values are summarized for the converters in Table 5.13. Since the largest capacitor needed for maintaining the voltage ripple below 10 % is at the lowest wind speed, the capacitor can be made smaller by allowing a larger voltage ripple at low wind speeds. In Table 5.13, the capacitor values needed for limiting the voltage ripple at all wind speeds are presented as well as the capacitor needed to limit the voltage ripple at wind speeds above 8 m/s.

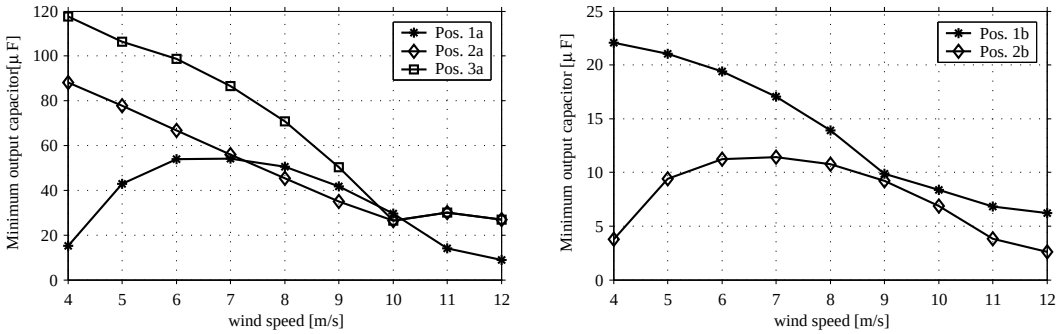

(a) Positions 1a, 2a and 3a.

(b) Positions 1b and 2b.

Fig. 5.42 Minimum output capacitor C_{load} for the LCC converter.

Table 5.13: Minimum values for the filter components for the LCC converters.

	Pos. 1a	Pos. 2a	Pos. 3a	Pos. 1b	Pos. 2b
C_{in}	1830 μF	1800 μF	1990 μF	660 μF	1080 μF
$C_{in} > 8\,m/s$	1670 μF	1610 μF	1720 μF	560 μF	1000 μF
C_{load}	54 μF	88 μF	118 μF	22 μF	11 μF
$C_{load} > 8\,m/s$	51 μF	45 μF	71 μF	14 μF	11 μF

5.5.2 Losses in the Series Parallel Resonant Converter

For the resonant converter, no snubber capacitors are needed to achieve soft switching and just one control strategy is considered. Therefore, the design of the converter is already determined as shown in Table 5.12. The resulting losses are plotted as a fraction of the input power in Fig. 5.43 (a) for positions 1a, 2a and 3a and in Fig. 5.43 (b) for positions 1b and 2b. Also note that the converter for position 3b is the same as the converter for position 1b.

The loss distributions for the converters are shown in Fig. 5.44 for positions 1a, 2a and 3a and in Fig. 5.45 for positions 1b and 2b. Also, the losses for the resonant converter are summarized in Table 5.14 for an average wind speed of 7.2 m/s.

The resulting losses for the resonant converter show no significant differences for positions 1a, 2a and 3a. For the group converter the losses are higher for position 2b than for position 1b caused by higher conduction losses in the switches. The higher conduction losses is a result of the lower input voltage due to the higher transformer ratio that gives a higher input current.

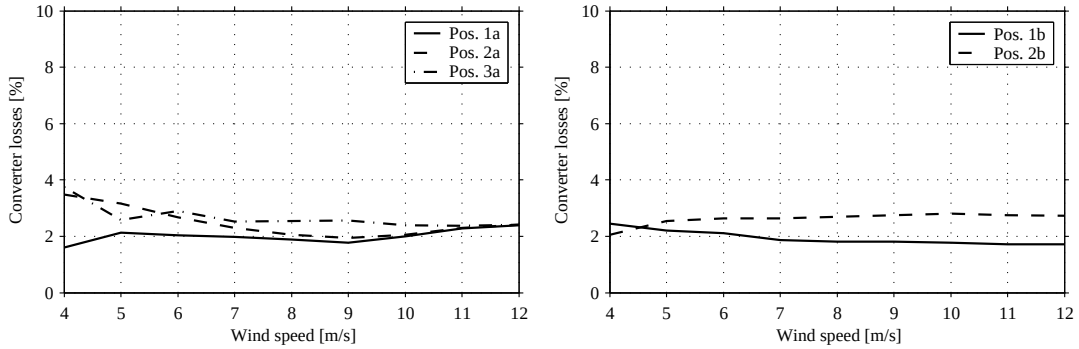

(a) Positions 1a, 2a and 3a.

(b) Positions 1b and 2b.

Fig. 5.43 Losses as a fraction of input power for the LCC converter.

Table 5.14: Average energy loss for the resonant converters at the average wind speed 7.2 m/s.

Position	
1 a	40.5 kW, 2.14 %
1 b	169 kW, 1.79 %
2 a	43.2 kW, 2.28 %
2 b	257 kW, 2.72 %
3 a	46.7 kW, 2.47 %
3 b	169 kW, 1.79 %

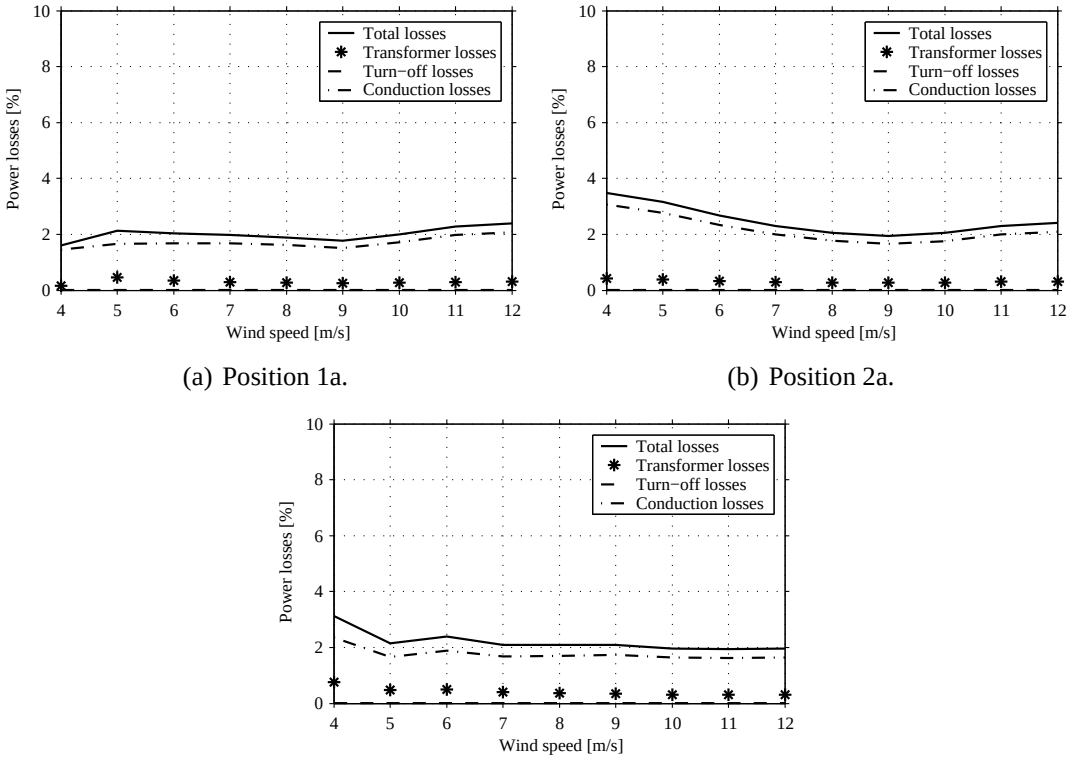

(a) Position 1a.

(b) Position 2a.

(c) Position 3a.

Fig. 5.44 Loss distribution for the LCC converter for positions 1a, 2a and 3a.

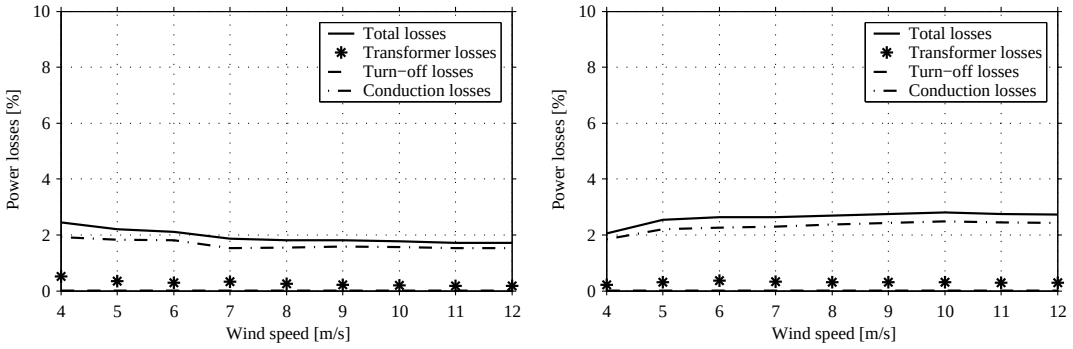

(a) Position 1b.

(b) Position 2b.

Fig. 5.45 Loss distribution for the LCC converter for positions 1b and 2b with snubber capacitor.

5.6 Evaluation of the Converters for the Local Wind Turbine Grid

In this chapter, the operating conditions for the converters have been determined using the local wind turbine grid. For all three topologies considered, the converters have been designed for each position in the local wind turbine grid and the losses have been calculated as a function of the wind speed. In this section, both the topologies and the control methods are evaluated regarding the losses and need of components. Comments are also made on how the converters are affected by the wide range of operating conditions in a wind farm application. Finally, the contribution to the energy production cost is determined for the different converters and the different control strategies.

5.6.1 Loss Comparison for the Local Wind Turbine Grid

In Tables 5.15, 5.16, and 5.17, the losses for the converters are shown for three different average wind speeds for the fullbridge converter, the single active bridge converter and the resonant converter. The chosen snubber capacitor for the fullbridge and single active bridge converters and the control method for the single active bridge converter used is what was found to give the lowest losses in the design of the converters. It should be noted that the average transferred power for the mean values 5.4 m/s, 7.2 m/s and 10 m/s for the wind for the speed is 1.03 MW, 1.89 MW and 2.90 MW for one turbine and 5.13 MW, 9.46 MW and 14.51 MW for the group converter. In Fig. 5.46, the losses are shown for each position for all three topologies.

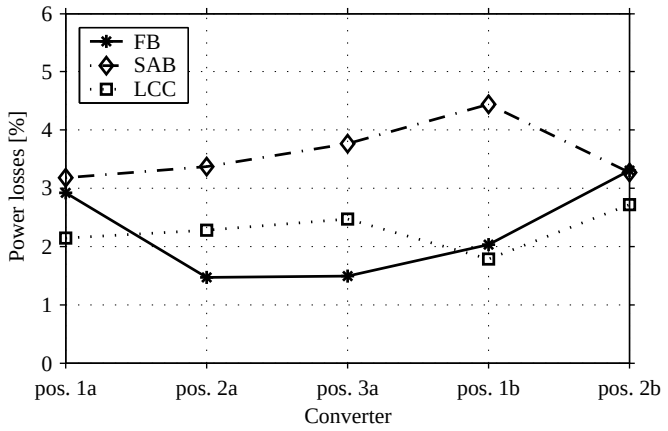

Fig. 5.46 Converter losses for each position for the average wind speed 7.2 m/s.

For the fullbridge converter, the losses are lowest for the converter at position 2a which has a constant ration between the input voltage and the output voltage as well as a low

Table 5.15: Energy loss for the fullbridge converters at different average wind speeds.

Pos.	snubber	5.4 m/s	7.2 m/s	10 m/s
1 a	C_s = 1 μF	27.8 kW, 2.71 %	55.3 kW, 2.92 %	89.0 kW, 3.07 %
1 b	C_s = 1 μF	110 kW, 2.15 %	192 kW, 2.03 %	288 kW, 1.98 %
2 a	C_s = 1 μF	15.5 kW, 1.52 %	27.8 kW, 1.47 %	42.2 kW, 1.46 %
2 b	C_s = 1 μF	158 kW, 3.08 %	305 kW, 3.30 %	503 kW, 3.47 %
3 a	C_s = 1 μF	16.4 kW, 1.60 %	28.3 kW, 1.50 %	42.4 kW, 1.46 %
3 b	C_s = 1 μF	110 kW, 2.15 %	192 kW, 2.03 %	288 kW, 1.98 %

input voltage at low power. The losses are higher for positions 1a and 2b where the converter has to compensate for the varying voltage level.

Table 5.16: Energy loss for the single active bridge converters at different average wind speeds.

Pos.	control	5.4 m/s	7.2 m/s	10 m/s
1 a	var. freq. C_s = 4.7 μF	31.9 kW, 3.11 %	60.2 kW, 3.18 %	93.9 kW, 3.23 %
1 b	var. freq. C_s = 4.7 μF	257 kW, 5.05 %	420 kW, 4.44 %	608 kW, 4.19 %
2 a	var. freq. C_s = 4.7 μF	35.5 kW, 3.47 %	63.8 kW, 3.37 %	96.6 kW, 3.33 %
2 b	var. freq. C_s = 4.7 μF	163 kW, 3.19 %	309 kW, 3.27 %	483 kW, 3.33 %
3 a	var. freq. C_s = 4.7 μF	44.6 kW, 4.35 %	71.2 kW, 3.76 %	101.5 kW, 3.50 %
3 b	var. freq. C_s = 4.7 μF	257 kW, 5.05 %	420 kW, 4.44 %	608 kW, 4.19 %

For the single active bridge converter where the losses are summarized in Table 5.16, the converters for positions 3a and 1b has the highest losses due to the high switching frequency at low wind speeds.

In Table 5.17 it is shown that the resonant converters have similar losses for all positions except positions 2b that has higher losses. This is due to the high transformer ratio needed that increases the current on the primary side and thereby also the conduction losses. Also,

Table 5.17: Energy loss for the resonant converters at different average wind speeds.

Pos.	5.4 m/s	7.2 m/s	10 m/s
1 a	20.9 kW, 2.04 %	40.5 kW, 2.14 %	65.1 kW, 2.24 %
1 b	94 kW, 1.84 %	169 kW, 1.79 %	254 kW, 1.75 %
2 a	23.5 kW, 2.29 %	43.2 kW, 2.28 %	67.4 kW, 2.32 %
2 b	138 kW, 2.70 %	257 kW, 2.72 %	396 kW, 2.73 %
3 a	25.7 kW, 2.51 %	46.7 kW, 2.47 %	70.7 kW, 2.44 %
3 b	94 kW, 1.84 %	169 kW, 1.79 %	254 kW, 1.75 %

the converter for position 3a has high losses.

The total converter losses for the local wind turbine grid, where the same converter topology is used for both wind turbine converter and group converter, are shown in Table 5.18 and the results are plotted in Fig. 5.47 for (a) the fullbridge converter, (b) the single active bridge converter and (c) the resonant converter.

Table 5.18: Energy losses for the control strategies at different average wind speeds.

Control	5.4 m/s	7.2 m/s	10 m/s
1 FB	249 kW, 4.86 %	468 kW, 4.95 %	733 kW, 5.05 %
2 FB	236 kW, 4.60 %	452 kW, 4.78 %	715 kW, 4.93 %
3 FB	192 kW, 3.75 %	333 kW, 3.52 %	500 kW, 3.45 %
1 SAB	417 kW, 8.14 %	721 kW, 7.62 %	1077 kW, 7.42 %
2 SAB	341 kW, 6.66 %	628 kW, 6.64 %	965 kW, 6.66 %
3 SAB	480 kW, 9.38 %	776 kW, 8.20 %	1115 kW, 7.69 %
1 LCC	199 kW, 3.89 %	372 kW, 3.93 %	580 kW, 4.00 %
2 LCC	256 kW, 4.99 %	473 kW, 5.00 %	733 kW, 5.05 %
3 LCC	223 kW, 4.35 %	402 kW, 4.25 %	608 kW, 4.19 %
Power	5.1 MW	9.5 MW	14.5 MW

It can be seen that control strategy 3 using the fullbridge converter is the control strategy

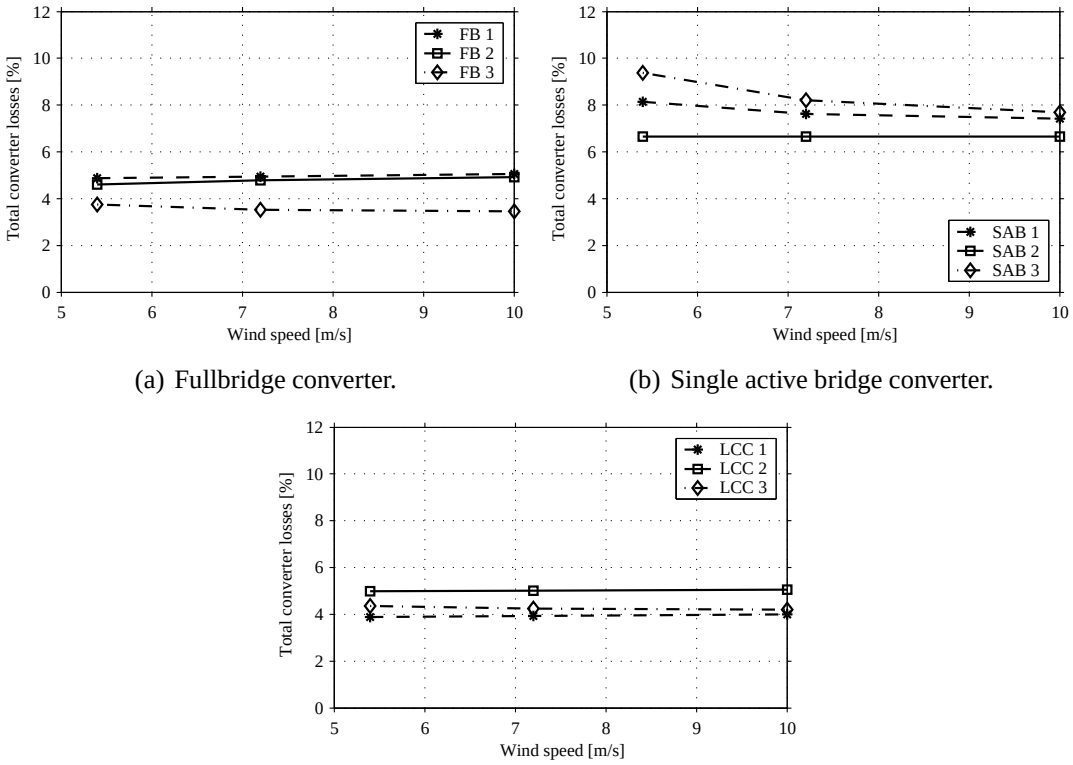

(a) Fullbridge converter.

(b) Single active bridge converter.

(c) Series parallel resonant converter.

Fig. 5.47 Total converter losses for the local wind turbine grid for the different topologies using control strategies 1, 2 and 3.

with the lowest losses. The local wind farm using the single active bridge converter has considerable higher losses than the other topologies.

5.6.2 Required Transformer, Filter and Semiconductor Components

As well as the losses of the converter, an important issue for the choice of converter topology and control strategy is the required transformer and the need for semiconductor components and filter components. Here, the weight of the transformer is considered as well as the number of IGBT and diode modules needed and the required filter components.

Transformer

The weight of the transformers for the different converters is presented in Table 5.19. It can be seen that the weight of the transformer increases with increased transformer ratio.

Table 5.19: Transformer parameters.

Converter	Transformer ratio	Leakage inductance	Weight
FB 1a	8.36	20 μH	2145 kg
FB 2a	3.32	20 μH	1579 kg
FB 3a	3.32	20 μH	1579 kg
FB 1b	5.48	20 μH	7532 kg
FB 2b	14.14	30 μH	13831 kg
SAB 1a	7.87	200 μH	1906 kg
SAB 2a	7.87	200 μH	1906 kg
SAB 3a	7.87	200 μH	1906 kg
SAB 1b	13.00	352 μH	9231 kg
SAB 2b	13.00	352 μH	9231 kg
LCC 1a	7.75	92 μH	3349 kg
LCC 2a	7.75	92 μH	3592 kg
LCC 3a	7.75	92 μH	3595 kg
LCC 1b	7.42	310 μH	16929 kg
LCC 2b	13.42	151 μH	60438 kg

For the fullbridge converter, the converters for positions 2a, 3a and 1b with constant ratio between the input and output voltage has the lowest weight of the transformer. Positions 1a and 2b has higher weight of the transformer. For the resonant converter, the transformer is a part of the resonant tank resulting in a higher peak voltage for the transformer. The high peak voltage as well as the high current in the transformer gives heavy and bulky converters.

Semiconductor Components

The second issue is the number of semiconductor modules for the converters, which is summarized in Table 5.20. Here, the number of modules with rated voltage 2.5-3 kV and rated current 2 kA are listed. In the cases where the rms-current is significantly lower than 2 kA, it is assumed that there is a module available with a lower number of sub-modules resulting in modules with ratings of 1 kA for 0.5 modules.

Table 5.20: Number of IGBT and diode modules needed for the converters.

	Input bridge		Output bridge	
Converter position	Parallel	Series	Parallel	Series
FB 1a	2	5	0.5	40
FB 2a	1	5	0.5	16
FB 3a	1	5	0.5	16
FB 1b	1	15	0.5	82
FB 2b	3	15	0.5	212
SAB 1a	2	5	0.5	15
SAB 2a	2	5	0.5	15
SAB 3a	2	5	0.5	15
SAB 1b	2	15	0.5	75
SAB 2b	3	15	0.5	75
LCC 1a	2	5	0.5	15
LCC 2a	2	5	0.5	15
LCC 3a	2	5	0.5	15
LCC 1b	2	15	0.5	75
LCC 2b	3	15	0.5	75

For the input bridge, the need for IGBT modules is 2 parallel connected and 5 series connected modules for the wind turbine converters and 2 parallel connected and 15 series connected modules for the group converters. The only exceptions are the fullbridge converters for position 2a, 3a and 1b with constant voltage ratio where just 1 module is needed in parallel and for position 2b for all topologies where 3 series connected modules are needed. For the output bridge, just 0.5 diode modules are needed in parallel for all converters. For the single active bridge converter and the resonant converters with voltage stiff output, 15 series connected modules are needed for the wind turbine converters

and 75 series connected modules are needed for the group converter. For the fullbridge converter, the current stiff output increases the maximum voltage across the rectifying bridge and thereby also a larger number of series connected diode modules are needed. This increase is largest for positions 1a and 2b with varying voltage ratio.

Filter Components

When designing the converters, the input and output filters are designed to limit the peak-to-peak ripple in the output and input currents and voltages to 10 % of the DC values. The dimensioning was done by approximating the voltage-stiff filter with a capacitor and the current-stiff output filter for the fullbridge converter with an inductance. The resulting demand for the filter components are shown in Table 5.21.

Table 5.21: Components needed for the input filter and output filter.

Converter position	C_{in}	C_{load}	L_{load}
FB 1a	641 μF	-	700 mH
FB 2a	97 μF	-	90 mH
FB 3a	97 μF	-	530 mH
FB 1b	49 μF	-	2400 mH
FB 2b	360 μF	-	3800 mH
SAB 1a	1200 μF	28 μF	-
SAB 2a	1200 μF	28 μF	-
SAB 3a	1200 μF	28 μF	-
SAB 1b	440 μF	10 μF	-
SAB 2b	440 μF	10 μF	-
LCC 1a	1830 μF	54 μF	-
LCC 2a	1800 μF	88 μF	-
LCC 3a	1990 μF	118 μF	-
LCC 1b	660 μF	22 μF	-
LCC 2b	1080 μF	11 μF	-

5.6.3 Sensitivity to Varying Operating Conditions

For the DC/DC converter topologies studied in this thesis, the fullbridge converter using phase shift control, the single active bridge converter and the series parallel resonant converter, previous work have been done considering design and losses for these topologies. In this thesis, these converters are studied for the wind farm application and it is therefore interesting to see how the losses of a converter are affected by this wide range of operating conditions. If a converter is designed for a single operating point, the losses can be reduced by choosing a suitable transformer ratio and leakage inductance as well as a suitable snubber capacitor. However, if the converter is designed for all operating points in a wind farm, the losses will be higher at most operating points compared to a converter designed for only one specific operating point. Here, the increase in losses due to the wide range of operating conditions will be discussed for all three topologies.

The Fullbridge Converter

The fullbridge converter has a current stiff output and the output voltage is proportional to the duty ratio of the converter for a constant input voltage. For the converters at positions 2a, 3a and 1b with constant ratio between the input and output voltage, the duty cycle is constant and can therefore be close to 0.5 for all operating points. If the voltage ratio is varying, as for positions 1a and 2b, the transformer must be designed for the case with the highest voltage ratio which is the lowest wind speed. When these converters are operating at higher wind speeds with lower transformer ratio, the duty cycle must be lower to achieve the desired output voltage. If this converter is compared to a converter designed for that high wind speed, the converter designed for one operating point would have a lower transformer ratio and also a lower on-state current for the input bridge for the same output current. The higher on-state current for the converter designed for all operating points will then result in higher turn-off losses that are proportional to the current at turn-off and therefore also higher total losses. In Figs. 5.16 and 5.17, it can be seen that converters 1a and 2b with varying voltage ratio have higher losses at higher wind speeds than converters 2a, 3a and 1b with constant voltage ratio. Also the conduction losses are higher for positions 1a and 2b since the rms-value of the current in the input bridge is higher. The semiconductor components are conducting also in the off-state, resulting in large conduction losses in the case of a large current even if the duty cycle is low. It should be noted that the converters for these positions have 2 and 3 IGBT modules connected in parallel for the switches in the input bridge compared to 1 module in parallel for the other topologies.

The wide range of operating conditions also makes the design of the snubber capacitor difficult. For a high wind speed where there is a high current, a large value is needed for the snubber capacitor to increase the rise time of the voltage and thereby achieve

soft switching. However, for a low wind speed with lower current the snubber capacitor needed at high wind speed is too large. The rise time of the voltage will then be very slow and it will also take a long time for the snubber capacitor to be discharged. This will result in high turn-on losses at low wind speeds as seen in Fig. 5.18, whereby the most suitable choice will be a small value of the snubber capacitor or no snubber capacitor.

The variable operating conditions gives a large fraction of core losses in the transformer at low power levels. Since the core losses just are dependent on the voltage applied at the transformer, the case with low current and high voltage with a high duty cycle gives a large fraction of core losses. This is most significant for positions 3a and 1b that have high voltage levels and high duty cycle even at low wind speeds.

The Single Active Bridge Converter

For the single active bridge converter, the duty cycle of the converter is affected both by the voltage levels and the transferred power. If the single active bridge converter is controlled using the constant frequency control, a high duty cycle is preferable in the same way as for the fullbridge converter. However, unlike the fullbridge converter, the single active bridge converter must be designed for the highest wind speed with the largest transferred power. For lower wind speeds, the duty cycle must be lowered to limit the transferred power. In the case of positions 1a and 2b with varying ratio between the input voltage and the output voltage, the duty cycle is also large at the lowest wind speed. For positions 3a and 1b with constant voltage levels, the current slope is constant for all operating points for both the positive and negative slopes. Therefore a large reduction in the duty cycle is needed to reduce the power contents in each pulse, which should be proportional to the output power. For position 2a, both the input and output voltages are lower at low wind speeds resulting in a slower increase in the current in the leakage inductance. A slower increase in the current as well as a lower output voltage gives a larger duty cycle at low wind speeds. For positions 1a and 2b with varying input voltage and constant output voltage, the duty cycle is slightly higher than for position 2a at low wind speeds due to the smaller difference between the input voltage and the output voltage. On the other hand, the fall time of the voltage is decreased by the larger sum of the input voltage and the output voltage resulting in a fairly constant off-time, except for the lowest wind speeds. In the same way as for the fullbridge converter, the efficiency is lowered in the operating points with a decreased duty cycle compared with a converter that is designed especially for that operating point. The difference is that the decrease in duty cycle occurs at low wind speeds with low transferred power compared to the fullbridge converter where the decrease in duty cycle occurs at high wind speeds with a large transferred power. In Figs. 5.29, 5.30 and 5.31 this is shown for the wind turbine converter and the converter for position 3a has the highest losses for low wind speeds due to the low duty cycle. The same applies for the group converters where the converter for position 1b has higher losses at

low wind speeds than the converter for position 2b.

For the single active bridge converter using variable frequency control, there is an increase in the frequency which is linked to the decrease in duty cycle for the constant frequency control. In Fig. 5.26, it is shown that the switching frequency is increased the most for positions 3a and 1b where the decrease in duty cycle also is most significant. An increased frequency results in increased losses as shown in Figs. 5.29, 5.30 and 5.31 as well as in Figs. 5.35 and 5.36.

The Series Parallel Resonant Converter

The resonant converter is controlled by varying the off-time between the resonant pulses by changing the switching frequency and, similar to the single active bridge converter, this off-time depends on both the transferred power and the voltage levels for the converter. The converters are designed to have zero off-time at full power, and the switching frequency is decreased at lower power levels to decrease the transferred power. For the converters at positions 3a and 1b with constant ratio between the input voltage and the output voltage, the shape of the resonant current pulse is the same with the same energy content for all operating points. The switching frequency will then be decreased proportionally to the decreasing power as seen in Fig. 5.40. For positions 1a and 2b where the input voltage varies and the output voltage is constant, the energy in each pulse and the peak current decreases with decreasing input voltage at low wind speeds. The switching frequency is then higher at low wind speeds due to the decreased energy in each resonant pulse compared to positions 1a and 2b. In the case of position 2a, both the input voltage and the output voltage are decreased at low wind speeds leading to even lower energy content in each pulse and therefore a higher switching frequency at low wind speeds. From the resulting losses shown in Fig. 5.43, it can be seen that the losses increase at low wind speeds where there is a long off-time between the current pulses. However, the main disadvantage with the long off-time at low wind speeds is the high demands on the input and output filters, and it is also hard to design the filters for a variable frequency.

5.6.4 Cost Evaluation

For evaluating the cost of the converters, the contribution from each converter to the energy production cost is estimated using both the investment cost for the converter and the cost for the losses in the converter.

Investment Costs

Starting with the investment costs, the costs are estimated for the different parts of the converter adding up to a total investment cost. It is assumed that the two most significant contributions to the investment cost are from the transformer and the semiconductor components, and the other costs will not be considered.

For the transformer, the cost is estimated using the volume of the core and the windings. The estimation is made that the total cost of the transformer is twice the cost of the core material and the copper in the windings. As a result, the cost of the transformer K_{trafo} is estimated as

$$K_{trafo} = 2\left(V_{core}Kr_{core} + V_{Cu}Kr_{Cu}\right), \tag{5.36}$$

where Kr_{core} and Kr_{Cu} are the costs for the core material and the copper for the windings per m^3 and V_{core} and V_{Cu} are the volumes for the core and the copper for the windings.

For the semiconductor components, the cost is the number modules times the cost for each module. Also, the mounting and drive circuit is assumed to be included in the prize of the semiconductor module whereby the total cost for the semiconductor components K_{semi} can be calculated as

$$K_{semi} = N_{IGBT}Kr_{IGBT} + N_{diode}Kr_{diode}. \tag{5.37}$$

Here, N_{IGBT} and N_{diode} are the number of IGBT modules and the number of diode modules in the converter and Kr_{IGBT} and Kr_{diode} are the costs for an IGBT module and a diode module. The assumed cost for a semiconductor module given in Table 5.23, is for one semiconductor module and the number of modules are summarized in Table 5.20. The total cost for the converter K_{conv} is assumed to be the sum of the cost of the components plus 50 % for additional costs. The total cost is then calculated by

$$K_{conv} = 1.5\left(K_{trafo} + K_{semi}\right). \tag{5.38}$$

The cost for each component and the total cost for each converter are summarized in Table 5.22. Additionally, the costs for the semiconductor modules and the material prize for the transformer used in the cost calculations are presented in Table 5.23.

Table 5.22: Investment costs for the converters and the different components.

Converter pos.	K_{trafo}	K_{semi}	K_{conv}
FB 1a	173 kSEK	1520 kSEK	2539 kSEK
FB 2a	127 kSEK	688 kSEK	1222 kSEK
FB 3a	127 kSEK	688 kSEK	1222 kSEK
FB 1b	567 kSEK	2676 kSEK	4865 kSEK
FB 2b	1035 kSEK	7416 kSEK	12676 kSEK
SAB 1a	159 kSEK	1070 kSEK	1844 kSEK
SAB 2a	159 kSEK	1070 kSEK	1844 kSEK
SAB 3a	159 kSEK	1070 kSEK	1844 kSEK
SAB 1b	673 kSEK	3750 kSEK	6634 kSEK
SAB 2b	673 kSEK	4950 kSEK	8434 kSEK
LCC 1a	269 kSEK	1070 kSEK	2009 kSEK
LCC 2a	289 kSEK	1070 kSEK	2036 kSEK
LCC 3a	289 kSEK	1070 kSEK	2037 kSEK
LCC 1b	1236 kSEK	3750 kSEK	7478 kSEK
LCC 2b	3954 kSEK	4950 kSEK	13355 kSEK

Cost Comparison

For comparing the costs for the different converters, the contribution from the converter to the energy production cost E_{conv} is calculated. There are two parts of the contribution, the investment cost and the cost for the losses. For the calculation of the contribution from the investment cost E_{inv}, the number of operational hours per year are assumed to be $T_o = 24 \cdot 365 = 8760$ h. For calculating the energy production cost, first the the total energy production for the wind farm E_{farm} is calculated as

$$E_{farm} = \frac{K_{farm}}{P_{out,avg} T_o} \frac{r(1+r)^{N_y}}{(1+r)^{N_y} - 1} \frac{100}{100 - Pr} = C_{cost} \frac{K_{farm}}{P_{out,avg}}. \tag{5.39}$$

where r is the interest rate, N_y is the life time in years, Pr is the profit in % and C_{cost} is a constant. The contribution to the energy production cost from the investment cost for the converter E_{inv} can be calculated as

$$E_{inv} = C_{cost} \frac{K_{conv}}{P_{in,avg}}. \tag{5.40}$$

Apart from the investment costs for the converter, the cost of the losses should be added

Table 5.23: Semiconductor device and material cost.

Component		Cost	
IGBT module	Kr_{IGBT}	20000	[SEK/st]
diode module	Kr_{diode}	9000	[SEK/st]
Core material	Kr_{core}	300000	[SEK/m^3]
Copper	Kr_{Cu}	440000	[SEK/m^3]

to the total cost for the converter. The contribution from the converter losses to the total energy production cost E_{loss} can be calculated as

$$E_{loss} = C_{cost}\frac{K_{farm}}{P_{in,avg}}\frac{P_{loss,avg}}{P_{out,avg}} = E_{farm}\frac{P_{loss,avg}}{P_{in,avg}}. \tag{5.41}$$

The total contribution to the energy production cost is then calculated as

$$E_{conv} = E_{inv} + E_{loss}. \tag{5.42}$$

Assuming an interest rate $r = 4$ %, a life time $N_y = 15$ years and a profit $Pr = 8$ %, the resulting energy production cost and the contributions from the investment cost and from the cost of the losses are found in Table 5.24 and in Fig. 5.48. The profit of 8 % might be underestimated, but since it varies between different energy producers, the value of $Pr = 8$ % is used in these calculations. Further, the calculation of the costs are based on an average wind speed of 7.2 m/s and that the assumption that the energy production cost of the wind farm E_{farm} is 0.5 SEK/kWh. The fact that the resonant converter does not require snubber capacitors is not considered, but on the other hand a large resonant capacitor is needed for the resonant converter.

From the figures, it can be seen that the contribution to the energy production cost from the losses is similar as the contribution from the investment cost for all converters. Regarding the investment cost, the cost of the semiconductor components is dominating for all converters.

Comparing the different topologies as in Fig. 5.49, it can be seen that the fullbridge converter has the lowest contribution to the energy production cost for positions 2a, 3a and 1b while the resonant converter has the lowest contribution for position 1a. For position 2b, the single active bridge converter has the lowest contribution to the energy production cost. Using the topologies with the lowest cost, the contribution to the energy production cost from he converters in the local wind turbine grid are shown in Fig. 5.50 and

Table 5.24: Contribution to the energy production cost from each converter.

Converter pos.	E_{inv} [SEK/kWh]	E_{loss} [SEK/kWh]	E_{conv} [SEK/kWh]
FB 1a	0.0150	0.0146	0.0296
FB 2a	0.0072	0.0074	0.0146
FB 3a	0.0072	0.0075	0.0147
FB 1b	0.0057	0.0101	0.0159
FB 2b	0.0150	0.0161	0.0311
SAB 1a	0.0109	0.0159	0.0268
SAB 2a	0.0109	0.0169	0.0278
SAB 3a	0.0109	0.0188	0.0297
SAB 1b	0.0078	0.0222	0.0300
SAB 2b	0.0099	0.0163	0.0263
LCC 1a	0.0119	0.0107	0.0226
LCC 2a	0.0120	0.0114	0.0235
LCC 3a	0.0120	0.0124	0.0244
LCC 1b	0.0088	0.0089	0.0178
LCC 2b	0.0158	0.0136	0.0293

Table 5.25.

It is seen that control strategy 3 has the lowest contribution to the energy production cost, and control strategies 1 and 2 have a higher contribution to the energy production cost. It should also be noted that the converter adjusting the voltage levels (at positions 1a and 2b) are the converters with the largest contribution to the energy production cost. With the assumption that the energy production cost for the wind farm is 0.5 SEK/kWh, the contribution from the converters in the local wind turbine grid is about 0.0304 / 0.5 = 6.1 % of the total energy production cost.

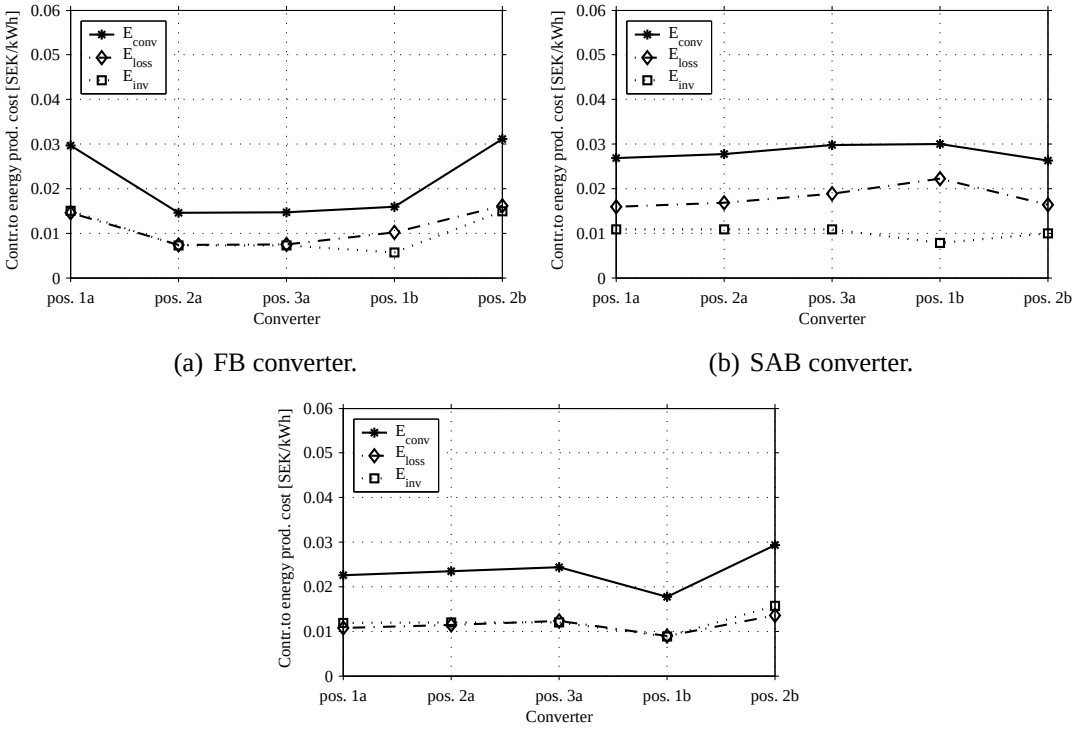

(a) FB converter.

(b) SAB converter.

(c) LCC converter.

Fig. 5.48 Contribution to the energy production cost for the different converters.

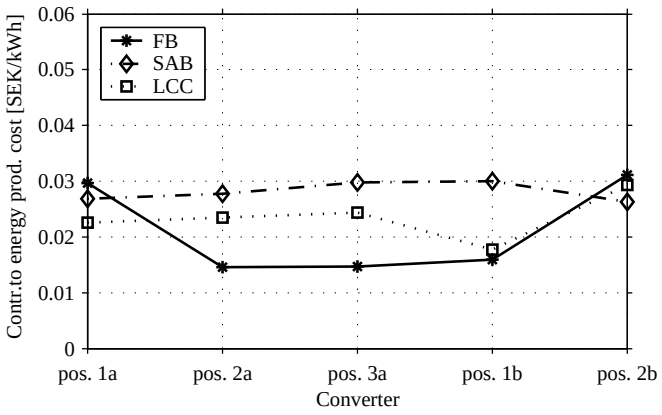

Fig. 5.49 Total contribution to the energy production cost for the different converters.

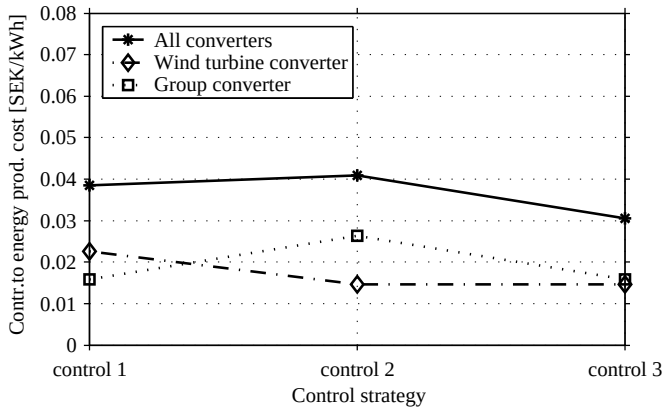

Fig. 5.50 Total contribution to the energy production cost for the converters in the local wind turbine grid using the economically most favorable converter.

Table 5.25: Total contribution to the energy production cost for the converters in the local wind turbine grid using the economically most favorable converter.

Control strategy	Turbine conv.	Group conv	All converters
1	0.0226 SEK/kWh	0.0159 SEK/kWh	0.0385 SEK/kWh
2	0.0146 SEK/kWh	0.0263 SEK/kWh	0.0409 SEK/kWh
3	0.0147 SEK/kWh	0.0159 SEK/kWh	0.0306 SEK/kWh

Comparison With an AC Transformer

The DC-based wind farm has the main advantages of using DC cables and smaller medium frequency transformers compared to the AC based wind farm that uses AC cables and large 50 Hz transformers. Here, a comparison is made between a DC/DC converter and a DC/AC converter with an AC transformer for a wind turbine converter. For example, consider the converter for position 3a, which is the wind turbine converter with constant voltage levels. In Fig. 5.51, the components in the wind turbine are shown both for a turbine with DC output voltage and for a turbine with an AC output voltage.

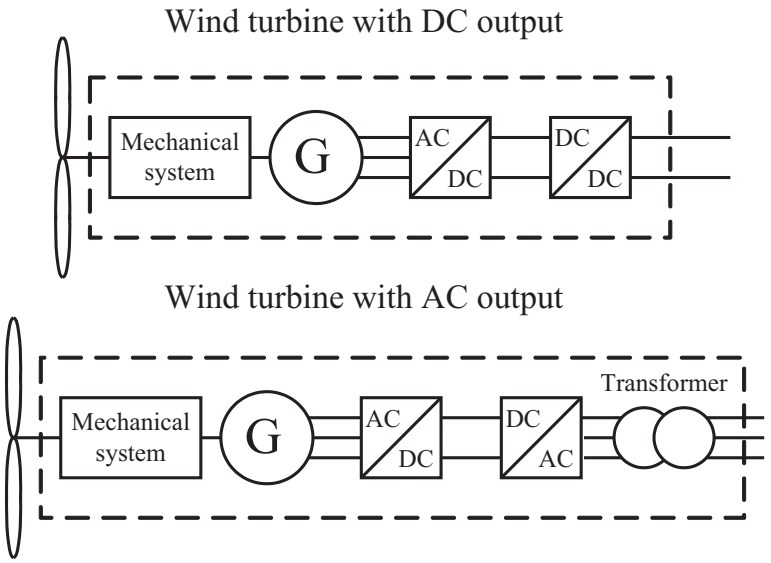

Fig. 5.51 Wind turbines with DC and AC outputs.

From the figure, it can be seen that the two systems have the same components in the generator and the rectifier. The difference is that for the case with a DC output there is a DC/DC converter including a medium frequency transformer instead of the DC/AC converter and the 50 Hz transformer for the case with the AC output. The large difference in contribution to the energy production cost between the DC/DC converter and the DC/AC converter including the transformer is the investment cost. For the cost of the semiconductor components, the DC/AC converter has three converter legs instead of two for the DC/DC converter so the cost for the IGBT modules are higher, but there is no rectifying bridge. Therefore the cost for the semiconductor components is assumed to be similar for the DC/DC and the DC/AC cases.

The main difference in investment costs is the cost for the transformer. For the DC/DC converter (assuming that the fullbridge converter is used), the transformer for the has a weight of 1579 kg (for core material, windings and insulation) and the corresponding

weight for the DC/AC converter is 12968 kg. Regarding the difference in investment cost, the DC/DC transformer with a steel core has a cost of 127 kSEK while the 50 Hz transformer with a steel core has a cost of 1039 kSEK. The increase in investment costs will increase the contribution from the converter to the total energy production cost with about 0.0076 SEK/kWh. If the losses for the DC/AC converter including the 50 Hz transformer is 2 % (38 kW), the reduction in energy production cost due to the lowered losses compared to the 55 kW for the fullbridge converter is 0.0045 SEK/kWh. The total increase in energy production cost if the DC/AC alternative is used is then 0.0031 SEK/kWh, and then the cheaper DC cables have not been considered.

5.7 Discussion

From the results shown in this section, the most obvious result is the low efficiency and and the resulting high contribution to the energy production cost of the single active bridge converter. The fullbridge converter and the resonant converter have comparable efficiency and therefore other factors will determine the choice of topology. The fullbridge converter has a constant switching frequency, and a current stiff output which requires a large filter inductance. A lower number of IGBT modules is required for the fullbridge converter than for the resonant converter, except for positions 1a and 2b where the numbers of IGBT modules are the same. However, a larger number of diode modules is required for the rectifying bridge in the fullbridge converter. Regarding the size of the transformer, the fullbridge converter has a smaller and less heavy transformer than the resonant converter. For the resonant converter, there is also an additional component in the resonant capacitor that must have a high voltage and current rating. The output of the resonant converter is voltage stiff, requiring a large filter capacitor, and the design of the filter will be complicated by the large range of switching frequencies.

The choice of topology will also depend on the cost and availability of additional components such as the filter capacitance and the resonant capacitor for the resonant converter and the filter inductance for the fullbridge converter. There is also a trade-off between the more heavy transformer for the resonant converter and the larger number of diode modules needed for the fullbridge converter. Further, the resonant converter has a number of disadvantages such as the high peak voltage, the large resonant capacitor, the large transformer and the variable frequency control. These factors will give a larger investment cost and then probably result in the fullbrige converter as the topology with the lowest contribution to the energy production cost.

When comparing the control strategies, control strategy 2 has the highest losses due to the low efficiency of the converter for position 2b both for the fullbridge converter and the resonant converter. Also, the fullbridge converter has a high number of diode modules in

the output bridge for position 2b and both topologies have a heavy transformer. Control strategy 1 has just slightly lower losses and there are large losses in the converter at position 1a. The lowest losses are obtained by using control strategy 3 with the fullbridge converter. However, it should be noted that for control strategy 1, a diode rectifier gives a variable voltage and for control strategy 3 an IGBT rectifier gives a constant output voltage.

It has also been shown that it is hard to find a suitable turn-off snubber capacitor that lowers the turn-off losses but does not cause any additional turn on-losses, and the result have been no snubber capacitor or a snubber capacitor with a low value. One way of making the use of a larger snubber capacitor possible is to adjust the voltage level in the local wind turbine grid so that the ratio between the current and the voltage is constant at all operating points. If the voltage level has the same variation in the whole local wind turbine grid, then all converters can have a constant duty cycle which gives low losses for the fullbridge converter. However, if a constant voltage is required for the HVDC transmission, the last converter must compensate for the voltage variations. This converter will then be similar to the converter at position 2b which is heavy and has a low efficiency.

Chapter 6

Experimental Setup

In Chapter 5, the fullbridge converter, the single active bridge converter and the series parallel resonant converter were studied and the losses were calculated for the application in a DC based wind farm. It was found that the fullbridge converter is an appropriate choice for this application with low losses, low peak values for the current and voltage and low investment cost. For the verification of the results from the simulations and calculations of the losses, a down scaled experimental setup of the fullbridge converter using phase shift control was constructed, which will be described in this chapter.

The purpose of the experimental verification is both to verify the resulting waveforms from the simulations and to investigate the losses for different operation points. First, since the loss calculations are based on the voltage and current waveforms obtained from the simulations, the waveforms from the ideal simulated model are compared with the measured waveforms. Then a refined simulation model is obtained that gives a more detailed representation of the experimental circuit. Finally, the losses are compared for the measurements and for the calculations from the simulations with the ideal model.

6.1 Design of the Fullbridge Converter

The design of the fullbridge converter aims to construct a down scaled converter suitable for tests that can be compared with simulations. It should be large enough to have similar characteristics as the full scale converter, but on the other hand it should be small enough to be realized using the existing laboratory equipment. The resulting converter is described in detail in [60] and will here be presented briefly. A photo of the experimental setup is shown in Fig. 6.1.

The power rating of the converter is 15 kW with an input voltage of 300 V and an input current of 50 A. The transformer of the converter has the ratio 1:1, which gives the maximum theoretical output voltage of 300 V. In reality, the output voltage is slightly lower due

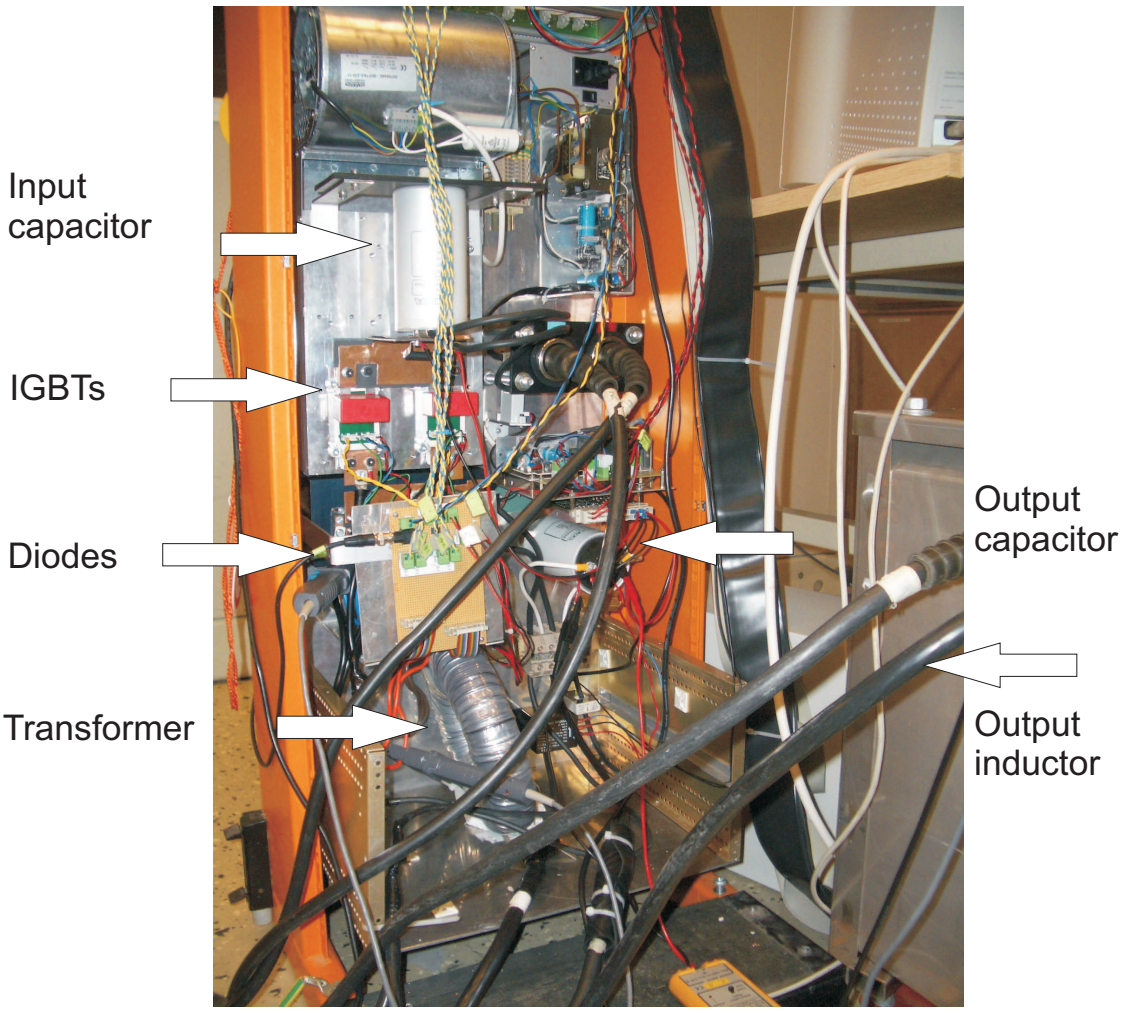

Fig. 6.1 Photo of the experimental setup.

to losses in the converter. The main components of the converter are the IGBT modules for the input bridge, the diode modules for the rectifying bridge, the transformer, the filter inductance and the control system. Additionally, there are auxiliary components such as the driver circuits, the measuring system, the cooling and the power supply to the auxiliary components. These different components will be explained briefly in this chapter and, in addition, more information about the experimental setup can be found in [60].

6.1.1 Semiconductor Components

The IGBT modules used in the input bridge are the SemixS302GB128D modules from Semikron with rated voltage 1200 V and rated current 320 A. As drive circuits for the IGBT modules, two *Skyper*^{TM}32*Pro* from Semikron are used. They are mounted on the corresponding evaluation boards *EvaluationBoard*1*Skyper*^{TM}32*Pro*.

For the rectifying bridge the SGS - ThomsonMicroelectronics BYT230PIV - 1000 modules are used with a rated voltage of 1000 V and a rated current of 30 A. However, using the rectifying bridge without over-voltage snubbers results in large oscillations at turn-off close to the maximum voltage for the diodes. To reduce these oscillations RC-snubbers are inserted across each diode with the values R_s = 60 Ω and C_s = 2.8 nF.

6.1.2 Transformer

The transformer used is a custom-made transformer with transformation ratio 1:1 which can be seen in Fig. 6.2. From the measurements of the transformer voltage and current, the stray inductance is determined to 10 μH and the main inductance to 14 mH. Further, the core material is the iron based magnetic alloy 2605SA1 from Metglas. However, it should be noted that the core material is no-field anneal and the given data for core losses in the data sheet is based on a core with longitudinal field anneal.

Fig. 6.2 Photo of the transformer.

6.1.3 Filter Components

As the input capacitor, a *Rifa Elyt Long Life PEH*169*UV*439*AQ* capacitor is used with the capacitance value of 3900 μF. In the output bridge, a *Rifa Elyt Long Life PEH*169*UV*433*OQ* capacitor with 3.3 μF is used. Since the fullbridge converter requires a current-stiff output,

the output filter inductance needs to be large, especially since the switching frequency is as low as 1 kHz. The inductance chosen was an existing free-standing inductor of 20 mH that can handle a current up to 80 A.

6.1.4 Control System and Measurements

For generating the control signals for the drive circuits, a Simulink/MATLAB file is used where the control signals are generated from the phase shift determined by the user. Further, the control signals are connected to the drive circuits via a dSPACE DS1103 controller board and two additional cards for obtaining the right voltage levels for the control signal to the drive circuits.

The measurements for the circuit are done in two different ways, either by an oscilloscope or by using a measuring card and feeding the measured signals back to the dSPACE system. The dSPACE system has the drawback of a limited bandwidth since the sampling time is 50 μs, and therefore, the high-frequency signals are measured with the oscilloscope. However, the input and output voltages are measured with the dSPACE system via a voltage transducer card. In the same way, the input and output currents are measured using LEM-modules and a measuring card, described in [60], together with the dSPACE system.

6.2 Measured and Simulated Waveforms

The resulting waveforms from the simulations of the ideal model of the experimental setup are compared with the measured voltage and current waveforms. The ideal model used in the simulations is shown in Fig. 6.3.

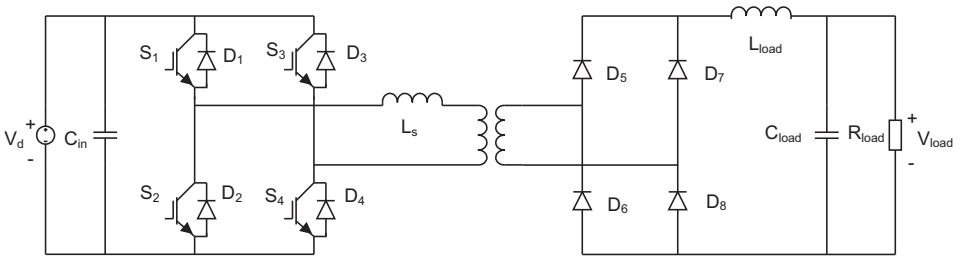

Fig. 6.3 Ideal simulation model for the experimental converter.

In the ideal simulation model, ideal switches are used and the components considered are the input capacitor, the leakage and main inductances of the transformer and the inductance and capacitance for the output filter. The load resistance is the same as the load

resistance in the experimental setup. In Fig. 6.4, the input and output voltages and currents are shown both for simulations and measurements, and in Fig. 6.5 the voltages and currents for the transformer are shown.

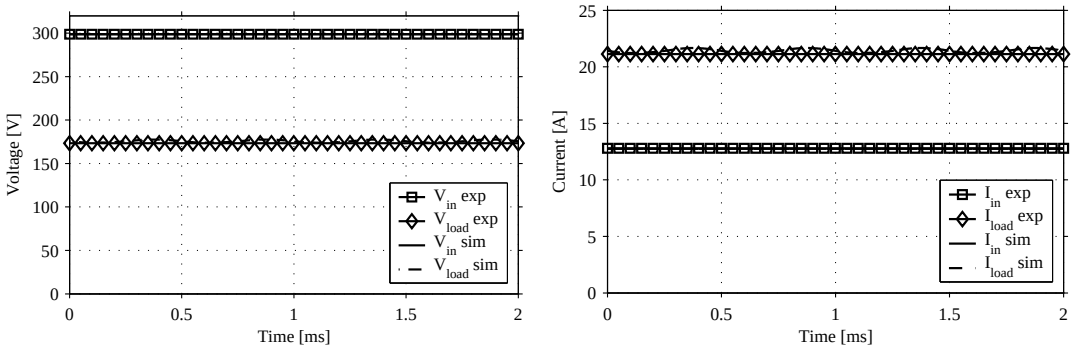

(a) Voltage. (b) Current.

Fig. 6.4 Ideal simulated and measured input and output current and voltage waveforms.

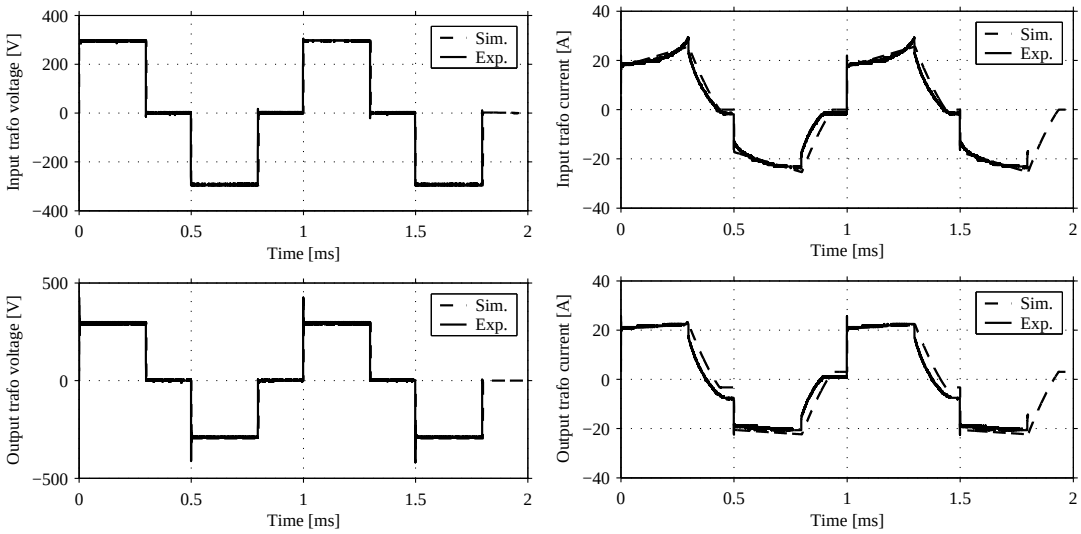

(a) Voltage. (b) Current.

Fig. 6.5 Ideal simulated and measured current and voltage waveforms for the transformer.

In the figures, it can be seen that neither the input and output voltage nor current levels show any significant differences between the simulations and the measurements. The noticeable difference is the higher output voltage and current for the ideal simulation model due to the lower losses in the ideal model. Regarding the transformer, the voltage levels are similar for the simulations and the measurements, but there are some differences in the current waveforms as seen in Fig. 6.5 (b).

One of the purposes with the experimental setup is to verify that the simulation model provides current and voltage waveforms good enough for loss calculations. Looking at the input current and voltage, the values match between the simulations and measurements giving accurate conditions for the diodes and switches in the input bridge. For the output diodes, both the current and voltage levels are slightly higher since the output current and voltage are higher in the ideal simulation, but this small change of about 1.5 % does not add a significant error in the loss calculations. Regarding the losses in the transformer, the transformer current is slightly higher which gives higher copper losses but since the voltage waveforms are the same, there should not be any significant difference in the transformer losses. The conclusion is therefore that the simulated waveforms are good enough for loss calculations, even though the currents in the output bridge and the transformer most likely are slightly overestimated in the simulations.

6.3 Refined Simulation Model

As seen in the previous section, there are some differences between the results from the ideal simulation model and the measurements. To achieve a more accurate representation of the experimental setup, a refined simulation model was obtained for the experimental setup. In this non-ideal simulation model, some loss components are included in the circuit. The ideal simulation model is modified by adding non-ideal switches, and also including the resistances of the transformer and the output filter. Finally, the resistances across the input and output capacitors are added. The added resistances can be seen in Fig. 6.6 and the values of the components are shown in Table 6.1. For the resistances R_{Cin} and R_{Cload}, the values are known and for the transformer and the filter inductance, the resistance values R_{Ls} and R_{Lload} are measured at 1 kHz for the transformer and at DC current for the filter. However, the value of the resistance for the filter inductance is increased from the measured 37.6 mΩ to 50 mΩ for obtaining the AC resistance.

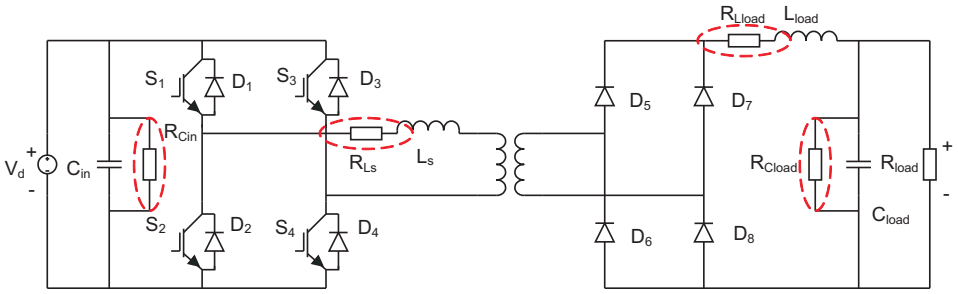

Fig. 6.6 Non-ideal simulation model for the experimental converter.

The IGBT module used in the experimental setup is not available in the Pspice library, instead the similar POWEREX IGBT module CM400HA-24H is used. The resulting wave-

Table 6.1: Calculated losses for the simulated circuit.

Component	Resistance
R_{Cin}	47 kΩ
R_{Cload}	10 kΩ
R_{Ls}	72 mΩ
R_{Lload}	50 mΩ

forms for the input and output current and voltages show no significant difference from Fig. 6.4, but for the transformer the currents follow the measured waveforms more closely which is shown in Fig. 6.7.

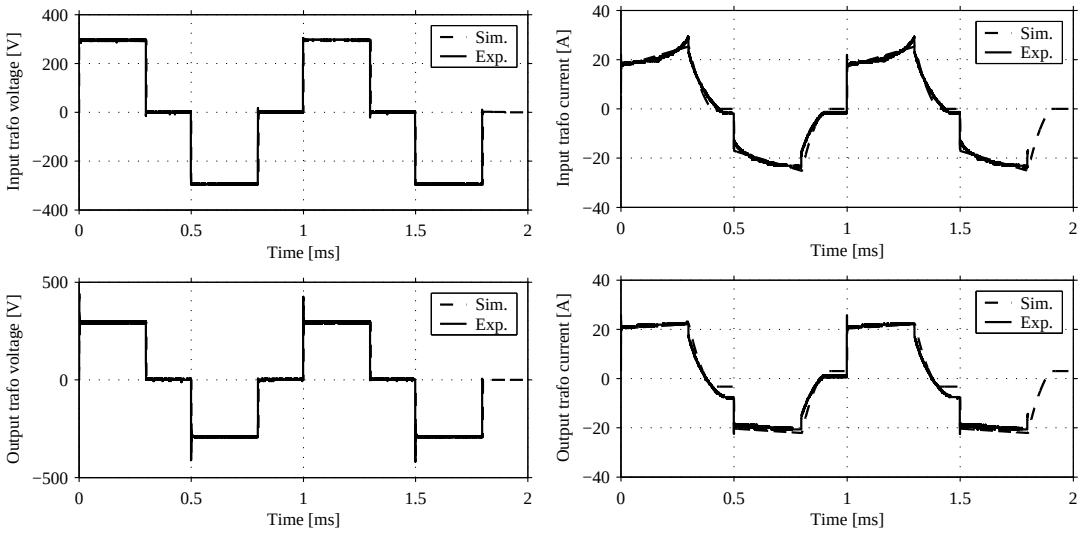

(a) Voltage. (b) Current.

Fig. 6.7 Non-ideal simulated and measured current and voltage waveforms for the transformer.

Even though it is not clearly visible in the figures, the non-ideal simulation model results in a lower output voltage, which is 0.3 % above the measured value compared to 1.5 % above the measured value for the ideal model. It can also be seen in Figs. 6.7 that the simulated current and voltage waveforms closely follow the measured values.

6.4 Loss Calculations

The second purpose of the experimental setup is to identify the losses in the converter and compare the results with the calculated losses. The losses are calculated using the current and voltage waveforms from the simulations together with the known properties of the components, and are then compared to the measured losses in the circuit.

6.4.1 Losses in the Semiconductor Devices

The first contribution to the losses is the losses in the semiconductor devices. Using the waveforms from the simulations, the losses for the semiconductor devices are calculated as described in Chapter 4. The losses in the semiconductor components is the sum of the conduction losses and the switching losses, and the resulting losses are shown in Table 6.2.

For calculating the on-state conduction losses, the values of the voltage drop over the components as a function of the on-state voltage are given in the data sheets. The on-state voltages for the IGBT modules and the diode modules are shown in Fig. 6.8 as a function of the forward current. The on-state voltage for the IGBT module V_{CE} is obtained from the forward current I_C as

$$V_{CE} = 0.53 + 0.0206 I_C - 8.56 \cdot 10^{-5} I_C^2. \tag{6.1}$$

The forward voltage V_F for the diode is calculated from the forward current I_F as

$$V_F = 0.92 + 0.0149 I_F - 6.10 \cdot 10^{-5} I_F^2. \tag{6.2}$$

Also the forward voltage $V_{F,IGBT}$ for the freewheeling diode in the IGBT module is calculated as a function of the forward current $I_{F,IGBT}$ as

$$V_{F,IGBT} = 0.73 + 0.0180 I_{F,IGBT} - 6.11 \cdot 10^{-5} I_{F,IGBT}^2. \tag{6.3}$$

The instantaneous conduction losses are then given by

$$P_c = V_{CE} I_C + V_F I_F + V_{F,IGBT} I_{F,IGBT}, \tag{6.4}$$

and the average conduction losses are given the average value over one switching period.

Apart from the conduction losses, there is energy dissipated at each switching of the IGBT devices. This energy for one switching period for one switching for the IGBT module is calculated as

$$E_s = E_{SRon} \frac{V_V}{V_{ref}} \frac{i_V}{i_{ref}} + E_{SRoff} \frac{V_V}{V_{ref}} \frac{i_V}{i_{ref}}. \tag{6.5}$$

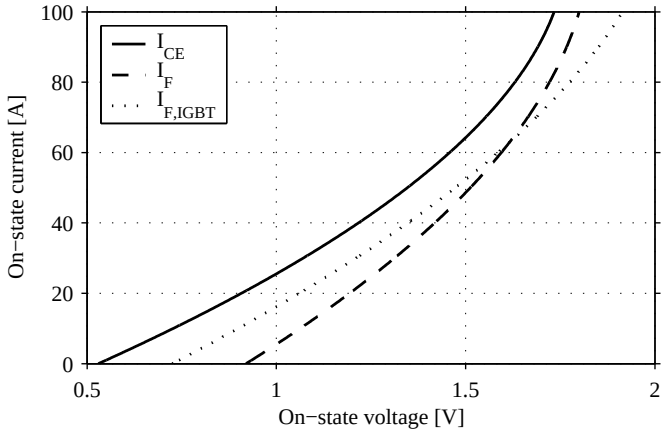

Fig. 6.8 On-state voltages V_{CE} for the diode module and V_F for the diode module.

Here, E_s is the actual switching loss at current i_V and voltage V_V, and $E_{SRon} = 20mJ$ and $E_{SRon} = 30mJ$ are the rated switching energies at the current $i_{ref} = 150A$ and voltage $V_{ref} = 600V$. The switching losses P_{sw} are then calculated as the switching energy times the switching frequency as

$$P_{sw} = E_s f_s, \tag{6.6}$$

and the total semiconductor losses are then given by

$$P_{semi} = P_{sw} + P_c. \tag{6.7}$$

Table 6.2: Calculated losses for the semiconductor devices.

ϕ	P_c	P_{sw}	P_{semi}
1	160 W	25 W	185 W
0.8	117 W	21 W	139 W
0.6	71 W	16 W	87 W
0.4	38 W	11 W	49 W
0.2	14 W	5 W	19 W

6.4.2 Losses in the transformer

The transformer losses are described in Chapter 3 and consists of copper losses in the windings and core losses.

For calculating the copper losses, the resistance of the windings are measured in a short-circuit test to find the resistance of the windings at the voltage and current waveforms used in the converter. The total ac-resistance of the windings were found to be 72 mΩ. Assuming that the resistances of the primary and secondary windings are equal, the ac resistance is $R_{pri,ac}$ 36 mΩ for the primary winding and $R_{sec,ac}$ 36 mΩ for the secondary winding. The losses in the windings P_w are then given by

$$P_w = P_{w,pri} + P_{w,sec} = R_{pri,ac} I_{pri}^2 + R_{sec,ac} I_{sec}^2. \tag{6.8}$$

For obtaining the core losses in the transformer, the no-load losses for the converter were measured. Since there is no load current, there are no losses in the output filter or the output diodes. The additional losses except the core losses for the transformer are the losses in the resistance across the input capacitor and the losses in the IGBT modules. When these two loss components are subtracted from the total losses, the remaining losses are the iron losses P_{core} of the transformer. These losses were measured to 43 W at full duty cycle and were assumed to be proportional to the duty cycle. The reason for not using measured values at lower duty cycles is that the current at these operating conditions is very small and it is therefore hard to measure with good accuracy.

The losses in the core are also calculated as described in Chapter 4 as

$$P_{core} = K_a 46.7 \cdot 10^3 f_{tr}^{1.51} B_{max}^{1.74} V_{core}. \tag{6.9}$$

The constant K_a used in (6.9) is a compensation for the no-field anneal core used in transformer in the experimental setup. In the data sheet for the core material, the losses are given for the longitudinal field anneal which gives considerably lower losses. To find a value of the constant K_a, the B-H curves were studied for the longitudinal field anneal and the no-field anneal. Assuming the maximum flux density 0.6 T, which is the case for full duty cycle at 300 V, the area covered at no-field anneal is K_a = 2.78 times the area covered at longitudinal field anneal. From the resulting losses in Table 6.3, it can be seen that the resulting core losses from the calculations are slightly lower than the measured values, with a deviation of 20 % for full duty cycle.

The core area is A_{core} =18 cm^2, the core volume is V_{core} = 990 cm^3 and the number of turns were measured to $N_{pri} = N_{sec}$ = 78. The resulting core losses $P_{core,calc}$ are shown in Table 6.3 together with the measured core losses $P_{core,meas}$.

The losses in the windings P_w are also shown in Table 6.3 and the total transformer losses P_{tr}, that are the sum of the core losses and the losses in the windings calculated as

$$P_{tr} = P_{core} + P_w. \tag{6.10}$$

Table 6.3: Calculated and measured losses for the transformer.

ϕ	P_w	$P_{core,calc}$	$P_{core,meas}$	P_{tr}
1	76 W	35 W	43 W	119 W
0.8	45 W	28 W	34 W	79 W
0.6	19 W	19 W	26 W	45 W
0.4	6 W	11 W	17 W	23 W
0.2	0.6 W	5 W	9 W	10 W

In Table 6.3, the core losses included in the total transformer losses are the losses based on the measurements of the no-load losses.

6.4.3 Losses in the Filter Inductance

There are also losses in the filter inductance, mainly due to the resistance in the windings. This resistance was measured to $R_{Lload} = 37.6\ m\Omega$ DC-resistance and since the dimension of the wire is not known and the core losses are not considered, the AC-resistance at 1 kHz is assumed to be $R_{Lload} = 50\ m\Omega$. The losses in the output filter P_{filter} is then calculated using the filter current I_{filter} as

$$P_{filter} = R_{Lload} I_{filter}. \tag{6.11}$$

6.4.4 Losses in the Blide Resistances

The last contribution to the losses that is considered is the losses P_{blide} in the resistances $R_{Cin} = 47k\,\Omega$ and $R_{Cload} = 10k\,\Omega$ across the input and output capacitances. These losses are calculated using the input voltage V_d and the output voltage V_{load} as

$$P_{blide} = \frac{V_d^2}{R_{Cin}} + \frac{V_{load}^2}{R_{Cload}}. \tag{6.12}$$

6.4.5 Loss Evaluation

The calculated losses for the different components in the circuit are summed up and compared to the measured total losses in the converter. The total power loss for the circuit is calculated using the measured values of the input and output current and voltage. Using these measured values, the losses $P_{loss,exp}$ are calculated as the difference between the input power and the output power as

$$P_{loss,exp} = P_{in} - P_{out} = V_d I_{in} - V_{load} I_{load}. \tag{6.13}$$

The different calculated loss components for the converter are shown in Table 6.4 and also in Fig. 6.9. The sum of the calculated losses are compared to the measured total losses in Table 6.5 and Fig. 6.10.

Table 6.4: Calculated losses for the simulated circuit.

ϕ	P_{semi}	P_{tr}	P_{filter}	P_{blide}	Sum of losses	
1	185 W	119 W	61 W	10 W	375 W	3.69 %
0.8	139 W	79 W	40 W	7 W	265 W	4.04 %
0.6	87 W	45 W	22 W	5 W	160 W	4.30 %
0.4	49 W	23 W	10 W	3 W	84 W	5.10 %
0.2	19 W	10 W	2 W	2 W	33 W	7.92 %

Table 6.5: Measured and calculated losses for the experimental circuit.

ϕ	Measured losses		Calculated losses	
1	383 W	3.76 %	367 W	3.61 %
0.8	280 W	4.27 %	259 W	3.95 %
0.6	162 W	4.36 %	153 W	4.77 %
0.4	87 W	5.28 %	79 W	4.74 %
0.2	45 W	10.66 %	29 W	6.97 %

It can be seen that the largest loss contribution is from the semiconductor components that contribute with more than half of the losses. The second largest source of losses is the transformer. For this converter, also the filter inductance contribute with a significant amount of losses. This is due to the filter design that was not optimized, but instead an existing inductance was used. Comparing the calculated losses with the measured losses, the calculated losses are similar even though the measured losses are slightly higher. This it not surprising since just the large loss components and not all loss components are considered.

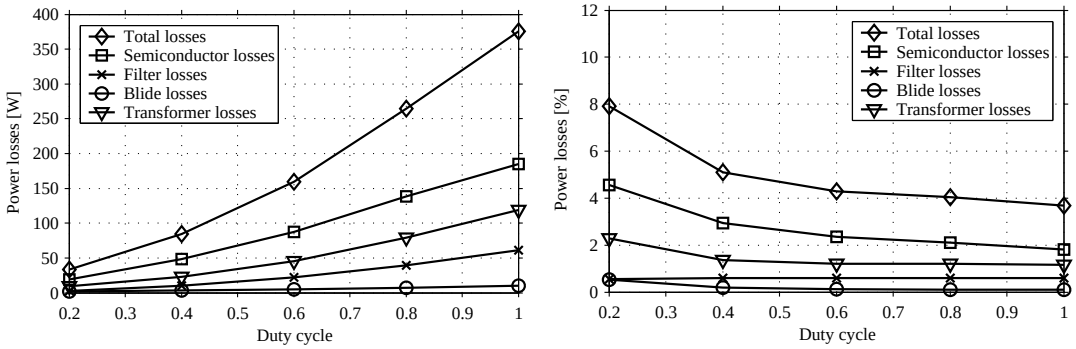

(a) Absolute losses. (b) Loss fraction.

Fig. 6.9 Calculated losses for the experimental setup.

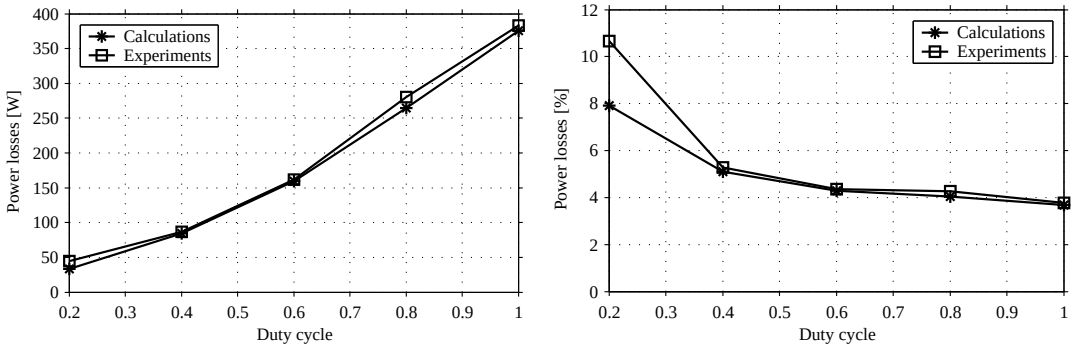

(a) Absolute losses. (b) Loss fraction.

Fig. 6.10 Calculated and measured losses for the experimental setup.

From the comparison between the calculated losses and the measured losses, it can be seen that the main loss contributions were identified. Also, the semiconductor losses and the transformer losses contribute to just above 80 % of the total calculated losses. Due to this, the loss calculations in Chapter 5, where the losses from the semiconductor components and the transformer are considered, gives reasonable values where the two main sources to the total losses are considered. The calculated values of the semiconductor losses and the transformer losses agrees with the measured values and therefore also the results in Chapter 5 should be valid. The only exception is the core material for the transformer where the correct losses for the material are not available, but for the steel core used in Chapter 5 there is available loss data.

Comparing the efficiency of the experimental converter just above about 3.5 % for input voltage 300 V to the efficiency of between 2 % and 3 % for the high-power converters in Chapter 5, it should be noted that the difference is due to the low voltage level. The IGBT and diode modules are rated for 1200 V and 1000 V but the input voltage is 300 V. Due to

the low input voltage, the current must be high in order to increase the power transfer and that will result in high conduction losses due to the high on-state voltage drop for the components. For the high-power converter in Chapter 5, the voltage across the 3.3 kV IGBT devices is approximately 1.7 kV and the on-state voltage drop is approximately twice the on-state voltage drop for the component in the experimental setup. The conduction losses will benefit from a high voltage and low current, and even with the same ratio between the current and the voltage a high voltage level, the ratio between the input voltage and the on-state voltage increases leading to a higher efficiency. Also, the losses decrease with decreasing duty cycle since the current is lowered but the voltage stays constant.

Chapter 7

Conclusions and Future Work

In this chapter, the results from this thesis will be summarized and some suggestions will be given for future research.

7.1 Summary and Concluding Remarks

In this thesis, three topologies of DC/DC converters are evaluated regarding their suitability for the application in a DC based wind farm. The energy efficiency and the contribution to the energy production cost of the converters, the fullbridge converter, the single active bridge converter and the series parallel resonant converter, are considered as well as the need of components. As stated in Section 4, the considered losses are the losses in the transformer and in the semiconductor components. Additional losses as the losses due to the cooling system, drive circuits and losses in the input and output filters are assumed to be similar for all topologies and are therefore not considered. The resulting losses should therefore be seen as a comparison between the different topologies more than an absolute value.

In Chapter 5, the operating conditions are obtained for the DC/DC converter in a local wind turbine grid consisting of five wind turbines. These operating conditions are used for designing the converters for all positions in the local wind turbine grid for three different control strategies. Knowing the designs of the converter and the operating conditions, the losses are calculated as a function of the wind speed. The average power loss for a certain average wind speed is obtained by integrating over the probability distribution of the wind speed.

It is found that the resonant converter and the fullbridge converter have the lowest losses of the three types for the DC wind farm application with about 1.79 - 2.47 % power losses for the resonant converter and about 1.47 - 2.92 % power losses for the fullbridge converter. The single active bridge converter has the highest losses for all positions and operating

points with 3.18 - 4.44 % losses. Since the fullbridge converter and the resonant converter have similar efficiencies, other factors will determine the choice of topology. The resonant converter requires a larger transformer and more IGBT modules, and therefore the contribution to the energy production cost is lower for the fullbridge converter than for the resonant converter for some positions in the local wind turbine grid, even though the losses are higher. Further, the fullbridge converter has the advantage of a constant switching frequency, a less heavy transformer and also low peak values for the voltage and current. The resonant converter has almost no switching losses but has a larger transformer, it requires a resonant capacitor with high current and voltage rating and also has large stresses for the input and output filters at low power levels. Also, the fullbridge converter has a current stiff output which requires a large filter inductance while the resonant converter has a voltage stiff output which requires a large filter capacitor. Regarding the control strategies, control strategy 3 (with constant voltage levels) using the fullbridge converter as the wind turbine converter and the resonant converter as group turbine is the choice with the lowest losses, which is 3.29 % including the losses for both the wind turbine converters and the group converter. Control strategy 2 (with voltage adjustment in the group converter) has the highest losses which is 4.19 % due to the low efficiency of the converter for position 2b. Control strategy 1 with voltage adjustment in the wind turbine has total losses of 3.93 %. For the choice of control strategy, also the rectifier used together with the generator should be considered. For control strategies 1 and 2, a diode rectifier gives a variable voltage and for control strategy 3 an IGBT rectifier gives a constant output voltage.

The lowest contribution to the energy production cost is given by using control strategy 3 with the fullbridge converter that contributes to the total energy production cost with 0.0306 SEK/kWh Moreover, the resonant converter will have a disadvantage of the large resonant capacitor, extra insulation due to the high peak voltage, large filters and also the variable frequency control. These factors will lead to an increasing investment cost for the converter and thereby make the fullbridge converter a suitable choice for the wind farm application.

The experimental results verified that the current and voltage waveforms from the ideal simulations agree with the measured waveforms for the fullbridge converter and are therefore appropriate to use in the loss calculations. Further, the losses were identified for the experimental setup and the calculated losses agree with the measured losses.

7.2 Proposals for Future Work

In this thesis, the DC/DC converter is studied that is a key component for the realization of a DC based wind farm. To further study the DC based wind farms, the properties of a DC grid should be studied including the DC/DC converters. For achieving that, one of the topologies should be chosen and a dynamic model should be obtained for that converter. Then, a model of the whole wind farm including wind turbines, cables, DC/DC converters and an HVDC connection should be used for the investigations.

There are some interesting aspects to investigate for the DC based wind farm:

- How the DC grid should be controlled during normal operation, both with and without communication between the different parts of the grid.
- How the internal DC grid should be designed, including choice of voltage levels, the need of auxiliary power and how the system should be grounded.
- How the wind farm can handle faults, both internal faults and ride-through properties in the case of a fault in the grid.

References

[1] B. Normark and E. Koldby Nielsen, “Advanced power electronics for cable connection of offshore wind,” in *Proc. Copenhagen Offshore Wind 05*, 2005.

[2] N. Barberis Negra, J. Todorovic, and T. Ackermann, “Loss evaluation of HVAC and HVDC transmission solutions for large offshore wind farms,” *Electric Power Systems Research 76 (2006) 916-927*.

[3] W. Kling, P. Bresesti, I. Valadè, D. Canever, and R. Hendriks, “Transmission systems for offshore wind farms in the Netherlands,” in *Proc. Copenhagen Offshore Wind 05*, 2005.

[4] S. Lundberg, “Configuration study of large wind parks,” Dep. Electric Power Eng., Chalmers University of Technology, Tech. Rep. 474L, 2003.

[5] R. L. Steigerwald, R. W. De Doncker, and H. Kheraluwala, “A comparison of high-power DC-DC soft-switched converter topologies,” *IEEE Trans. Industry Applications*, vol. 32, no. 5, pp. 1139–1145, September/October 1996.

[6] J.-G. Cho, J. A. Sabate, H. Guichao, and F. C. Lee, “Zero-voltage and zero-current-switching full bridge PWM converter for high-power applications,” *IEEE Trans. Power Electronics*, vol. 11, no. 4, pp. 622 – 628, July 1996.

[7] A. Bendre, S. Norris, D. Divan, I. Wallace, and R. W. Gascoigne, “New high power DC-DC converter with loss limited switching and lossless secondary clamp,” *IEEE Trans. Power Electronics*, vol. 18, no. 4, pp. 1020–1027, July 2003.

[8] L. Mihalache, “A modified PWM control technique for full bridge ZVS DC-DC converter with equal losses for all devices,” in *Proc. IEEE IAC’04*, vol. 3, 2004, pp. 1776–1781.

[9] G. D. Demetriades, “Evaluation of different topologies for high-power DC-DC converters,” Dep. Electrical Eng., Royal University of Technology, Tech. Rep. ISSN-1404-8248, 2001.

[10] G. D. Demetriades, "On small-signal analysis and control of the single- and dual-active bridge topologies," Dep. Electrical Eng., Royal University of Technology, Tech. Rep. ISSN-1650-674X, 2005.

[11] J. Walter and R. W. De Doncker, "High-power galvanically isolated DC/DC converter topology for future automobiles," in *Proc. IEEE PESC'03*, vol. 1, 2003, pp. 27–32.

[12] N. Mohan, T. M. Undeland, and W. P. Robbins, *Power Electronics: Converters, Applications and Design*. John Wiley and Sons INC., third edition, 2003.

[13] L. Helle and S. Munk-Nielsen, "Comparison of converter efficiency in large variable speed wind turbines," in *Proc. IEEE APEC'01*, vol. 1, 2001, pp. 628–634.

[14] W. Dong, J.-Y. Choi, Y. Li, H. Yu, J. Lai, D. Boroyevich, and F. C. Lee, "Efficiency considerations of load side soft-switching inverters for electric vehicle applications," in *Proc. IEEE APEC'00*, vol. 2, 2000, pp. 1049–1055.

[15] J. S. Lai, R. W. Young, and J. W. Mc Keever, "Efficiency consideration of DC link soft-switching inverters for motor drive applications," in *Proc. IEEE PESC'94*, vol. 2, 1994, pp. 1003–1010.

[16] E. R. C. da Silva, M. C. Cavalcanti, and C. B. Jacobina, "Comparative study of pulsed DC-link voltage converters," *IEEE Trans. Power Electronics*, vol. 18, no. 4, pp. 1028–1033, July 2003.

[17] S. Munk-Nielsen, M. M. Bech, R. Teodorescu, and J. K. Pedersen, "Simulink model of a three level converter leg including device losses," in *Proc. IEEE PCC'00*, vol. 2, 2002, pp. 559–564.

[18] M. H. Kheraluwala, R. W. Gasgoigne, D. M. Divan, and E. Bauman, "Performance characterization of a high power dual active bridge DC/DC converter," in *Proc. IEEE IAC'90*, vol. 1, 1990, pp. 1267–1273.

[19] R. Asensi, J. A. Cobos, O. Garcia, R. Prieto, and J. Uceda, "A full procedure to model high frequency transformer windings," in *Proc. IEEE PESC'94*, vol. 2, 1994, pp. 856–863.

[20] M. C. Caponet, F. Profumo, and A. Tenconi, "Evaluation of power losses in power electronic converters for industrial applications: comparison among hard switching, ZVS and ZVS-ZCS converters," in *Proc. IEEE PCC 02*, vol. 3, 2002, pp. 1073–1077.

[21] T. Ackermann, *Wind Power in Power Systems*. Chichester, England: John Wiley & Sons, Ltd, 2005.

[22] G. L. Johnson, *Wind Energy Systems*. New Jersey, USA: Prentice-Hall, 1985.

[23] A. Petersson, “Analysis, modeling and control of doubly-fed induction generators for wind turbines,” Dep. of Energy and Environment, Chalmers University of Technology, Tech. Rep. ISSN-0346-718X, 2005.

[24] T. Thiringer and J. Linders, “Control by variable rotor speed of a fixed-pitch wind turbine operating in a wide speed range,” *IEEE Trans. Energy Conversion*, vol. 8, no. 3, pp. 520–526, September 1993.

[25] Horns Rev homepage. [Online]. Available: http://www.hornsrev.dk,2006-09-15

[26] J. van der Tempel, D. Gerda Salzmann, T. J. Mulder, J. M. L. Koch, F. W. B. Gerner, O. F. C. Calkoen, A. J. Göbel, H. T. Brinkhuis, R. C. Lagers, and W. G. S. van Korven, “Scale model testing of the Ampelmann, safe and easy access to offshore wind turbines,” in *Proc. Copenhagen Offshore Wind 05*, 2005.

[27] S. Vestergaard, “Offshore technology/operation & maintenance - accessibility,” in *Proc. Copenhagen Offshore Wind 05*, 2005.

[28] N.-E. Ottesen Hensen, “Experiences with simple and repititive offshore foundations,” in *Proc. Copenhagen Offshore Wind 05*, 2005.

[29] P. Vølund, “Concrete is the future for offshore foundations,” in *Proc. Copenhagen Offshore Wind 05*, 2005.

[30] P. Schaumann and C. Böker, “Can jackets and tripods compete with monopiles,” in *Proc. Copenhagen Offshore Wind 05*, 2005.

[31] S. Meier, S. Norrga, and H.-P. Nee, “New topology for more efficient AC/DC converters for future offshore wind farms,” in *Proc. Nordic Wind Power Conference, NWPC 04*, 2004.

[32] R. L. Hendriks, J. H. den Boon, C. G. Paap, and W. L. Kling, “Connecting offshore wind farms to (VSC-)HVDC interconnectors,” in *Proc. Nordic Wind Power Conference, NWPC 06*, 2006.

[33] T. Ackermann, N. Barberis Negra, J. Todorovic, and L. Lazardis, “Evaluation of electrical transmission concepts for large offshore wind farms,” in *Proc. Copenhagen Offshore Wind 05*, 2005.

[34] S. G. Johansson, L. Liljestrand, F. Krogh, J. Karlstrand, and t. . Jutta Hansson.

[35] Information about HVDC and HVDC Light from ABB. [Online]. Available: http://www.abb.com/hvdc,2006-09-15

[36] Information about HVDC and HVDC Plus from Siemens. [Online]. Available: http://www.siemens.com/hvdc,2006-09-15

[37] R. W. Erickson and D. Maksimović, *Fundamentals of Power Electronics, Second Edition*. Massachusetts, USA: Kluwer Academic Publishers, 2002.

[38] R. L. Steigerwald, "A comparison of half-bridge resonant converter topologies," *IEEE Trans. Power Electronics*, vol. 3, no. 2, pp. 174–182, April 1988.

[39] T. Kjellqvist, S. Norrga, and S. Östlund, "Design considerations for a medium frequency transformer in a line side power conversion system," in *Proc. IEEE Power ELectronics Specialists Conference, PESC 04*, 2004.

[40] R. Petkov, "Optimum design of a high-power, high-frequency transformer," *IEEE Trans. Power Electronics*, vol. 11, no. 1, pp. 33 – 42, January 1996.

[41] M. Sippola and R. E. Sepponen, "Accurate prediction of high-frequency power-transformer losses and temperature rise," *IEEE Trans. Power Electronics*, vol. 17, no. 5, pp. 835 – 847, September 2002.

[42] M. Albach, T. Durbaum, and A. Brockmeyer, "Calculating core losses in transformers for arbitrary magnetizing currents a comparison of different approaches," in *Proc. PESC 96*, vol. 2, 1996, pp. 1463 – 1468.

[43] M. S. Chinthavali, L. M. Tolbert, and B. Ozpineci, "4H-SiC GTO thyristor and p-n diode loss models for HVDC converter," in *Proc. IEEE IAC 04*, vol. 2, 2004, pp. 1238 – 1243.

[44] M. Trivedi, S. Pendharkar, and K. Shenai, "Switching characteristics of MCT's and IGBT's in power converters," *IEEE Trans. Electron Devices*, vol. 43, no. 11, pp. 1994–2003, Nov 1996.

[45] M. T. Aydemir, A. Bendre, and G. Venkataramanan, "A critical evaluation of high power hard and soft switched isolated DC-DC converters," in *Proc. IEEE IAC'02*, vol. 2, 2002, pp. 1338–1345.

[46] D. Linzen and R. W. De Doncker, "Simulation of power losses with MATLAB/simulink using advanced power device models," in *Proc. IEEE CPE'02*, vol. 1, 2002, pp. 71–75.

[47] M. H. Bierhoff and F. W. Fuchs, "Semiconductor losses in voltage source and current source IGBT converters based on analytical derivation," in *Proc. IEEE PESC 04*, vol. 4, 2004, pp. 2836–2842.

[48] R. Kraus, P. Turkes, and J. Sigg, "Physics-based models of power semiconductor devices for the circuit simulator SPICE," in *Proc. IEEE PESC 98*, vol. 2, 1998, pp. 1726 – 1731.

[49] R. Azar, F. Udrea, M. De Silva, G. Amaratunga, N. Wai Tung, F. Dawson, W. Findlay, and P. Waind, "Advanced SPICE modeling of large power IGBT modules," *IEEE Trans. Industry Applications*, vol. 40, no. 3, pp. 710–716, May/June 2004.

[50] O. Al-Naseem, R. W. Erickson, and P. Carlin, "Prediction of switching loss variations by averaged switch modeling," in *Proc. IEEE APEC 00*, vol. 1, 2000, pp. 242–248.

[51] "5SLF 20H2500 data sheet," ABB, Doc. No. 5SYA1584-02, May 2004.

[52] "5SNR 20H2500 data sheet," ABB, Doc. No. 5SYA1582-02, May 2004.

[53] "FF200R33KF2C data sheet," Eupec, June 2003.

[54] D. I. M. de Silva, N. K. Shrestha, P. R. Palmer, F. Udrea, G. A. J. Amaratunga, D. Chamund, L. Coulbeck, and P. Waind, "Accurate conduction and switching loss models of IGBTs for resonant converter design," in *Proc. IEEE PESC 04*, vol. 4, 2004, pp. 2950–2955.

[55] M. Trivedi and K. Shenai, "Modeling the turn-off of IGBT's in hard- and soft-switching applications," *IEEE Trans. Electron Devices*, vol. 44, no. 5, pp. 887–893, May 1997.

[56] I. Widjaja, A. Kurnia, K. Shenai, and D. M. Divan, "Switching dynamics of IGBTs in soft-switching converters," *IEEE Trans. Electron Devices*, vol. 42, no. 3, pp. 445 – 454, March 1995.

[57] Technical bulletin for the Metglas® POWERLITE® inductor core. [Online]. Available: http://www.metglas.com/downloads/powerlite.pdf,2006-10-03

[58] T. Kjellqvist, S. Norrga, and S. Östlund, "Switching frequency limit for soft-switching MF transformer system for AC-fed traction," in *Proc. IEEE PESC 05*, 2005.

[59] Datasheet for thin non-oriented fully processed electrical steel. [Online]. Available: http://www.cogent-steel.com,2006-10-03

[60] T. Nyikos and T. Tomaschett, "Experimental verification of a DC-DC converter for a DC wind farm," Dep. of Energy and Environment, Chalmers University of Technology, Tech. Rep., 2006.